ELSEVIER

S0032-3861(97)00071-2

Polymer Vol. 38 No. 13, pp. 3151–3212, 1997

0032-3861/97/$17.00 + 0.00

polymer papers

Kinetics of crystallization from the melt and chain folding in polyethylene fractions revisited: theory and experiment

John D. Hoffman*
Department of Materials Science and Engineering, 102 Maryland Hall, The Johns Hopkins University, Baltimore, MD 21218, USA

and Robert L. Miller
Michigan Molecular Institute, 1910 W. St. Andrews Road, Midland, MI 48640, USA
(Received 25 September 1996; revised 22 October 1996)

The rate of growth of chain-folded lamellar crystals from the subcooled melt of polyethylene fractions is treated in terms of surface nucleation theory with the objective of illuminating the origin of the chain folding phenomenon and associated kinetic effects in molecular terms. An updated version of flux-based nucleation theory in readily usable form is outlined that deals with the nature of polymer chains in more detail than previous treatments. The subjects covered include: (i) the origin of regimes I, II, III, and III-A and the associated crystal growth rates, including the effect of forced steady-state reptation and reptation of 'slack' in the subcooled melt; (ii) the variation of the initial lamellar thickness with undercooling; (iii) the origin of the fold surface free energy σ_e and the lateral surface free energy σ; (iv) the generation and effect of nonadjacent events (such as tie chains) on the crystallinity and growth rates; and (v) 'quantized' chain folding at low molecular weight. The topological limitation on nonadjacent re-entry and the value of the apportionment factor ψ are discussed. Key experimental data are analysed in terms of the theory and essential parameters determined, including the size of the substrate length L involved in regime I growth. The degree of adjacent and/or 'tight' folding that obtains in the kinetically-induced lamellar structures is treated as being a function of molecular weight and undercooling. New evidence based on the quantization effect indicates a high degree of adjacent re-entry in regime I for the lower molecular weight fractions. The quality of the chain folding at higher molecular weights in the various regimes is discussed in terms of kinetic, neutron scattering, i.r., and other evidence. Application of the theory to other polymers is discussed briefly. © 1997 Elsevier Science Ltd.

(Keywords: polyethylene; nucleation theory; chain folding; surface free energy; physical adsorption; Kuhn length; characteristic ratio; growth rate; regime transition; lamellar thickness; substrate length; forced reptation; reptation of slack; friction coefficient; Gambler's Ruin; molecular trajectory; crystallinity)

CONTENTS

I. INTRODUCTION

Our overall goal is to give a treatment of the kinetics of crystallization from the subcooled melt of linear polyethylene (PE) fractions that exhibit chain folding with emphasis on what occurs in molecular terms. We do this in the light of continued interest, having over a period of time noted important work of others while at the same time ourselves further developing the original Lauritzen–Hoffman (LH)[1,2] nucleation approach in some detail. In the process we were able to clarify and quantify certain aspects of the theory and to extend considerably its range of applicability.

A rather full deposition of the elementary theory is

* To whom correspondence should be addressed

given, which updates an earlier version[3] published as a book chapter in 1976. The emphasis in that chapter was on polymers of moderate molecular weight and dealt only with regimes I and II. Many developments have occurred since then. These include: (i) a treatment of regime III[4] which we shall improve herein; (ii) the incorporation of the reptation concept into polymer crystallization theory[5–7]; (iii) a theory for the physical origin and magnitude of the lateral surface free energy σ[8,9]; (iv) a nucleation-based treatment permitting fluctuations of the fold period during substrate completion[10]; (v) a nucleation-based treatment of the onset of 'quantized' chain folding at low and then approaching moderate molecular weights[11–13] which is extended and applied herein; (vi) development of the Gambler's Ruin and related treatments which place a topological lower bound on the degree of 'tight' folding[14–18]; and (vii) theoretical studies giving the lower bound of the degree of adjacency as a function of chain stiffness[19,20]. Questions related to the apportionment factor ψ are also dealt with, as are concerns related to other aspects of the LH approach and its recent derivatives.

In the present work we shall deal with the reptation concept in some detail with the object of connecting it in a more unified and quantitative manner with the growth rate treatments for regimes I, II, III, and III-A. (Forced steady-state reptation and reptation of slack provide mechanisms for transport of chain segments in the subcooled melt to the growth front that are sufficiently rapid to allow some chain folding.) Attention is given to assigning a direct physical meaning to the rate constants that govern the forward and backward reactions for surface nucleation and substrate completion. An improved treatment of the initial lamellar thickness, including the interfacial zone, is outlined. Care is taken in generating the pre-exponential factors for the growth rate expressions applicable to fractions of moderate molecular weight since these are essential to estimating fundamental parameters such as the substrate length L characteristic of regime I. This affords a particularly probing test of the theory and asks much of the experiments.

Special interest attaches to extension of the nucleation treatment to lower and higher molecular weight PE than had been carried out heretofore. We shall treat with 'quantized' chain folding in lower molecular weight fractions that exhibit a high degree of adjacent re-entry in regime I. Also, we shall deal with the reduced crystallinity, tie chain formation, and 'perturbed' reptation effects caused by nonadjacent events at moderately high molecular weights and then discuss the disappearance of the regime I $\rightarrow$ II transition effect and associated changes in spherulite morphology at still higher chain lengths. Some observations related to the crystallization behaviour of ultrahigh molecular weight PE fractions are noted.

It will be indicated at appropriate places in this work why we adopt a model featuring a substantial fraction of 'tight' folds in the case of melt-crystallized PE fractions. Definitions are in order here. A 'tight' fold is defined in this work as one that is formed by an emergent chain that executes a transit to an adjacent (probability $= p_{ar}$) or next-nearest adjacent (probability $= p_{aar}$) site where it re-enters the lamella of origin and which in each case has no substantial amorphous character in the traverse. The sum $p_{ar} + p_{aar}$ is the probability of 'tight' folding p_{tf}, which thus embraces all first- and second-nearest neighbour re-entries that have little or no amorphous component in their traverses. A 'sharp' fold is defined here as one involving a transit to an adjacent site that has a minimal, or close to minimal, traverse length with little or no amorphous contribution. We urge the reader to note these definitions since they are sometimes employed elsewhere with different meanings. The term 'regular folding' is occasionally employed and refers to systems where 'tight' folding is prevalent.

The above definitions set the stage for raising a question that has led to much discussion, namely that of the nature of the 'fold' surface. Following hard upon Keller's recognition of chain folding in solution-grown PE single crystals[21], it was known even in 1959[22] that melt-crystallized PE exhibited a decidedly lamellar morphology with a considerable degree of chain folding of some type on the upper and lower surfaces of each lamella. While this morphology certainly replaced the older 'fringed micelle' model, a dispute promptly arose concerning the nature of the fold surface in melt-crystallized PE. Was the surface a 'random switchboard' with only accidental adjacency[23], or was there a rather high degree of adjacency, or, put in a somewhat less demanding but nevertheless trenchant form, was there a rather high degree of 'tight' folding? The archetypical 'random switchboard' model was based on the idea that any adjacent re-entry was largely of accidental origin so that the lamella had a p_{ar} near zero, i.e. a preponderance of isolated single stems. We shall discuss the adjacency and 'tight' fold issues at various places in the main body of the text. To arrive at supportable estimates of the quality of the chain folding as it relates to specific situations will involve what can be deduced from theoretical treatments as well as from kinetic, i.r., neutron scattering, and other experimental studies. In this connection we note that for well-formed lamellae of large lateral extent there exists a topological lower bound on the allowed degree of 'tight' folding (Gambler's Ruin limit[14–18]) which for PE of moderate molecular weight is not less than about one-half and often notably higher, and further that the actual degree of 'tight' folding and strictly adjacent re-entry are from both a theoretical and experimental standpoint decidedly a function of molecular weight and the regime of crystallization. In the event, we shall not have to repent of employing basically chain-folded models.

Since the emphasis is on linear fractions, most of the issues addressed are principally of scientific interest. With this framework we have noted a number of theoretical endeavours that are worth considering and have also mentioned gaps in the experimental picture for PE which, if filled, would lead to an even more complete understanding of the crystallization behaviour and physical properties of fractions of this polymer. Despite the emphasis on fractions, it is believed that the phenomena to be discussed for these prototypical systems may provide a more firm basis than was heretofore available for treating more practical PE systems such as those with a broad distribution of molecular weight. The general concepts developed here may prove useful in dealing with other highly crystallizable linear polymers that possess an appropriate degree of chain flexibility. It will be brought out that extension of the theory can predict crystallization behaviour differing markedly from that of PE for

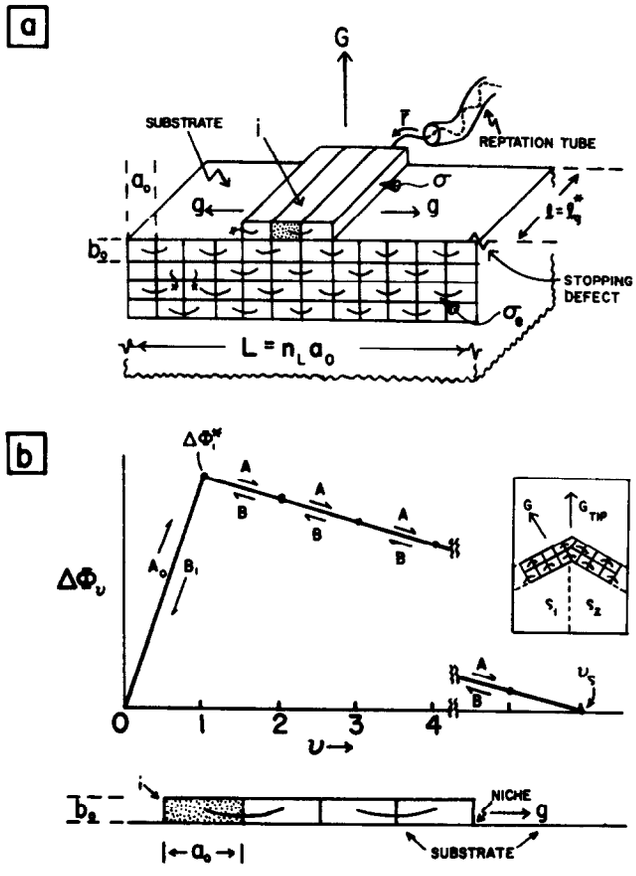

Figure 1 *Model for surface nucleation and growth.* (a) Physical relationships showing substrate of length L, nucleation rate i, substrate completion rate g, reptation velocity $\bar{r}$, fold surface free energy σ_e, lateral surface free energy σ, initial lamellar thickness l_g^*, and growth rate G (schematic). (b) Corresponding barrier system showing rate-determining forward and backward rate constants A_0, B_1, A and B. Shaded stems represent initial (primary) surface nucleation acts injected at rate i. Inset depicts {1 1 0} growth front with two sectors s_1 and s_2: the two slower-growing lateral {2 0 0}-type sectors not shown

polymers where the transport mechanism is for intrinsic molecular reasons restricted to reptation of slack.

It will be seen in various places in the text to follow that we emphasize certain connections between surface nucleation theory, on the one hand, and aspects of general polymer science, on the other. Thus, in addition to reptation which has already been mentioned, one will see reference to such topics as physical adsorption, the friction coefficient, the Kuhn segment length, the rotational isomeric state (RIS) model, and the statistical mechanics of confined chains, as in each case they relate to polymer crystallization. While acceptance is at the discretion of the reader, the authors believe that the overall understanding of the crystallization behaviour of PE (and possibly similar polymers) will prove to be furthered by these connections.

II. THE SURFACE NUCLEATION MODEL

A. Background

In developing the model, we recognize at the outset that no equilibrium treatment can possibly give a proper accounting of the initial thickness of the chain-folded lamellae, let alone the rate of crystallization. The equilibrium state is that with the extended-chain conformation and not the chain-folded one, and it is clear enough that the folds are incorporated in a lamellar crystal as it is being formed. If a further indication that chain-folding is in major aspect kinetic in character is required, one only need note that on storage the initially thin chain-folded lamellae of thickness l_g^* begin spontaneously to thicken if the crystallization (storage) temperature is high enough to permit the requisite molecular motions. Of course, the kinetic equations of nucleation theory conform at certain points to the prevailing thermodynamics associated with Gibbsian surface physics and, in another sense, where detailed balance is invoked in the rate expressions. We shall proceed on the basis that, when coupled with certain considerations based on chain flexibility and topology, a proper application of even a quite simple version of flux-based nucleation theory can lead to a meaningful molecular picture of the interesting, unusual, and sometimes seemingly counterintuitive phenomena that attend the occurrence of chain folding.

The developments to follow in this section apply specifically to specimens of isothermally melt-crystallized PE of intermediate molecular weight ($M \simeq 15$K to $M \simeq 90$K) in which regime I → II and II → III transitions appear, where the degree of crystallinity is relatively high, and where the effects of reptation can be sorted out. The theory is subsequently tested against experiment in Section III where the intermediate molecular weight range is divided into two parts, ranges B–B′ and C–C′, depending upon the nature of the reptation process. 'Quantized' chain folding at low molecular weights (range A–A′, $M \sim 3.4$K to ~11K), where adjacent re-entrant clusters with up to at least four stems appear, is treated in a later section. Also treated later is the extension of nucleation concepts to high molecular weight systems, ranges D–D′, $M \sim 103$K to ~640K, and E–E′, $M \geq$ ~1000K, in both of which the regime I → II transition is absent, reptation is highly restricted, and the crystallinity is low. The reader may obtain an immediate grasp of the extent of these molecular weight ranges by turning briefly to *Figure 7* in Section III.C.

The treatment to follow is intended to describe the formation from the subcooled melt of chain-folded lamellae where the interior stems are in an orthorhombic arrangement, which represents the stable phase at ordinary pressures. At high pressures near and above the triple point, the hexagonal form appears directly from the subcooled melt and leads to highly interesting crystallization effects involving 'thickening growth' that differ significantly from those discussed here[24].

B. Model

The basic surface nucleation model is shown schematically in *Figure 1*. This depiction refers to the growth front that is observably the kinetically dominant one in PE, namely {1 1 0}, which is also the most densely packed. In PE, as in certain other polymers, more than one type of growth front can be observed in the same crystal, which for PE includes the dominant {1 1 0} and the slower growing {2 0 0} front. This slower growing (subordinate) growth front is associated with lateral sectors containing {2 0 0} folds, these sectors having curved edges at high growth temperatures[25–27] from the melt just as do single crystals of PE grown from dilute solution at high temperatures[28,29]. A special nucleation-based treatment is required to deal with the curved

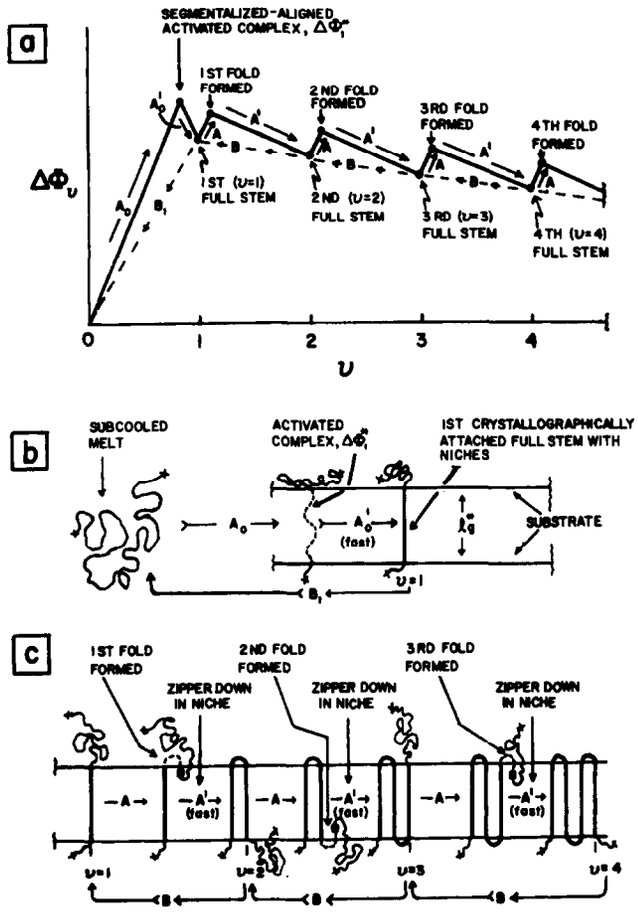

Figure 2 *Details of barrier system for surface nucleation including both slow and fast steps: also corresponding molecular configurations.* (a) Barrier system showing all rate constants. Rate-determining slow steps A_0, B_1, A, and B; fast steps A_0' and A'. (b) Formation of the physically adsorbed 'segmentalized–aligned' rate-determining activated complex (no niches) leading to subsequent formation in rapid step A_0' of first crystallographically-attached stem with niches at $\nu = 1$. (c) Fold formation by excursion to nearby site in niche ('proximity' effect) at rate A followed by rapid zippering down at rate A' adding a new fully attached adjacent stem in substrate completion process

{2 0 0} edges[30–32] (see Section III.G), but we concentrate in the present work mainly on the behaviour of the kinetically dominant {1 1 0} growth front that advances into the subcooled melt at a rate G. As shown in the inset in *Figure 1*, the actual optically observable growth rate of spherulites and axialites is controlled by G_{tip} which, for practical purposes, may be taken to be the same as G for the {1 1 0} growth front. Details concerning the nature of the {1 1 0}-type growth front at high T_x (regime I) and lower T_x (regime II) are important and will be given subsequently.

The first stem (designated $\nu = 1$ and shaded in *Figure 1b*) is the most difficult to put on the previously-formed growth front and involves a process with a high free energy barrier as shown in the figure. In the conventional LH nucleation model this barrier is thought of as the work $2b_0\sigma l$ of building the two lateral surfaces of the new $\nu = 1$ surface nucleating stem of length l. Here, b_0 is the layer thickness and σ the lateral surface free energy. The length l is treated as a variable, the mean value of which will subsequently define the initial lamellar thickness l_g^*.

The conventional view that the barrier height at $\nu = 1$ is a result of forming the two new lateral 'σ' surfaces is useful and we shall retain it in virtually all of the treatment to follow, but the reader should be aware that a recent theoretical development concerning the origin and *a priori* calculation[8,9] of σ places this measurable parameter in a new light. It is helpful to digress briefly here to describe this development. The new theory relates the σ of nucleation theory to the parameter C_∞ of the RIS model of the melt state of polymers.

The treatment of σ involves the problem of putting down the first stem on a 'flat' niche-free substrate and begins with the fact that when a random coil chain molecule in the melt (initial state) closely approaches such a 'flat' surface, it is forced by the mere near-presence of the surface to lose configurations by developing structure and thus reduce its entropy. The 'flat' substrate is assumed to have no niches that invite consecutive zippering down of $-CH_2-$ units, wherein each unit would immediately give up its full heat of fusion. The loss of entropy occurs without actual crystallographic attachment to the niche-free surface so that the section of molecule involved is in a somewhat flattened mobile state resembling that of weak physical adsorption with occasional point contacts at separated sites on the substrate[3]. A short section of molecule in this semi-confined but as yet crystallographically unattached state is envisioned as becoming, after many trials, 'straightened' and 'segmented' and, at a point in time, aligned with a full stem pair on the substrate such that the fall in entropy as measured relative to the melt as the initial state is taken to be $-\Delta S_f/C_\infty$ (hereinafter sometimes denoted $-\Delta S_1^*$). The short section of as yet crystallographically unattached molecule consists of on the order of n^* $-CH_2-$ units, which suffices to subsequently form a crystalline stem of length l_g^*. Here ΔS_f is the full entropy of fusion of the short section and C_∞ the characteristic ratio of the polymer in the melt. The characteristic ratio enters the theory through the approximation that the thermodynamically active segment length of the aligned portion of chain that forms the activated complex in proximity to the surface is related to C_∞ according to $l_{seg} - l_b$ where l_{seg} is the Kuhn length $C_\infty l_b$[9]. The associated large free energy change (work) in the absence of any significant heat of fusion is $(-T)(-\Delta S_1^*)$ or $T\Delta S_f/C_\infty$, which is *higher* than that of the unperturbed melt and corresponds to the peak value of $\Delta\phi_\nu$, i.e. $\Delta\phi_1^*$, as in *Figures 1b* and *2a*. *It is this crystallographically unattached 'aligned' and 'segmentalized' assemblage proximate to the substrate in a state of physical adsorption that is taken to be the most difficult to form spontaneously and which thus represents the activated complex, i.e. the rate-determining step in putting down the first crystallographically-attached stem.* (From an entropic standpoint, this segmentalized-aligned activated state has at least a passing resemblance to a crystallographically unattached but weakly physically adsorbed and mobile rotator phase-like stem with some point contacts on the substrate.) The heat of physical adsorption for the n^* units in the activated complex involves only a limited number[9] of weak van der Waals contacts, with the result that it is much less than the full heat of fusion of the n^* $-CH_2-$ units. In the absence of any significant heat of fusion, the nucleation free energy barrier $\Delta\phi_1^*$ for putting down the first stem on the niche-free substrate in this treatment is seen through the relation $T\Delta S_1^*$, or $T\Delta S_f/C_\infty$, to be of basically entropic origin. Shortly after attaining the crystallographically unattached rate-determining activated state,

the segmentalized and aligned section of adsorbed chain in that state snaps onto the substrate at a rapid rate A_0', forming a crystallographically attached first stem on the {1 1 0} face (final state, orthorhombic lattice) of length l_g^* with a niche on either side and with simultaneous release of the bulk of the heat and free energy of fusion of the stem[13] (*Figure 2b*).

While the concept that a chain in proximity (but not crystallographically attached) to a surface develops structure is new to polymer nucleation theory, there is nothing *ad hoc* or physically obscure in the general proposition. For example, Chan *et al.*[33] have shown by simulations that an isolated chain on a cubic lattice in proximity to a surface, but not actually attached thereto, develops an enhanced degree of internal structure; this clearly calls for a reduced entropy in the crystallographically unattached surface state. That a polymer chain loses entropy on a close approach to a surface is in any case widely accepted by theorists. Meanwhile, we note that the concept of physical adsorption of a section of polymer chain on a niche-free substrate is surely a reasonable one.

As has been described in detail[8,9], the physical concepts noted above lead to the expression valid under 'theta' conditions

$$\sigma = T\left(\frac{\Delta h_f}{T_m}\right)\frac{a_0}{2}\left(\frac{l_b}{l_u}\right)\frac{1}{C_\infty} \qquad (1)$$

where σ is the lateral surface free energy of conventional nucleation theory, Δh_f the heat of fusion, T_m the melting point, a_0 the width of the chain, l_b the bond length, and l_u the C–C distance as projected along the chain axis. [Equation (1) is readily derived by setting the conventional expression for the barrier height for $\nu = 1$ in *Figure 1* (which is given by $2b_0\sigma l = 2b_0\sigma l_u n^*$) equal to $T\Delta S_1^* = T(\Delta S_f)/C_\infty$ in the units $a_0 b_0 l_b n^* \times [T(\Delta h_f/T_m)]/C_\infty$ where it is recalled that n^* represents the number of $-CH_2-$ units in the initial lamellar thickness.] This formulation has been successful in predicting σ (or alternatively C_∞) for a number of melt-crystallized polymers having a range of C_∞ values; these include PE ($C_\infty = 6.7$); *it*-polypropylene, *it*-PP ($C_\infty = 5.7$); and poly(L-lactic acid), PLLA ($C_\infty = 2.1$). Originally *it*-polystyrene (*it*-PS) was included in the list[8,9], but recent work by Marand[34] suggests that there is considerable uncertainty in the experimental value of σ and σ_e from crystallization studies. Current evidence suggests that the theory for σ applies best for high polymers for which the I → II transition has been clearly observed, as in the cases of PE, *it*-PP, and PLLA.

The extended theory with C_∞ replaced by C_n (the latter approaching unity at very low n[35,36]) also predicts the marked increase of $\bar{\alpha}_1$ and thus σ observed by Turnbull and Spaepen[37,38] at very low chain lengths ($n < 40$) in the $-(CH_2)_n-$ system, the approach outlined here then evidently applying with fair accuracy from pentane to polyethylene[9,40]. In the 'negentropic' model proposed by Turnbull and Spaepen in 1978, the general concept of 'segmentalization' was an inherent part of the explanation given for the increase in σ at low chain lengths[9,37]. (Spaepen[41] had earlier presented a persuasive case for the entropic origin of surface free energies in atomic systems.) Our equivalent of the 'negentropic' approximation is that the entropy of the activated state for the first stem is $-\Delta S_1^* = -\Delta S_f/C_\infty$ or, alternatively, $-a_0 b_0 l_b n^*[\Delta h_f/T_m]/C_\infty$ in the units appropriate to that stem; for very small n^* or very short chains, C_∞ would be replaced by C_n.

A different class of model for lamellar crystallization featuring surface roughening and a barrier of entropic origin that avoids the concept of a surface nucleus of the general type discussed here has been proposed by Sadler and Gilmer[42,43]; see also the more recent work of Goldbeck-Wood[44] and of Spinner *et al.*[45]. As will be noted subsequently, their treatments are not free of question. Here and earlier[8,9] we pursued the alternative of enlarging on the approach initiated by Spaepen[41] and Turnbull and Spaepen[37] that emphasizes the entropic origin of the normal surface free energy σ. Thus, we came to consider the problem of explaining the physical origin of one of the most important parameters of polymer nucleation theory in entropic terms including the introduction of the Kuhn length $C_\infty l_b$ to account for the segmental nature of the polymer chain.

It is essential to observe that the model presented here has σ in effect being created by a special-condition corresponding to the rate-determining activated state that prevails in proximity to the substrate *before* actual crystallographic attachment of the first stem. Recall here that actual crystallographic attachment of this stem, with full release of the heat and free energy of fusion, occurs in a rapid step A_0' immediately after attainment of the locally aligned and segmentalized physically adsorbed activated state. Thus the *net* entropy change (melt) → (crystallographically attached first stem) is $-\Delta S_f$ in appropriate units. As will appear shortly, these characteristics are compatible with the well-known 'low ψ' formulation of polymer surface nucleation theory.

Contrary to an objection[46], the theory for σ does *not* imply that the full entropy of fusion of a polymer depends on C_∞. In the treatment of σ, only the entropy of the rate-determining *activated state* for the first stem $-\Delta S_1^*$ was taken to depend on C_∞ according to $-\Delta S_f/C_\infty$—this does not imply that the full entropy change $-\Delta S_f$ on going from the initial state (random coil melt) to the final state (crystallographically attached stem) depends on C_∞ for *any* stem added, including the first.

The overall process described above for the formation of a first stem, e.g. (random coil) → (segmentalized-aligned adsorbed activated state) → (crystallographically attached first stem), does in fact lead to the creation of two new lateral σ-type surfaces with niches as assumed in conventional nucleation theory and as depicted in *Figure 1*. There is no contradiction between the new theory for σ and the conventional approach—see following thermodynamic relationship for the first stem.

After crystallographic attachment of the first stem, new stems ($\nu \geq 2$) add in sequence to the energetically favourable 'niche' on either side of the first stem. This leads to a relatively rapid substrate completion process that produces a new layer of thickness b_0 on the face of the lamella (*Figure 1*). Repetition of the nucleation and substrate completion processes leads to the growth rate G. In the simplest ideal model, each stem added in the substrate completion process requires the formation of a chain fold with its concomitant work of formation, the latter being ultimately overborne by the full free energy of fusion associated with the stem that fills the niche.

To assist the reader who wishes to follow the treatment in numerical as well as conceptual terms,

Table 1 Useful input data for analysis of PE crystallization kinetics

Quantity	Value
Crystallographic	
a_0, width of stem	4.55×10^{-8} cm
b_0, layer thickness	4.15×10^{-8} cm
a_0, b_0, cross-sectional area of chain	18.88×10^{-16} cm^2
l_b, C–C bond length	1.54×10^{-8} cm
l_u, projected length per $-CH_2-$ unit in straight PE chain	1.273×10^{-8} cm
Thermodynamic	
Δh_f, heat of fusion	2.80×10^9 erg cm^{-3}
T_m^0, equilibrium melting temperature	145.5°C = 418.7 K
Nucleation constants and parameters	
σ_e, fold surface free energy	90 erg cm^{-2}
σ, lateral surface free energy	11.8 erg cm^{-2}
q, work of chain folding	4.90 kcal mol^{-1} = 3.404×10^{-13} erg molecule^{-1}
$K_{g(I)}$, nucleation constant for regime I	1.91×10^5 deg^2
$K_{g(II)}$, nucleation constant for regime II	0.955×10^5 deg^2
$K_{g(III)}$, nucleation constant for regime III	$\sim 1.91 \times 10^5$ deg^2
Q_D^*, activation energy for reptation and centre-of-mass diffusion[47]	5736 cal mol^{-1}
Physical constants and conversion factors	
R, gas constant	1.987 cal mol^{-1} deg^{-1}
k, Boltzmann's constant	1.3806×10^{-16} erg molecule^{-1} deg^{-1}
h, Planck's constant	6.626×10^{-27} erg s

erg molecule^{-1} × 1.4393×10^{16} = cal mol^{-1}; 1 cal = 4.184 J; 1 mJ m^{-2} = 1 erg cm^{-2}

Table 1 provides input data that will be found useful throughout this work.

C. Surface nucleation rate

In thermodynamic terms, the net free energy of formation of a new layer comprised of ν stems is given by

$$\Delta\phi_\nu = \underbrace{2b_0\sigma l - a_0 b_0 l(\Delta G)}_{\text{first stem, } \nu=1} - \underbrace{(\nu-1)a_0 b_0[l(\Delta G) - 2\sigma_e]}_{\text{substrate completion, } \nu\geq 2} \quad (2a)$$

where the driving potential for crystallization (free energy difference between subcooled melt and crystal in erg cm^{-3}) is to a sufficient approximation

$$\Delta G = \frac{(\Delta h_f)(T_m - T_x)}{T_m} = \frac{\Delta h_f(\Delta T)}{T_m} \quad (2b)$$

Here, T_m is the melting point of a large extended-chain crystal with an equilibrium degree of perfection (corresponding to the equilibrium content of localized chain ends) for the molecular weight under consideration, T_x the isothermal crystallization temperature (often used in the text without the subscript), and $T_m - T_x = \Delta T$ the undercooling. In certain instances where large undercoolings ΔT are to be considered, the quantity ΔG is multiplied by a factor[3,48] $f = 2T/(T_m + T)$ to account approximately for entropic and enthalpic effects arising from the decrease in the heat of fusion with lowering temperature, but this is a relatively trivial correction in the case of PE fractions for the low undercoolings normally encountered in the growth rate studies and we shall accordingly not apply it in the present case. Our use of T_m as a reference temperature in dealing with the behaviour of chain folded systems, including the 'quantized' ones of low molecular weight, is justified in Section V.B.

Observe from the last term in equation (2a) that substrate completion cannot occur unless $l(\Delta G)$ is at least slightly greater than $2\sigma_e$, which means that l has an absolute lower bound of $2\sigma_e/(\Delta G)$. This is important and its origin will be discussed shortly.

The treatment of surface nucleation and growth for chain folded lamellar systems presented below considers both the forward and backward reactions for each elementary step in calculating the total flux and thence the surface nucleation rate. It is therefore related in this context to the work of Turnbull and Fisher[49] who earlier gave a treatment involving forward and backward reactions for the step-by-step formation of a homogeneous nucleus for atoms or small molecules. The problem of the conversion to surface nucleation and growth in lamellar polymeric systems requires consideration of a number of new features, such as accounting for the work of chain folding q, the quite different nature of the transport mechanism (reptation) in the polymeric melt, the effect of chain length, the segmental nature of the polymer chain, and questions related to the substrate length and the nature of a surface nucleus on a bladelike structure.

To obtain the surface nucleation rate i and the substrate completion rate g, it is necessary to construct expressions for the so-called 'rate constants' A_0, B_1, A, and B in *Figure 1* that describe the rate of the essential forward and backward reactions. We shall do this in what follows in a manner that attaches a direct physical meaning to each and which adheres to the principle of detailed balance. This principle requires that for each elementary step, the equilibrium distribution delineated in equation (2a) be recovered.

For the rate constant for attainment of the activated state $\Delta\phi_1^*$, which represents the barrier for the subsequent deposition of the first ($\nu = 1$) stem, we write

$$A_0 = \beta e^{-2b_0\sigma l/kT} \quad (3a)$$

This expresses the rate-determining (slow) step in conventional form. For the backward reaction (removal of the first stem) one has

$$B_1 = \beta e^{-a_0 b_0 l(\Delta G)/kT} \quad (3b)$$

which requires the full free energy of fusion $a_0 b_0 l(\Delta G)$ to convert the stem back to the melt state. The factor β, which is in units events s^{-1}, represents the retardation of the nucleation process associated with transport of chain segments through the subcooled melt to or from the growth front. A form of β consistent with both nucleation and reptation concepts will be presented in due course.

Observe that the rate constant A_0 to the approximation of equation (3a) does not involve the free energy of fusion in accord with the above discussion of the origin of σ. The fast step A_0', wherein the 'segmentalized–aligned' portion of chain of length l snaps onto the surface forming a first stem with full crystallographic

attachment is not a rate-determining factor in the deposition of that stem and need not be considered in the rate process above. It is only important that this fast step releases the full free energy of fusion on deposition of the first stem. This is consistent with the formulation of B_1, which states that the full free energy of fusion must be supplied to remove the stem. The overall process for the first stem obeys the principle of detailed balance, since the ratio A_0/B_1 recovers the equilibrium distribution for $\nu = 1$ required by equation (2a).

Figure 2a illustrates the detailed arrangement of all the rate constants leading to deposition and removal of the first ($\nu = 1$) stem. The rate-determining activated state, which has no niches, is formed at a rate A_0. Because there is no niche in the segmentalized activated complex, there is yet no tendency for fold formation so that there is no factor $\exp(-q/kT)$ in A_0. After the 'segmentalized–aligned' activated state is attained, the section of molecule involved shortly thereafter snaps onto the substrate at the rapid rate A_0', leading to the first fully crystallographically attached stem with a niche on either side (*Figure 2b*). This full stem can occasionally be removed by the backward reaction B_1. The important feature of the first fully attached stem (as opposed to the preceding activated complex) is that it has a niche that promotes fold formation in the subsequent substrate completion process (*Figure 2c*). (Note that the scheme depicted in *Figure 2* for forming the first fully attached stem avoids the altogether less probable high-barrier nucleation path involving the work of chain folding q wherein $\Delta\phi_1^*$ would be $2b_0\sigma l + q$ rather than $2b_0\sigma l$.) *Figure 1* shows only the important rate-determining rate constants A_0 and B_1 that appear in equations (3a) and (3b), and it omits the fast step A_0' which does not influence the overall kinetics of deposition of the first fully attached stem at $\nu = 1$.

The reader familiar with early versions[3,50] of the theory will recognize that equations (3a) and (3b) represent the so-called '$\psi = 0$' or 'low ψ' formulation for the first stem, which clearly avoids the 'δ catastrophe'. (In these versions, A_0 was written as $\beta\exp[-2b_0\sigma l/kT + \psi a_0 b_0 l(\Delta G)/kT]$ and B_1 as $\beta\exp[-(1-\psi)a_0 b_0 l(\Delta G)/kT]$ where $0 \leq \psi \leq 1$.) If it actually occurred, the 'δ catastrophe' would lead to a relatively abrupt upswing in l_g^* and the growth rate toward very large values at the undercooling $\Delta T_c = 2\sigma T_m/(\Delta h_f)a_0\psi$; for the upper bound of ψ of unity, this comes to about 77°C for PE. No such upswing of l_g^* is currently known to occur for any polymer crystallized isothermally directly from the subcooled melt at low T_x and the 'low ψ' formulation for l_g^* to be presented shortly is free from any 'catastrophe' effect. It was noted at an early date by LH[50] that the ψ for the first stem, often later denoted ψ_1, could be different than the ψ for substrate completion, and further that physical adsorption could play a role in causing ψ_1 to be small and thus eliminate the 'δ catastrophe'. For PE, a ψ_1 of $\sim$0.2 already puts the 'δ catastrophe' close to absolute zero, so 'low ψ' may be taken to mean $0 \leq \psi \leq 0.2$.

The present treatment provides an additional rationale for the choice of a low or nil ψ for the first stem. The successful *a priori* calculation of σ for PE, *it*-PP, and PLLA[9] in terms of a difficult-to-attain segmentalized and aligned physically adsorbed conformation associated with the presence of the surface, but without crystallographic attachment thereto and thus little or no immediate free energy of fusion corresponding to a low or nil ψ as implied by equation (3a), provides the rationale. What Nature was trying to tell us by letting only the 'low ψ' formulation of the earlier versions of the theory correspond best to experiment with respect to the behaviour of l_g^* was that attainment of the rate-determining activated state for the first stem involved little or no release of the available free energy of fusion. Since the issue of the appropriate value of ψ has important ramifications, we deem it helpful to introduce the following commentary.

In the past there was concern about the fact that a large ψ for the first stem could lead to prediction of a 'δ catastrophe'. The current theoretical approach clarifies the true origin of the low or nil ψ for the first stem and makes it clear on fundamental grounds (beginning with the entropy loss of a polymer chain proximate to a surface in a condition of physical adsorption prior to crystallographic attachment) that the appearance of a 'δ catastrophe', though conceivable in an exceptional case, is not commonly to be expected. The overall result of the 'low ψ' model for the first stem is that one now has an understanding of why a 'δ catastrophe' is unlikely and, in addition, one has a theory for σ in terms of C_n^{-1} that is noteworthy not only because it predicts σ for chain-folded PE but also because it evidently holds[38,40] for short extended-chain *n*-alkanes. Further, it is satisfactory that the entropically active segment length in the theory for σ for PE is directly related to the Kuhn length $C_\infty l_b$ rather than some arbitrary fraction or multiple thereof. Taken together, these findings provide substantial support for the surface nucleation model outlined here. Other findings that support the model will be noted in due course.

Further comment concerning ψ and the addition of the first stem is required to put matters in full perspective. The assumption for PE that the first stem simply 'zippers down' in sequence directly from the random coil melt onto the niche-free substrate, with each $-CH_2-$ unit immediately giving up its full heat and free energy of fusion, corresponds to $\psi \simeq 1$ and predicts a 'δ catastrophe' at $\Delta T_c \simeq 77°$ for which there is no experimental support; moreover, because of the immediate generation of the heat and free energy of fusion, this model exhibits the additional debility of preventing the development of a theory for σ. It is therefore evident that this extreme version of the model wherein the first stem was supposed to zipper down directly as just described onto the niche-free substrate is questionable. Further, it is evident that the present segmentalized-aligned rate-determining activated state model involving physical adsorption with its inherently low ψ is superior to it for PE and gives a more insightful and productive picture of the molecular physics involved in putting down the first stem. It needs to be appreciated that the heretofore much-questioned 'low ψ' approximation for this stem, which leads to agreement with experiment for σ, the behaviour of l_g^* and, as will emerge later, the surface nucleation rate and the growth rate, is now based from the outset on how flexible polymer chains actually behave entropically when they closely approach a 'flat' niche-free surface. The conventional zippering down mechanism, wherein each $-CH_2-$ group directly deposited in sequence from the subcooled melt immediately gives up its heat and free energy of fusion, is

properly reserved for situations involving the filling of a niche during substrate completion (see below).

Consider now the substrate completion process $\nu \geq 2$. Here the slow rate-determining step for the forward reaction for the deposition of each stem is represented by

$$A = \beta e^{-q/kT} \tag{3c}$$

which recognizes the necessity of accounting for the work of chain folding q. The implication of equation (3c) is that a preliminary fold structure with essentially typical chain-fold energetics forms early in the overall process of stem addition during substrate completion—the emergent chain is pictured as normally turning back and attaching a few segments nearby in the adjacent niche ('proximity' effect) thus creating a chain fold with adjacent re-entry (*Figure 2c*). That the attachment to the niche can under appropriate circumstances be quite close to the point of emergence is supported by the 'first passage' argument for a random walker given in 1971 by Sanchez and DiMarzio[51]. From a kinetic point of view, this turning back process is opposed by the work of chain folding q and is, therefore, slow and rate-determining for substrate completion $\nu \geq 2$ as expressed by the rate constant A. After this 'proto-fold' with its relatively normal q is formed, the bulk of the free energy of fusion is delivered in the fast step A' as segments of the much longer remainder of the dangling chain are rapidly zippered down in the niche forming a new crystallographically attached stem (*Figure 2c*). The new stem has a niche and the process can be repeated. As in the case of A_0', the fast step A' does not appear in the final rate expressions. Thus, as in *Figure 1b*, only A and B are involved in determining the substrate completion rate g.

While tending to promote adjacent re-entry because of the higher concentration of chain segments belonging to the emergent chain at the potential site of fold formation, the 'proximity' effect noted above and illustrated in *Figure 2c* obviously does not exclude a certain amount of nonadjacent re-entry. In the melt there are segments of a 'strange' (i.e. a different) molecule naturally present. These could with some probability enter the niche and complete a stem thereby creating a nonadjacent event. For intermediate molecular weights, it will subsequently be shown that adjacent re-entry is considerably more likely in regime I (low ΔT) than in regime III (high ΔT).

For the slower backward (stem removal) reaction we write

$$B = B_1 = \beta e^{-a_0 b_0 l(\Delta G)/kT} \tag{3d}$$

where the relevant energetic quantity is the free energy of fusion, just as for the removal of the first stem. Detailed balance is preserved since the ratio A/B recovers the equilibrium distribution required by equation (2a) for $\nu \geq 2$. There is no term in σ in equation (3c), since no new lateral surface is formed at a niche.

The above picture for substrate completion is in the 'low ψ' class[3] insofar as the number of $-CH_2-$ units in the niche just as the proto-fold is formed is small in relation to the total number n^* of $-CH_2-$ units in a complete stem (*Figure 2c*). In such a case the free energy of fusion associated with initial fold formation is small. (The expression[3] for A including ψ is $\beta \exp[-q/kT + \psi a_0 b_0 l(\Delta G)/kT]$ and that for $B = B_1$ is $\beta \exp[-(1-\psi)a_0 b_0 l(\Delta G)/kT]$; no analogue of the '$\delta$ catastrophe' occurs in substrate completion in this model for any allowed value of ψ.) As implied earlier, the more general formulation of the theory assigns a value of ψ_1 to the first stem and another ψ to the substrate completion process[50]. The arguments given above provide a molecular basis for employing the 'low ψ' approximation for both the first stem and the stems $\nu \geq 2$ in the substrate completion process. This will prove to be altogether adequate for PE, but the general formulation may need to be invoked in an exceptional case. Observe that the physical cause for a low ψ_1 for the first stem is different than that for a low ψ for substrate completion.

In the above, the mean work of chain folding q is given by

$$q = 2a_0 b_0 \sigma_e \tag{4}$$

Here we recognize that q and σ_e are the averages $\langle q \rangle$ and $\langle \sigma_e \rangle$, respectively, over the predominant fraction of 'tight' folds, most of which are adjacent, together with some smaller contributions from the less numerous but still relatively nearby nonadjacent re-entries. Except at a later point where we mention the case of low molecular weight PE fractions with only a few folds per molecule where, for instance, the presence of short chain ends reduces the effective value of σ_e to one-half its full value in the case of once-folded molecules, we employ the notation of equation (4) in what follows with the understanding that these quantities represent the averages noted.

It is generally agreed that the work of folding a PE chain back on itself and re-entering the orthorhomic lattice forming a sharp {1 1 0} fold has a large contribution from the introduction of a number of *gauche* bonds in the fold. *Trans* bonds are also present in the fold. Depending upon the particular type of sharp {1 1 0} fold considered, 5–7 C–C bonds are involved, and there is some additional twist energy present in both the *gauche* and *trans* bonds in the fold in order to achieve correct re-entry into an adjacent site. Molecular energy calculations for {1 1 0} folds have in the past yielded q_{110} values ranging from 14.6[52], 5.61[53], to 4.0[54] kcal mol^{-1}. Recent computations[55] for the three lowest energy {1 1 0} folds yielded a value centring around 4.94 ± 0.69 kcal mol^{-1} corresponding to a σ_e of 90.7 ± 12.7 erg cm^{-2}, which is close to the experimental result listed in *Table 1*. Interestingly, we find that the Boltzmann-weighted average for q_{110} for all five types of fold structures treated in ref. 55, which range from 4.49 to 6.15 kcal mol^{-1}, is 4.87 kcal mol^{-1}: this holds within narrow limits for the entirety of regimes I and II. (As will be brought out later, the initially-formed fold surface is likely rougher than the annealed one and the energetics slightly different.) For a discussion of the nature of 'ideal' sharp {1 1 0} folds as revealed by i.r. studies, see ref. 56 and citations therein. The *net* work W_{200} of chain folding for {2 0 0} folds, counting *gauche* and twist energies in the normal work of folding q_{200}, as well as rather strong fold–fold interactions with the accompanying lattice strain effects, is known from experiment to be larger than q_{110}; the latter point will be raised again in Section III.G.

We now calculate the net flux S_T over the barrier in *Figure 1b*, and thence the surface nucleation rate i. The flux over the barrier is given in the general case[50,57] by $S(l) = N_0 A_0[(A-B)/(A-B+B_1)]$, which in the present situation where $B = B_1$ is

$$S(l) = N_0 A_0(1 - B/A) \tag{5a}$$

Here, N_0 is the number of reacting species which we

define as

$$N_0 \equiv C_0 n_L \tag{5b}$$

where C_0 is the configurational path degeneracy and n_L the number of stems of width a_0 comprising the substrate length L (see *Figures 1* and *3*). Note that N_0 is seen as being proportional to the substrate length, which is given by $L = n_L a_0$. We take L to be an inherent property of the underlying crystal (see later). The *net* flux across the barrier is given by

$$S_T = \frac{1}{l_u} \int_{2\sigma_e/(\Delta G)}^{\infty} S(l)\, dl \tag{5c}$$

where l_u is the monomer length. With the definition for the surface nucleation rate

$$i\,(\text{stems s}^{-1}\,\text{cm}^{-1}) \equiv S_T/L = S_T/n_L a_0 \tag{5d}$$

one obtains exactly

$$i = \frac{C_0}{a_0}\,\beta\,\frac{1}{l_u}\left[\frac{kT}{2b_0\sigma} - \frac{kT}{2b_0\sigma + a_0 b_0(\Delta G)}\right] e^{-4b_0\sigma\sigma_e/(\Delta G)kT} \tag{5e}$$

For low and moderate undercoolings in PE, $a_0 b_0(\Delta G)$ is substantially less than $2b_0\sigma$ giving, to an approximation sufficient for most purposes,

$$i \cong C_0\beta\left[\frac{kT(\Delta G)}{4b_0 l_u \sigma^2}\right] e^{-4b_0\sigma\sigma_e/(\Delta G)kT} \tag{6}$$

There is an important point upon which much depends that should not be missed here, which involves the lower bound of integration in equation (5c). The integration is intended to cover all possible values of l. That the lower bound of l is $2\sigma_e/(\Delta G)$ is readily seen from the thermodynamic melting point expression for a thin lamella with large lateral dimensions

$$T_m' = T_m[1 - 2\sigma_e/(\Delta h_f)l] \tag{7a}$$

Substitution of $l = 2\sigma_e/(\Delta G) = 2\sigma_e T_m/\Delta h_f(T_m - T_x)$ yields $T_m' = T_x$, showing that $l = 2\sigma_e/(\Delta G)$ represents the thinnest possible lamella, justifying the lower bound in equation (5c). It follows, as will be shown explicitly below, that the correct average value of l, denoted l_g^*, is slightly larger than $2\sigma_e/(\Delta G)$ by an amount δ, which happily leads to the formation of a bladelike crystal that melts above its temperature of formation. Specifically, with $l = l_g^* = 2\sigma_e/(\Delta G) + \delta$ substituted into equation (7a) and noting that δ is small compared to $2\sigma_e/(\Delta G)$, one finds that the melting point T_m' of an unthickened chain-folded crystal is

$$T_m' \cong T_x + (\Delta T)^2\left[\frac{\delta(\Delta h_f)}{2\sigma_e T_m}\right] - (\Delta T)^3\left[\frac{\delta(\Delta h_f)}{2\sigma_e T_m}\right]^2 + \cdots \tag{7b}$$

For PE melt-crystallized at $\Delta T = 20°$, T_m' is calculated to be about 1.4° above T_x. 'First melting' experiments confirm that the youngest, i.e. the essentially unthickened, lamellae melt slightly above T_x, as indicated by equation (7b)[58]. During the crystallization process, and also during slow melting, isothermal thickening leads to increases in T_m' that are reflected as $\gamma > 1$ in the familiar Hoffman–Weeks T_m' vs. T_x plot.

It is appropriate to interject a comment here on the use of the T_m' vs. T_x plot as a vehicle for estimating T_m. Though originally proposed to explain why the melting point of a polymer depended on the crystallization temperature, the T_m' vs. T_x plot has come to be widely used to estimate T_m. This plot is based on the expression[3,59]

$$T_m' = T_m(1 - 1/\gamma) + T_x/\gamma \tag{7c}$$

where γ is the fractional degree of thickening above l_g^*. Under ideal experimental conditions (constant γ) a plot of T_m' vs. T_x data should yield a nearly straight line at low and moderate ΔT with slope γ^{-1}. (See equation (7d) below for excess curvature induced by δ at large ΔT.) The intercept of this line with the line $T_m' = T_x$ under such conditions can give an estimate of the melting point T_m of a very large extended-chain crystal for the molecular weight under consideration. There are some hazards in using this procedure to estimate T_m, including among others an increased thickening rate which may occur even during the measurement of T_m'—thickening is an activated process that is more rapid the higher the temperature[58]. This effect, as well as others, can indeed (in some instances) lead to failure to obtain a useful T_m. But with care, credible T_m values can often be obtained as in the case of PE to be noted below. It is best to rely provisionally on T_m values from the T_m' vs. T_x plot only if the data for a fixed low degree of crystallinity χ describe a well-defined and relatively long and essentially straight line indicative of a constant γ. If such a line is found, but with a few high T_m' points at the highest growth temperatures, these high T_m' points may be ignored in the extrapolation to obtain T_m provided there is collateral evidence that these high points are a result of increased thickening. In the case of PE, there appears to be a metastable minimum present after the lamellae have about doubled in thickness, which causes γ to hold well for a time at ~2.0 in regime II[60]. The most convincing circumstance is that where a properly executed T_m' vs. $1/l$ plot based on equation (7a) and a T_m' vs. T_x plot based on equation (7c) yield essentially the same T_m. This has been attained in the case of a PE fraction $M_w = 32.1$K—both plots give virtually identical T_m values which, significantly, agree well with the T_m from the Flory–Vrij equation (see Section III.B).

The expression for T_m' carried to higher order yields the term[3]

$$\delta(\Delta h_f)(T_m - T_x)^2/2\gamma\sigma_e T_m \tag{7d}$$

which is to be added to the right-hand side of equation (7c). Thus, the theoretical T_m' vs. T_x line even for constant γ is not absolutely straight. The deviation from linearity is ordinarily quite small at low and moderate ΔT and leads to little error in estimating T_m. However, at large ΔT this term leads to the prediction of a region where T_m' vs. T_x plot is roughly constant for a considerable range of low T_x values. Examples of this effect are known. Of course, extrapolation from this region to the line $T_m' = T_x$ does not lead to a valid T_m.

Though absent in early nucleation-based treatments for lamellar polymers, the quantity δ is clearly essential to the understanding of melting behaviour and, as will be developed below, it plays a major role in crystallization kinetics. We turn now to the calculation of the initial lamellar thickness l_g^* and thence δ.

D. Initial lamellar thickness

The initial lamellar thickness consistent with the mean rate of passage over the barrier shown in *Figure 1b* is

calculated according to

$$\langle l \rangle = l_g^* = \frac{1}{l_u}\int_{2\sigma_e/(\Delta G)}^{\infty} lS(l)\,dl \Big/ \frac{1}{l_u}\int_{2\sigma_e/(\Delta G)}^{\infty} S(l)\,dl \tag{8a}$$

where the values of the rate constants A_0, B, and A to be used for $S(l)$, equation (5a), are the 'low ψ' expressions given as equations (3a), (3b) or (3d), and (3c), respectively. This yields the result

$$l_g^* = \frac{2\sigma_e}{\Delta G} + \frac{kT}{2b_0\sigma}\left[\frac{(\Delta G) + 4\sigma/a_0}{(\Delta G) + 2\sigma/a_0}\right] \tag{8b}$$

where the second term on the right-hand side is the exact expression for δ. Thus, we have the useful relations

$$l_g^* = \frac{2\sigma_e}{\Delta G} + \delta = \frac{2\sigma_e T_m}{(\Delta h_f)(\Delta T)} + \delta \tag{9a}$$

where δ may be approximated at low and moderate undercoolings by

$$\delta \cong kT/b_0\sigma \tag{9b}$$

This treatment of l_g^* does not deal explicitly with fluctuations of fold period during substrate completion. It suffices for the time being to note that such fluctuations lead to an initially rough fold surface, a small temperature dependence of σ_e, and a somewhat larger δ than given in equation (9b)[10]. It is emphasized that l_g^* refers to the *initial* lamellar thickness prior to any significant isothermal thickening. Observe that equations (9) predict no discontinuities in l_g^* at the regime transitions to be discussed subsequently. Note also that the 'low ψ' rate constants employed in calculating l_g^* lead to a δ that does not behave abnormally at low T_x, i.e. there is no 'δ catastrophe'. There is a distribution of lamellar thicknesses[3] about l_g^*. The mean square deviation $\langle (l - l_g^*)^2 \rangle$ comes to $\sim(1/2)(kT/b_0\sigma)^2$ at low undercoolings, which leds to an r.m.s. value of *ca.* 8 Å for PE. This means that an ensemble of unthickened lamellae will have a slightly broadened melting point centering about the T_m' of equation (7b).

The predicted magnitude of l_g^* in equations (8b) or (9) increases the lower the undercooling. On an historical note, it is of interest that many years ago Keller and O'Connor[61], on observing the increase in lamellar thickness of solution-grown PE single crystals with diminishing undercooling, suggested the possibility that the size of a nucleus was at the root of the variation. In retrospect, this must in our view be accorded the status of a correct and significant observation.

From an experimental standpoint, the interlamellar spacing l_{obs} obtained for melt-crystallized PE of moderate molecular weight and high crystallinity by real-time small-angle X-ray scattering (SAXS) is mainly due to l_g^* as given above, but there are two other features in addition to δ that contribute small and approximately constant terms to equations (9) to make up l_{obs}. One of these is a term resulting from the roughness of the chain-folded surface; this is consistent with the Lauritzen–Passaglia (LP) extension[10] of surface nucleation theory that deals with fluctuations of fold period during substrate completion and, depending on details, some or much of it is actually a part of the crystalline core of l_g^* (see later). The other is the presence of a thin amorphous or quasi-amorphous layer resulting from cilia and nonadjacent events, which is not part of the crystalline core. These concepts will be pursued later in this work.

Perhaps the most important observation is that the initial lamellar thickness is determined as in equation (8a) by the net rate of passage over the barrier, i.e. by kinetics. The surface nucleation process is, in effect, in a kinetic snare. If the stems are of length $2\sigma_e/(\Delta G)$, the nucleus remains metastable and its net rate of formation is nil. If the stems involved are rather longer than $2\sigma_e/(\Delta G) + \delta$, the nucleation rate is also very small. The only path out of the trap is to deposit successive stems closely centering around the length $l_g^* = 2\sigma_e/(\Delta G) + \delta$, which then leads to a large and definite rate of surface nucleation. Such nuclei then allow formation of a stable surface layer and thence a thermodynamically stable chain-folded lamella of initial mean thickness l_g^*. As will be brought out in more detail later, multiple nucleation acts on the substrate of length L (as well as another effect related to the energy cost of protruding folds) tend to re-establish the initial lamellar thickness at l_g^* on a practically continuous basis during substrate completion. To this we would add that the increment δ, which confers a suitable degree of stability upon the newly-formed bladelike crystal, will be found to be pervasive in the rate expressions to follow.

E. Substrate completion rate (nucleation theory)

Given the above, one readily calculates the substrate completion rate as shown in *Figure 1* as

$$g \equiv a_0(A - B) \tag{10a}$$

where A and B are given by equations (3c) and (3d), respectively. Thus the substrate completion rate is simply proportional to the net rate of the forward and backward reactions depicted in *Figure 1b*. This yields

$$g = a_0\beta e^{-q/kT}[1 - e^{-a_0b_0\delta(\Delta G)/kT}] \tag{10b}$$

where for the most exact case we would use the δ as in equation (8b). However, one can at low-to-moderate undercoolings expand the exponential and employ $\delta \cong kT/b_0\sigma$ as in equation (9b) to obtain the useful expression

$$g_{nuc.}\,(cm\,s^{-1}) \cong a_0\beta\left[\frac{a_0b_0\delta(\Delta G)}{kT}\right] e^{-q/kT}$$

$$= a_0\beta\left[\frac{a_0(\Delta G)}{\sigma}\right] e^{-q/kT} \tag{11}$$

where the subscript 'nuc.' is added to indicate the origin of the expression. Shortly we shall obtain an expression for g with the help of reptation theory which, when brought into the form of $g_{nuc.}$, will lead to a unified description of β as well as of the substrate completion rate. In the process, we shall evaluate parameters that permit an estimate of the absolute value of g.

Observe that the substrate completion rate is, as to be expected, opposed by the work of chain folding and approaches zero as $T_x \to T_m$ because the driving potential for crystallization $\Delta G \to 0$ at T_m. Note also that the case $\delta = 0$ gives $g_{nuc.} = 0$. The quantity β is in events s^{-1}, σ in erg cm^2, and ΔG in erg cm^{-3}.

F. Reptation in the melt—role in polymer crystallization

It is essential at this juncture to introduce the concept of reptation, which is required to understand the form and magnitude of the retardation factor β. The basic idea

is that in one limit (slow crystallization) the mean force associated with the crystallization process draws a molecule through the reptation tube in the subcooled melt onto the crystal surface (*Figure 1a*). The reptation tube consists of neighbouring molecules in the melt. In the near-ideal steady-state region (which appears in PE) this allows major sections of a given molecule to engage in the chain folding process during substrate completion, even though there may be interruptions resulting from nonadjacent re-entry events or fold formation. Thus, the force of crystallization in effect acts to 'reel in' the chain molecule through the reptation tube onto the growth front. As noted by Frank[62], the concept is rather analogous to taking in hand one end of a strand of spaghetti, whose main section is otherwise entangled in a plateful of like neighbours, pulling on it gently while lightly agitating the plate, and as he said 'I shall have it out within a minute'—meaning soon and easily. We emphasize that our model does *not* require abandoning the idea that a polyethylene bulk melt is an intertwined mass of long molecules, which exhibit the end-to-end distance typical of an unperturbed (theta condition) system as Flory proposed in another connection[63]. The steady-state reptation idea makes it much easier to understand and quantify how a given molecule is pulled out of the highly intertwined system onto the growth front. At no time in our studies have we employed the artifice of assuming pre-existing folded structures in the bulk subcooled melt state as playing a role in polymer crystallization.

There are some important points concerning the reptation idea that need to be highlighted. The first is that the 'curvilinear' or 'lengthwise' diffusion process characteristic of reptation in the melt applies not only near but also well *above* the critical molecular weight M_e where entanglements cause the melt viscosity to change from an $\eta \propto M^1$ to an $\eta \propto M^{3.4}$ law. In brief, the practical point here is that the forced steady-state reptation process under appropriate conditions does not experience impediments from entanglements in the melt such as those that affect the molecular weight dependence of the viscosity. Thus, when a force is exerted on one part of a long molecule (e.g., the force of crystallization f_c), the portion of the molecule remaining in the melt responds in its entirety to that force in the case of slow crystallization and travels through the contour of the reptation tube in the direction demanded by the force. The result is that with a constant average force $\bar{f}_c$ (as for a fixed undercooling ΔT) acting on a dangling chain of $\bar{n}$ $-CH_2-$ units, the crystal growth rate for slow crystallization (regimes I and II) is predicted to vary as $1/\bar{n}$ both well above and somewhat below M_e. (At various places in what follows we shall denote the process just described wherein the force of crystallization draws a pendant chain in a reptation tube in the subcooled melt on to the growth front as involving 'forced reptation' or 'forced steady-state reptation'.) The attribute of being able to minimize the effect of entanglements commends the forced steady-state reptation concept for application in the present case, where almost all the PE fractions to be dealt with here have a molecular weight well in excess of $M_e \cong 3740$, $n_e \cong 267$. It had been argued in the past that the then conventional picture of diffusion in polymer melts (which did not include steady-state reptation or reptation of slack) foreclosed the possibility of any significant degree of adjacent re-entry[64]. In the absence of these reptation concepts, one would indeed encounter difficulties in explaining either the ready formation from the melt of gross structures such as lamellae in PE, or the attendant chain folding.

Another point is that the force of crystallization cannot rapidly undo structures resulting from double or multiple attachment of a long molecule at distant sites in the same or a different lamella; these clearly will increase in number with increasing molecular weight. Accordingly, one cannot expect the forced steady-state reptation concept to apply in unperturbed form above a certain molecular weight where such effects become prevalent. In addition, if the crystallization rate is very high, as in regime III, the forced steady-state reptation process becomes too slow so that eventually only rapid reptation of sections of 'slack' (i.e. 'stored length' toward the end of the reptation tube)[5] can occur. Thus, we may anticipate that the treatment embodying forced steady-state reptation to follow will apply in regimes I and II where the growth rate is relatively slow, and in a range of molecular weights whose upper bound is far above M_e but not so high that multiply-attached long molecules on the growth front impede transport of chain segments to that front on a considerable scale. We shall subsequently identify the undercooling and molecular weight ranges where the aforementioned disturbances of the normal near-ideal forced steady-state reptation mechanism take place in melt-crystallized PE fractions, as well as identify those ranges where reptation of slack prevails.

G. Unified reptation-nucleation theory of substrate completion rate

In dealing with the problem of the retardation factor β involved in steady-state reptation we shall through a conjoining of reptation theory and surface nucleation theory find that it is appropriate to cast β in form

$$\beta = \frac{\kappa}{n}\left(\frac{kT}{h}\right) e^{-Q_D^*/RT} \tag{12}$$

Here kT/h is a frequency factor in events per second, Q_D^* the activation energy for reptation, which is the same as that of centre-of-mass diffusion, n the number of $-(CH_2)-$ units in the chain consistent with the appropriate moment of the molecular weight, and κ a numerical constant that we shall evaluate from a determination of the monomeric friction coefficient as it enters into the rate that a molecule is reeled on to the surface as given by reptation theory. The procedure will directly justify the factor n^{-1} in equation (12). The above expression holds in the Arrhenius range—see later remarks in the vicinity of equation (33d) regarding a shift to a Vogel law at low T_x.

Consider now the reptation approach for calculating g, which is directly related to the reeling rate $\bar{r}$ by the relation $g = \bar{r}(a_0/l_g^*)$—see later for the reason that use of this expression is restricted to regimes I and II. To find $\bar{r}$ requires an evaluation of the force of crystallization and the friction coefficient.

There are two ways of estimating the mean force $\bar{f}_c$ urging the reptating molecule onto the substrate. The first of these, ${}_1\bar{f}_c$, is based on the thermodynamic relation

equation (2a) according to[7,65]

$$ {}_1\bar{f}_c\,(\mathrm{erg\,cm^{-1}}) = \frac{1}{l_g^*}\left[\frac{\mathrm{d}(\Delta\phi_\nu)}{\mathrm{d}\nu}\right] = -\frac{1}{l_g^*}a_0 b_0[l(\Delta G) - 2\sigma_e] $$
$$ = -a_0 b_0(\Delta G)[\delta/l_g^*] \qquad (13) $$

where the substitution $l = 2\sigma_e/(\Delta G) + \delta$ derived previously as equation (9) has been employed. The minus sign signifies that the force is drawing the pendant chain onto the crystal. The result given in equation (13) is simply related to the *net* decrease in free energy on adding a stem with a fold to the substrate and thus represents a 'mean field' approximation. With the simplification that $l_g^* = 2\sigma_e/(\Delta G)$, equation (13) can be cast in the form $-a_0^2 b_0(\Delta G)^2 kT/\sigma q$ showing that ${}_1\bar{f}_c$ diminishes with increasing work of chain folding. The factor δ/l_g^* is the reduction factor in the maximum possible force of crystallization caused by the presence of the chain folds.

The second method of estimating $\bar{f}_c$, denoted ${}_2\bar{f}_c$, uses the concept of a time-average force. It is assumed that no force is exerted during fold formation, the long time required to form the fold being proportional to $(l_f/l_u)\exp(q/kT)$ where l_f is the length of a fold. It is further assumed that the short time involved in subsequently putting down the stem in the rapid zippering down process in the niche is proportional to l_g^*/l_u; during this time the maximum force $-a_0 b_0(\Delta G)$ is exerted. This leads to a reduction factor

$$ \frac{(l_g^*/l_u)}{(l_g^*/l_u) + (l_f/l_u)\exp(q/kT)} \cong (l_g^*/l_f)\,\mathrm{e}^{-q/kT} \qquad (14a) $$

giving the time-average force as[7]

$$ {}_2\bar{f}_c\,(\mathrm{erg\,cm^{-1}}) \cong -a_0 b_0(\Delta G)[(l_g^*/l_f)\,\mathrm{e}^{-q/kT}] \qquad (14b) $$

which holds for $q \geq 3kT$. The force ${}_2\bar{f}_c$ falls off with increasing q, but more rapidly than ${}_1\bar{f}_c$. The reduction factors δ/l_g^* and $(l_g^*/l_f)\exp(-q/kT)$ have virtually identical numerical values for PE in the region of interest, i.e. at the regime I → II transition temperature and do not differ greatly in regime I and the upper part of regime II.

The 'reeling in' rate, denoted as $\bar{r}$ in *Figure 1*, associated with the forced steady-state reptation process is given by[66]

$$ \bar{r}_{\mathrm{rept.}}\,(\mathrm{cm\,s^{-1}}) \equiv \bar{f}_c/\xi = \bar{f}_c/\xi_r n \qquad (15a) $$

Here, ξ is the friction coefficient of the entire chain, ξ_r the monomeric friction coefficient for a $-CH_2-$ unit in erg s cm^{-2} in the melt (or subcooled melt at a specified crystallization temperature T_x), and n the number of $-CH_2-$ units corresponding to the appropriate molecular weight average to be noted shortly for the near-ideal forced steady-state reptation case. (By 'near-ideal' we refer to the case where the molecules are not so long that they frequently form multiple attachments at distant sites on the same or a different growth front and thereby seriously interfere with the reeling process.) Since experiments leading to determination of the monomeric friction coefficient were carried out in the melt state mostly at a reference temperature $T_0 = 449\,\mathrm{K}$ (or corrected thereto), we convert equation (15a) to

$$ \bar{r}_{\mathrm{rept.}} = (\bar{f}_c/\xi_0 n)\,\mathrm{e}^{Q_D^*/RT_0}\,\mathrm{e}^{-Q_D^*/RT_x} \qquad (15b) $$

where ξ_0 is the monomeric friction coefficient at T_0 and Q_D^* the activation energy of the reptation process. Here Q_D^* is identified with the observed activation energy for centre-of-mass diffusion, which is close to 5736 cal mol^{-1} for PE[47]. While in the 'coupling' model[67] the 'primitive' activation energies for self-diffusion and viscosity in the Arrhenius region are the same for PE, the treatment still has the observed activation energy for viscosity being larger than that for diffusion as is found experimentally.

The substrate completion rate for the forced steady-state reptation model is seen from *Figure 1a* to be

$$ g_{\mathrm{rept.}}\,(\mathrm{cm\,s^{-1}}) = \bar{r}_{\mathrm{rept.}}(a_0/l_g^*) $$
$$ = (\bar{f}_c/\xi_0 n)\left[\frac{a_0}{l_g^*}\,\mathrm{e}^{Q_D^*/RT_0}\right]\mathrm{e}^{-Q_D^*/RT_x} \qquad (16) $$

It is emphasized that the steady-state 'reeling in' rate $\bar{r} = g(l_g^*/a_0)$ implied above holds only in regimes I and II. In regime III the 'reeling in' velocity is dominated by the nucleation rate according to $\bar{r}_{III} \cong a_0 i l_g^*$, which causes the onset of reptation of slack when $\bar{r}_{III}$ becomes large because of the high value of i at low T_x in this regime (see Sections III.D and III.H).

It is now a straightforward matter to bring the nucleation and reptation treatments for the substrate completion rate into a unified expression. Equating equation (11) for $g_{\mathrm{nuc.}}$ to equation (16) for $g_{\mathrm{rept.}}$, and utilizing equation (12) for the form of β, one readily finds the unified expression for the substrate completion rate in regimes I and II comes to

$$ g\,(\mathrm{cm\,s^{-1}}) = a_0\frac{\kappa}{n}\left[\frac{kT}{h}\right]\left[\frac{a_0(\Delta G)}{\sigma}\right]\mathrm{e}^{-Q_D^*/RT}\,\mathrm{e}^{-q/kT} \qquad (17) $$

where the number κ is

$$ {}_1\kappa = h\exp(Q_D^*/RT_0)\exp(q/kT)/\xi_0 l_g^{*2} \qquad (18a) $$

for the case ${}_1\bar{f}_c = -a_0 b_0(\Delta G)(\delta/l_g^*)$ and

$$ {}_2\kappa = h\exp(Q_D^*/RT_0)/\xi_0\delta l_f \qquad (18b) $$

for the case where ${}_2\bar{f}_c = -a_0 b_0(\Delta G)(l_g^*/l_f)\exp(-q/kT)$, i.e. for the time-average mean force.

It is seen from equation (17) that a numerical value of κ is needed if one is to estimate the absolute value of the substrate completion rate. This requires an evaluation of the monomeric friction coefficient ξ_0 at T_0. Below we carry out the evaluation of κ for future use. Besides giving the ξ_0 required to evaluate κ above, the method reveals essential details of the forced reptation concept and how it relates to centre-of-mass diffusion.

The diffusion coefficient $D_{\mathrm{rept.}}$, and hence the friction coefficient ξ for reptation for an entire molecule, is linked to the usual centre-of-mass diffusion coefficient D_{CM} by the relation

$$ D_{\mathrm{rept.}} \equiv \frac{kT}{\xi} = \frac{3D_{CM}\mathscr{L}_{\mathrm{tube}}^2}{\langle r^2\rangle} \qquad (19a) $$

Here $\mathscr{L}_{\mathrm{tube}}$ is the length of the reptation tube (which has a diameter larger than the cross-section of a molecule) and $\langle r^2\rangle$ the average square end-to-end distance of the random-coil molecule in the melt. The physical picture here is that as the molecule engages in lengthwise curvilinear diffusion in the reptation tube, which it creates as it tunnels through the random coil melt in such a way as to maintain $\langle r^2\rangle$, the centre-of-mass of the molecule changes accordingly.

Table 2 Melting points and crystallization rates for PE fractions of intermediate molecular weight[a]

Fraction No.	M_n	M_w	M_w/M_n	M_z	$\bar{M}_{nw}$	$\sqrt{M_n M_w}/14 = \bar{n}_{nw}$	$M_z/14 = n_z$	T_m (°C)[b]	$\Delta T_{I\to II}$ (°C)	G_I (cm s^{-1}) at $\Delta T = 14.96$°C	G_{II} (cm s^{-1}) at $\Delta T = 17.96$°C	MW range
1	13.0K	18.1K	1.39	28K	15.34K	**1100**	**2000**	142.43	17.23	1.92×10^{-7}	1.58×10^{-5}	B–B′
2	18.5K	19.8K	1.07	22.3K	19.14K	**1370**	**1590**	142.68	16.48	1.40×10^{-7}	6.73×10^{-6}	B–B′
3	23.0K	24.6K	1.07	27.7K	23.79K	**1700**	**1980**	143.19	16.79	1.77×10^{-7}	9.96×10^{-6}	B–B′
4	25.7K	30.6K	1.19	38.4K	28.0K	**2000**	**2740**	143.61	16.41	1.23×10^{-7}	8.74×10^{-6}	B–B′
5	26.8K	30.0K	1.12	35.4K	28.35K	**2025**	**2520**	143.58	16.18	2.92×10^{-7}	5.99×10^{-6}	B–B′
5′[c]	26.8K	30.0K	1.12	35.4K	28.35K	**2025**	**2520**	143.58	16.18	2.22×10^{-7}	3.68×10^{-6}	B–B′
6	34.2K	37.6K	1.10	43.8K	35.86K	**2560**	**3120**	143.94	16.64	2.49×10^{-7}	3.33×10^{-6}	B–B′
7	34.9K	42.6K	1.22	53.5K	38.56K	**2755**	**3810**	144.11	16.11	1.43×10^{-7}	4.45×10^{-6}	B–B′
8	45.8K	62.8K	1.37	98.6K	53.63K	**3830**	**7030**	144.54	16.14	3.87×10^{-8}	1.43×10^{-6}	C–C′
9	66.4K	74.4K	1.12	86K	70.29K	**5020**	**6130**	144.68	15.88	4.03×10^{-8}	9.48×10^{-7}	C–C′
10	71.4K	115K	1.61	204K	90.61K	**6475**	**14 500**	144.97	16.87	1.27×10^{-8}	7.37×10^{-7}	C–C′

$\overline{\Delta T}_{I\to II} = 16.37 \pm 0.50$°C[d]

[a] For the various molecular weights listed, the symbol K stands for '×1000'. Samples arranged in increasing order of $\bar{n}_{nw} = \sqrt{M_n M_w}/14$

[b] Calculated with Flory–Vrij expression as given numerically in ref. 7 as corrected[75]; value of T_m^0 for $n \to \infty = 145.5$°C = 418.7 K. This expression is:

$$T_m = T_m^0(\mathrm{K})\left[\frac{n - 2.903}{n + 0.565[2.45 + R\ln n - 0.5n(1 - T_m/T_m^0)]}\right]$$

In ref. 7, the numerator in this expression was misprinted as '$n - 2.093$' but the melting points in the table in that paper as well as this one were calculated with the correct expression as give above. This expression closely reproduces the original Flory–Vrij[76] results from $n = 44$ upward, i.e. in the range where the orthorhombic form is that which melts directly to liquid

[c] Total re-run beginning with separate solution crystallization, filtration, vacuum drying, and growth rate steps (HFRL[77])

[d] Average with $\Delta T_{I\to II}$ for sample 1 omitted. Error limit covers all values for fractions 2–10

The value of $\langle r^2 \rangle$ is given by the usual relation

$$\langle r^2 \rangle = C_\infty n l_b^2 \tag{19b}$$

where C_∞ is the characteristic ratio, n the number of $-CH_2-$ units in the chain, and l_b the C–C bond length. In the case of PE, C_∞ is 6.7 and l_b is 1.54×10^{-8} cm. Because the reptation tube has a diameter greater than that of the chain, the tube is shorter than the contour length $\mathscr{L} = nl_b$ of the chain contained therein. Following Klein and Ball[5], we find

$$\mathscr{L}_{\text{tube}} \cong (C_\infty l_b/a) n l_b = 0.344 n l_b \tag{19c}$$

for their assigned tube diameter of $a = 30$ Å. In early work, the reptation tube was approximated as having the same diameter as the molecule and this was rightly criticized[68]. Equation (19c) deals with this point. Now the centre-of-mass diffusion coefficient for PE in the melt is known from tracer and other experiments to vary at a given reference temperature T_0 as

$$D_{CM} = D_0/M^2 = D_0/(14n)^2 \tag{19d}$$

where M is the molecular weight. This variation of D_{CM} as M^{-2} is in accord with an important basic prediction of de Gennes[69]. This law holds for PE (actually hydrogenated-deuterated polybutadiene systems[70]) up to a molecular weight of at least 2×10^5, which is much greater than M_e.

By combining equations (19a) through (19d), and with

$$\xi = \xi_0 n \tag{20a}$$

as assumed in equations (15a) and (15b), one finds that the monomeric friction coefficient ξ_0 for PE comes to

$$\xi_0 = kT/2.70 \times 10^{-4} D_0 \tag{20b}$$

Tracer diffusion measurements by Klein and Briscoe[71] give $D_0 = 0.32\,\text{cm}^2\,\text{s}^{-1}$ at $T_0 = 449$ K and a study by Graessley[72], based on the Doi–Edwards[73] form of reptation theory, yields $D_0 = 0.34\,\text{cm}^2\,\text{s}^{-1}$ corrected to the same reference temperature. With a D_0 of $0.33\,\text{cm}^2\,\text{s}^{-1}$ it is found that

$$\xi_{0(449\,\text{K})} \cong 7.0 \times 10^{-10}\,\text{erg s cm}^{-2} \tag{21}$$

It is a remarkable fact that the tracer diffusion experiments of Klein and Briscoe and the viscoelastic data analysis of Graessley based on the Doi–Edwards approach lead to essentially the same D_0. The reality of tube-like motion for a single fluorescently labelled DNA molecule acting under a force exerted at one end has recently been demonstrated by optical microscopy[74]. This notable work verifies a number of features of reptation theory.

It is now a simple matter to calculate ${}_1\kappa$ and ${}_2\kappa$ for use in equation (17) and thereby permit the estimation of the absolute substrate completion rate. The κ to be calculated is for use for melt-crystallized PE specimens in the intermediate molecular weight range such as those listed in *Table 2*, which exhibit clear-cut regime I → II transitions. (The origin and analysis of the data in this table will be given later.) We first find ${}_1\kappa$ at $T \cong 400.4$ K, the nominal temperature of the regime I → II transition. The value of Q_D^* is 5736 cal mol^{-1} and q is 4900 cal mol^{-1} (*Table 1*). With equation (9) with $T_m = 143.61$°C as for fraction 4 in *Table 2*, and $\sigma_e = 90\,\text{erg cm}^{-2}$, $\sigma = 11.8$ erg cm^{-2}, and $\Delta h_f = 2.8 \times 10^9\,\text{erg cm}^{-3}$ from *Table 1*, l_g^* is found to be $\sim 175 \times 10^{-8}$ cm. Then, with ξ_0 from equation (21) and $T_0 = 449$ K, it is found that ${}_1\kappa = 0.91$. A closer estimate is obtained by noting that the 'rough fold surface' version of l_g^* to be mentioned later adds ~10–15 Å to equation (9) giving $l_g^* \simeq 190$ Å. This yields

$${}_1\kappa \simeq 0.77 \tag{22}$$

For ${}_2\kappa$ one needs an estimate for the length of a fold. If we use the estimate that a sharp fold contains 5 bonds giving $l_f = 6.36 \times 10^{-8}$ cm, then, with $\delta = 10.27 \times 10^{-8}$ cm as given by equation (8b) (exact form) for ΔG based on $T_m = 416.81$ K and $\Delta T = 16.37°$ and the $\xi_{0(449\,\text{K})}$ just cited, one finds ${}_2\kappa \simeq 0.91$. With the perhaps more realistic use of six bonds for l_f, the result comes to

$${}_2\kappa \simeq 0.76 \tag{23}$$

We shall employ the κ of 0.77 in calculation of the substrate completion rate to be given in Section III. The values of ξ_0 and κ are entered in *Table 3*, where important results are gathered.

It remains to indicate what the near-ideal steady-state forced reptation approach implies about the molecular weight averages that correspond to the n in equation (17) and other expressions such as equation (12). The question concerning the proper moment of the molecular weight to employ with the reptation concept was posed by Phillips in a recent review[80]. It has been shown that the time $t_{\text{rept.}}$ required to pull in a specific chain of length $l_u n$ is given by[7,65,81]

$$t_{\text{rept.}} = \frac{1}{2}\left(\frac{l_u n}{\bar{r}_{\text{rept.}}}\right) = \text{const.} \times n^2 \tag{24a}$$

Thus, for a constant average force, it takes four times longer to reel in a molecule of length $2l_u n$ than one of length $l_u n$. Equation (24a) provides the necessary clue concerning what happens when a distribution of chain lengths is available, as in even a good fraction. The above expression leads to a mean reptation time $\bar{t}_{\text{rept.}}$ that is proportional to the square of the molecular weight according to[82]

$$\bar{t}_{\text{rept.}} \propto \frac{\sum N_i M_i^2}{\sum N_i} = \frac{\sum N_i M_i}{\sum N_i} \times \frac{\sum N_i M_i^2}{\sum N_i M_i} = M_n \times M_w \tag{24b}$$

It follows that the 'n' in equation (24a), and hence in equations (12) and (17), is proportional to $\bar{n}_{nw} = (M_n M_w)^{1/2}/14 = \bar{M}_{nw}/14$.

The following argument will bring out the fact that $\bar{n}_{nw}$ is in addition to be multiplied by 2/3. We begin by assuming that during the substrate completion process, each new molecule of length nl_u initially attaches to a niche toward one of its ends giving one quite short cilium and one considerably longer pendant chain of length $nl_u - l_g^*$ or $\sim nl_u$ for the case $nl_u \gg l_g^*$. This type of initial attachment, illustrated in *Figures 2b* and *c*, minimizes the free energy associated with this 'short cilium–long pendant chain' system (Section V.B). Given a pendant chain of initial length of $\sim nl_u$ that is to be drawn on to the substrate, it is readily found that its mean length averaged over its lifetime, which ends when its length is zero, is

$$\langle nl_u \rangle = l_u \times \int_n^0 n^2\,dn \Big/ \int_n^0 n\,dn = (2/3) n l_u \tag{24c}$$

The factor of 2/3 arises from the fact that the 'reeling in' rate is slower while the pendant chain is long—the

Table 3 Summary of numerical results for fractions of intermediate molecular weight, range B–B′

1.	*Reptation*	*Quantity*	*Value*
	ξ_0	monomeric friction coefficient for reptation in PE at 449K	7.0×10^{-10} erg s cm^{-2}
	κ	numerical constant in equation (12) for retardation factor β	0.77

2. *P_{tf}, lower bound for degree of tight folding, calc. from equation (36); also observed angles of tilt θ*

P_{tf} (lower bound)	Angle of tilt	Observed values of θ[a]
0.657	0.0°	Not found
0.637	19.0°	Low to moderate MW, regime I[78]
0.581	35.0°	Frequent at moderate MW, regimes I, II, and upper part of III
0.514	45.0°	Moderate MW, hard quench to regime III[79]
0	69.9°	Not found

3. *Surface nucleation and related parameters (regimes I and II)*

	MW range B–B′	
C_I, pre-exponential constant for regime I growth	$2.10 \pm 0.72 \times 10^{13}$ cm s^{-1}	
C_{II}, pre-exponential constant for regime II growth	$7.267 \pm 2.530 \times 10^{6}$ cm s^{-1}	
C_0, configurational path degeneracy	4.408×10^5	
n_L, number of stems of width a_0 in substrate length L	Predicted from kinetics Equation (40)	Experimental (D_{110} from X-ray line widths)
	190 within a factor of ~1.5	85.7 and 158.2
L, substrate length, regime I (from kinetics)	865 within a factor of ~1.5	390 Å and 720 Å
$\Delta T_{cut\ off}$, undercooling below which regime I theory is inapplicable	~9.7°C	

4. *Surface nucleation and related parameters (regime III)*

	for $S_\kappa/a_0 = 2$	for $S_\kappa/a_0 = 2.5$
C_{III}, pre-exponential factor for regime III	2.326×10^{11} cm s^{-1}	2.88×10^{11} cm s^{-1}
$\Delta T_{II \to III}$, predicted undercooling at onset of regime III	23.4°C	22.9°
	Calc. by equation (46) $S_\kappa/a_0 = 2.0$	Observed (Barham)
G_{III}, growth rate in regime III at 90°C, $n = 2000$	3.4 cm s^{-1}	~3.5 cm s^{-1}
G_{III}, growth rate in regime III at 100°C, $n = 2000$	0.61 cm s^{-1}	~0.55 cm s^{-1}

5. *Estimated degree of adjacency and tight folding at $M \sim 40$K, melt crystallized PE*

	P_{ar}	P_{tf}
Regime I	~0.66	~0.8
Regime III	0.3–0.4	0.51–0.58 depending on angle of tilt

[a] Observed angle of tilt θ intended to reflect that present in interior of a melt-crystallized specimen for the molecular weight and regime noted

overall friction coefficient decreases as the chain gets shorter so that the pendant chain accelerates as it is drawn onto the substrate. It is evident from the above that for the near-ideal steady-state forced reptation process in PE, the 'n' in equation (12) for β and equation (17) for g subject to the approximations noted is

$$n = (2/3)\bar{n}_{nw} = (2/3)(M_n M_w)^{1/2}/14 = (2/3)\bar{M}_{nw}/14 \quad (25)$$

The form of n given in equation (25) for near-ideal forced reptation applies in regimes I and II in the part of the intermediate range denoted B–B′ in *Table 2*. Here the crystallinity is high, indicative of a minimal degree of multiple attachments of a chain at widely separated sites. In the part of the intermediate range denoted C–C′ in *Table 2* an incipient fall in the crystallinity and growth rate indicates an increasing presence of multiple attachments, which leads to 'perturbed' forced reptation. Here, n in equations (12) and (17) is related to M_z (see Section III.E). At still higher molecular weights (range D–D′), the regime I → II transition becomes diffuse and disappears, the degree of crystallinity is in a steep decline, and a definite change occurs in spherulite morphology. These phenomena will be brought out after the actual growth rate, degree of crystallinity, and morphological results for the PE fractions are introduced in Section III.

H. Growth rates in regimes I, II, and III

It is now possible to set down the growth rate expressions for regimes I, II, and III with the exponential and pre-exponential factors appropriate to each. The basic premise underlying the treatment of regimes I and II is that there is a relatively short and molecularly generally flat and continuous substrate length L [as shown in *Figure 3* and already noted in equation (5d)] that is naturally present on the {1 1 0} growing face of the crystal. In *Figure 3*, this length is depicted for convenience as being terminated on either end by a 'stopping' defect. Alternatively, one may prefer to think of L as reflecting a 'domain' or 'grain' size in the body of the crystal that makes itself felt on the {1 1 0}-type growth front. In special situations, the actual {1 1 0} growth tip in regime I could be very small and approach dimensions on the order of L. This apparently occurs in

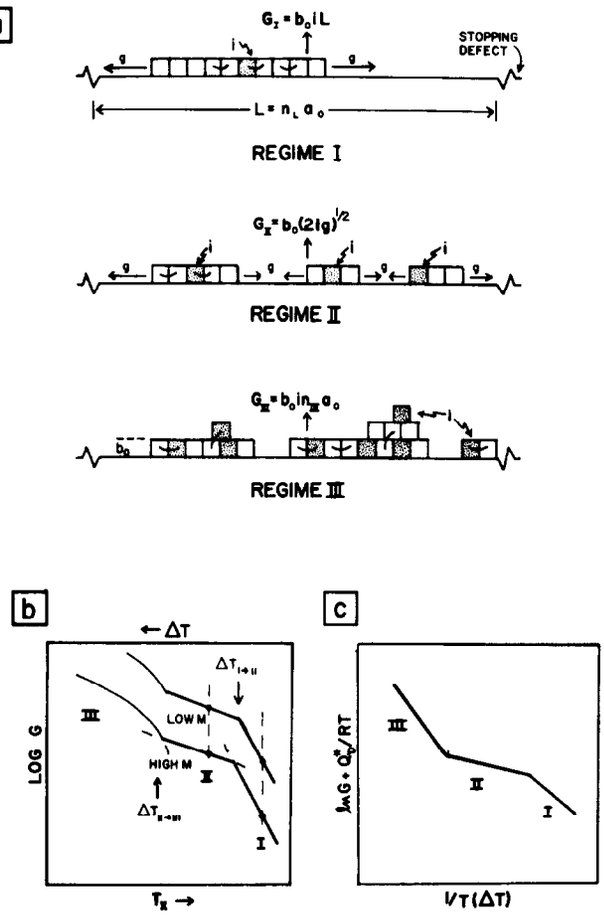

Figure 3 *Regimes I, II, and III.* (a) Regime I: one surface nucleus injected at rate i (shaded) leads to complete filling of substrate of length L at rate g creating layer of thickness b_0 and leading to growth rate G_I. Regime II: multiple nucleation at rate i on substrate (shaded stems) combined with substrate completion at rate g completes new layer leading to growth rate G_{II}. Regime III: layer addition governed mainly by injection of stems at rate i leading to growth rate G_{III}. (b) Schematic of predicted growth rate G as a function of isothermal crystallization temperature T_x for two molecular weights. (c) Schematic plot of $\ln G + Q_D^*/RT$ vs. $1/T(\Delta T)$ of the type employed to determine K_g showing predicted change of slope of factor of 2 accompanying regime I → II and II → III growth rate transitions

the case of melt-crystallized PE, but not in solution-grown PE single crystals (see below).

It is clear that L must be quite small—it is difficult to envision that the face of a polymer crystal is such that a single nucleus could cause the substrate completion process to propagate without hindrance over a distance of many micrometres. Moreover, the assumption of a small value for L avoids the incorrect prediction of accelerated nonlineal growth in regime I; such an effect is not observed even for very small crystals. We shall later estimate from an analysis of the growth rates that L at the regime I → II rate transition is within a factor of about 1.5 of 865 Å in PE fractions.

In melt-crystallized PE, for special reasons to be noted in Section III, the actual physical size of the overall macroscopic {1 1 0}-type growth front falls somewhat with increasing T_x in regime II, and then rather abruptly attains a small value (apparently as low as the order of L itself for the 'leading' lamellae) in the immediate vicinity of the regime II → I growth rate transition when regime I is entered. Experiments by Toda[27] have shown that there is a change in crystal type (truncated lozenge) → (symmetrical lenticular crystal) at the growth rate transition, the regime I lenticular crystal having the very small {1 1 0} growth front. This transformation of crystal type is evidently associated[27] with the well-known change of gross morphology[77] (spherulitic) → (axialitic) that occurs in the immediate vicinity of the II → I rate transition in the crystallization from the subcooled melt for PE fractions. (For future reference we note that screw dislocations can arise in the symmetrical lenticular crystals with very fine growth tips referred to above which lead to asymmetrical 'lenticular' crystals[25] that likely play a role in generating an active front for the 'leading' lamellae for regime I growth in the subcooled melt.) The change of crystal type in melt-crystallized PE proximate to the II → I transition does not necessarily define a universal pattern, since polymers in general do not always appear to exhibit an abrupt change of crystal type at regime transitions. Following up on the latter point, it is important to note that the regime I → II rate transition observed by Organ and Keller in solution-grown PE single crystals is *not* accompanied by a change of crystal type, the crystals in both regimes being elongated truncated lozenges with macroscopic {1 1 0}-type growth fronts and curved {2 0 0} edges at all T_x including regime I[32,83]. Here the regime I → II rate transition (which is associated with the {1 1 0} front) is clearly apparent in $\ln G$ vs. $1/T(\Delta T)$ plots with a slope change close to 2 just as it is in the case of melt-crystallized PE (Section III.B).

The treatment to follow deals directly with the more general situation where there is no change of crystal type in the T_x range considered, and where a macroscopic {1 1 0}-type growth front divided into sections of mean length L is assumed to be present in both regimes I and II. The results are readily adapted to the melt-crystallized PE problem. In no case can the existence of regime I and the I → II rate transition, as manifested in growth rate studies, be predicted without introducing the concept of a small substrate of length L. In general, we take the I → II growth rate transition to be associated with single nucleation on a substrate of length L in regime I and multiple nucleation on L in regime II—a change of crystal type alone can hardly provide a general basis for a slope change of 2 in plots of $\ln G + Q_D^*/RT$ vs. $1/T(\Delta T)$. In his treatment of the subject, Frank[84] suggested that the substrate length L might be associated with the range of lattice coherence. Our results will support this suggestion.

It is important to bear in mind that we hold that *the substrate length L is a natural physical property of the underlying chain-folded crystal and not an artifact of nucleation theory*. We would at the same time emphasize another point. A macroscopically observable '1 1 0' growth front (such as may appear on a scale of microns in an electron micrograph) need not be flat and straight over its entirety to justify the existence of L; it is only required that this much larger growth front be broken up (by 'stopping defects' in our terminology) into a set of smaller and crystallographically coherent sections each of mean length L. Calculations by Mansfield and Klushin[85] employing the Eden model of crystal growth by surface nucleation show that both the regime I and regime II effects can occur in systems where the growth face is not only slightly rough on a macroscopic scale but also slightly curved. In fact, the presence of such roughness and curvature on a macroscopic scale does not

preclude the use of surface nucleation theory to predict all three regimes[85]. This work counters the occasional misconception that the existence of regime I growth is questionable or even impossible because the observed growth front is slightly curved and slightly rough on a macroscopic scale.

In regime I, which occurs at high growth temperatures where the surface nucleation rate i is low, one primary nucleus is sufficient to cause, through subsequent rapid addition of stems at a rate g, the completion of the substrate of length L, thus adding to the crystal a new layer of thickness b_0 (*Figure 3a*). Here, $G_I \propto i$. In regime II, which occurs at lower growth temperatures where the surface nucleation rate is higher, numerous primary nuclei occur on the substrate of length L so that the surface is somewhat rough on a molecular scale, as noted by Lauritzen in his treatment of the subject[86], and the different growth rate law $G_{II} \propto (2ig)^{1/2}$ prevails (*Figure 3a*). Thus, in regime II, $G_{II} \propto i^{1/2}$. Our treatment of regimes I and II is arranged in such a way as to allow a reasonably accurate value of L to be estimated from observed growth rate data for the PE fractions listed in *Table 2*. We note here that the melting points given in *Table 2* are based on a numerical form of the Flory–Vrij equation[76] devised by Miller[7] as corrected[75]. The numerical expression is given as a footnote to the table.

The growth rate in regime I is given by

$$G_I\,(\mathrm{cm\,s^{-1}}) \equiv b_0 iL = b_0 i(n_L a_0) \tag{26}$$

which, with equations (6) and (12), gives the working expression

$$G_I = \left(\frac{C_I}{n}\right) e^{-Q_D^*/RT}\, e^{-K_{g(I)}/T(\Delta T)} \tag{27a}$$

where

$$C_I = C_0 \kappa n_L \left[\frac{b_0 kT}{h}\right]\left[\frac{kTa_0(\Delta G)}{4b_0 l_u \sigma^2}\right] \tag{27b}$$

and

$$K_{g(I)} = \frac{[4]b_0\sigma\sigma_e T_m}{\Delta h_f k} \tag{27c}$$

In the near-ideal forced reptation region, n in equation (27a) is $(2/3)\bar{n}_{nw}$ as from equation (25). In the perturbed region, n is proportional to n_z as determined empirically (see Section III.H). Both $K_{g(I)}$ and C_I can be determined by experiment, as can $K_{g(II)}$ and C_{II} to be given below.

In regime II, where numerous nuclei are put down on the substrate of length L, the observable growth rate is defined as

$$G_{II} \equiv b_0(2ig)^{1/2} \tag{28}$$

With equations (6), (11), and (12) one obtains

$$G_{II} = \left(\frac{C_{II}}{n}\right) e^{-Q_D^*/RT}\, e^{-K_{g(II)}/T(\Delta T)} \tag{29a}$$

where the pre-exponential factor is

$$C_{II} = C_0^{1/2}\kappa\left(\frac{b_0 kT}{h}\right)\left(\frac{a_0(\Delta G)}{\sigma}\right)\left(\frac{kT}{2b_0\sigma l_u}\right)^{1/2} e^{-q/2kT} \tag{29b}$$

and

$$K_{g(II)} = \frac{[2]b_0\sigma\sigma_e T_m}{\Delta h_f k} \tag{29c}$$

The nature of n in equation (29a) is the same as that described for regime I.

Observe that $2K_{g(II)} = K_{g(I)}$; this leads to the change of slope of close to a factor of 2 in plots of $\ln G + Q_D^*/RT$ vs. $1/T(\Delta T)$ at the regime I → II rate transition which are employed to determine $K_{g(I)}$ and $K_{g(II)}$ from growth rate data. The nature of this plot is shown schematically in *Figure 3c*. That $2K_{g(II)}$ is equal to $K_{g(I)}$ derives fundamentally from the scaling laws $G_I \propto i$ and $G_{II} \propto i^{1/2}$ inherent in equations (26) and (28), the latter being based on g having only a weak variation with T_x compared with that of i as will subsequently be shown to be the case. These scaling laws for G_I and G_{II} as a function of i for lamellar systems were noted in early times by Sanchez and DiMarzio[51], Lauritzen[86], Lauritzen and Hoffman[50], and Frank[84].

Equations (26) and (28) are well-known solutions of the Seto–Frank[84,87] differential equations for a nominally flat surface exhibiting nucleation and substrate completion on a substrate of length L. Mansfield[88] has recently given comments on what is meant by 'flat' in the derivation of equation (28) and has also remarked on the origin of the mean separation of nucleation sites $(2g/i)^{1/2}$, which we later denote S_k. Mansfield also dispels the misunderstandings that in some cases attend the special solutions of the Seto–Frank equations for moving boundary conditions that have to do with curved {2 0 0} edges.

Entirely apart from experimental difficulties connected with very slow growth at high T_x, regime I and the I → II transition may fail to appear in a number of situations. As will be discussed, this failure occurs in PE at high molecular weight because multiple attachment events force the system from steady-state reptation into reptation of slack, thereby causing regime I and II behaviour to be replaced by regime III-A—see Section IV. More generally, if some inherent feature of a polymer chain (e.g. a large side group or hydrogen bonding) strongly inhibits steady-state reptation with the result that reptation of slack dominates the transport mechanism, regime III-A crystallization, where $G \propto i$, may in one limit prevail over the entire T_x range where growth rates can be measured. Notwithstanding these points, there is no doubt about the existence of regime I growth and the I → II transition in melt-crystallized PE fractions of intermediate molecular weight (see Section III).

In regime I and the main body of regime II, the majority of the stems are added to the crystal during the substrate completion process. As will be noted shortly, this situation changes as regime III is entered. In regime III almost every other stem is injected onto the substrate at the rate i, and this replaces the concept of 'substrate completion' in the sense of g in equations (16), (17), and (28).

By eliminating C_0 from equations (27b) and (29b), one finds

$$n_L = 2\kappa\left(\frac{b_0 kT}{h}\right)\left(\frac{a_0(\Delta G)}{\sigma}\right)\left(\frac{C_I}{C_{II}^2}\right) e^{-q/kT} \tag{30}$$

Thus, with κ being known as described previously, and given experimental values of C_I and C_{II} from growth rate data on the PE fractions, one can estimate the substrate length L through the relation $L = n_L a_0$. Note that equation (30) is valid only at the regime I → II transition. With κ being known within reasonable limits, it will also prove to be possible to estimate the

configurational path degeneracy C_0. As will be shown later, the value of C_0 is key to predicting the onset temperature for regime III.

There remains one point concerning the applicability of the regime I concept at very low undercoolings that requires attention. By setting the thermodynamic expression for $\Delta\phi_\nu$ [equation (2)] equal to zero and letting l in this expression be $l = l_g^* - 2\sigma_e/(\Delta G) + \delta$ (with $\Delta G \cong \Delta h_f(\Delta T)/T_m$), one readily derives the expression for ν_s, the number of stems required to form a just stable surface nucleus: see *Figure 1*. The result is

$$\nu_s = \frac{4\sigma\sigma_e}{a_0\delta(\Delta G)^2} - \frac{2}{\Delta G}\left[\frac{\sigma_e}{\delta} - \frac{\sigma}{a_0}\right]$$

$$\cong \frac{4\sigma\sigma_e T_m^2}{a_0\delta(\Delta h_f)^2(\Delta T)^2} - \frac{2T_m}{\Delta h_f(\Delta T)}\left[\frac{\sigma_e}{\delta} - \frac{\sigma}{a_0}\right] \quad (31)$$

with the understanding that δ is given by $kT/b_0\sigma$ as in equation (8b), or more precisely as in equation (7b). The point here is that n_L should be equal to or larger than ν_s for the 'leading' lamellar for regime I growth to occur at a normal rate. The condition $n_L \geq \nu_s$ is evidently fulfilled in the case of the PE data to be treated subsequently, even at the lowest undercoolings employed. We mention this because a claim has been made[89,90] to the effect that regime I theory is generally invalid because $n_L < \nu_s$. This assertion was refuted[91]; we shall subsequently return to this issue in numerical terms in Section III.D. If for some reason the actual {1 1 0} growth tip in some of the crystals is smaller than the range of lattice coherence $L = n_L a_0$, regime I growth with its typical $G_I \propto \exp(-K_{g(I)})/T(\Delta T)$ behaviour will still occur, but with a reduced absolute growth rate because of the smaller effective substrate length. These slower growing lamellae with the {1 1 0} growth front of reduced size can attain stability by developing a somewhat larger than normal δ.

We turn now to the prediction of regime III, which is a natural result of the nucleation model shown in *Figures 1* and *3*. The transition from regime II to regime III occurs at large undercoolings where the surface nucleation rate has become so high that the mean gap distance between the surface nuclei (which are injected at the rate i) is on the order of the width a_0 of a molecule. As noted, in this situation the normal substrate completion process is in effect replaced by the surface nucleation act itself, so the growth rate follows the relationship $G_{III} \propto i$. Thus, the form of the growth rate in regime III will be similar to that of regime I, but with a smaller pre-exponential factor. In regime III, the growth face is quite rough on a local scale.

The theory to follow is based generally on an earlier treatment given in 1983[4] but is more complete. There was recognition as early as 1979 of the existence of regime III and the II → III transition in polymers—see the work of Phillips[92] and also that of one of the authors[66,93]. Even prior to this, Sanchez noted in a review[94] that G would vary as i at very high nucleation rates rather than i to some lower power at lesser rates. Though not pursued further at the time, this may be regarded as a preliminary hint of the existence of a II → III type of transition.

The growth rate in regime III is defined[4] according to

$$G_{III}\,(\text{cm s}^{-1}) \equiv b_0 i(n_{III} a_0) \quad (32)$$

where n_{III} is a number on the order of 2.0–2.5. For the case of single stems with no folds, a simulation by Guttman and DiMarzio[95] gave n_{III} as ~1.5 at the onset of regime III. For PE, where a substantial fraction of 'tight' folds must occur even in regime III because of the Gambler's Ruin topological requirements, n_{III} can be estimated to be ~2.0–2.5 (see later). Then, with equation (6) for i and equation (12) for β, one has

$$G_{III} = \left(\frac{C_{III}}{n}\right) e^{-Q_D^*/RT}\, e^{-K_{g(III)}/T(\Delta T)} \quad (33a)$$

in which the pre-exponential factor is

$$C_{III} = C_0 \kappa n_{III}\left(\frac{b_0 kT}{h}\right)\left(\frac{kTa_0(\Delta G)}{4b_0 l_u \sigma^2}\right) \quad (33b)$$

and the exponent

$$K_{g(III)} \cong K_{g(I)} = \frac{[4]b_0\sigma\sigma_e T_m}{(\Delta h_f)k} \quad (33c)$$

A slope change of 2 is predicted at the II → III transition in plots involving $\ln G + Q_D^*/RT$ vs. $1/T(\Delta T)$, which is in the opposite sense to that predicted for the I → II transition (*Figure 3c*). The main difference between regimes I and III resides in the pre-exponential factors C_I and C_{III}, the former being proportional to n_L, which is about 190 for PE, and the latter being proportional to n_{III} which is ~2.0–2.5.

The form of n in equation (33a) is to be provisionally taken as equal to $(2/3)\bar{n}_{nw}$ at $T_{II\to III}$, $\Delta T_{II\to III}$ if the crystallization in regime II is in range B–B′ and $(2/3)n_z$ if it is in the molecular weight range C–C′.

The steady-state forced reptation of the near-ideal (B–B′) or perturbed (C–C′) type cannot be expected to persist throughout regime III. Instead, it is to be anticipated because of the very high surface nucleation rate that the transport process will soon begin to utilize reptation of the 'slack' near the end of the reptation tube, a clever idea introduced into crystallization theory by Klein and Ball[5]. Then the n in equation (33a) will ultimately become n_{slack} which represents the number of $-CH_2-$ units in the effective slack length; the latter is expected to correspond approximately to the contour length of a coiled chain between entanglements in that part of the reptation tube near the substrate. Since the limiting value of n_{slack} will not depend markedly on the remaining length of the pendant molecule, the growth rate in regime III at a sufficiently large fixed undercooling will tend to vary but little with molecular weight. A treatment of the reeling rate associated with reptation of slack deep in regime III is given in Section III.H.

It is of interest to mention that at crystallization temperatures near and below about $T_g + 100°$, where T_g is the glass transition temperature, the factor $\exp(-Q_D^*/RT)$ in equation (33a) is to be replaced by $\exp[-U^*/R(T - T_\infty)]$ on an empirical basis, i.e. a shift from Arrhenius to 'Vogel' behaviour[3]. Then one has the general form useful below a nominal temperature of about $T_g + 100°$

$$G = G_0\, e^{-U^*/R(T-T_\infty)}\, e^{-K_g/T(\Delta T)f} \quad (33d)$$

where $f \cong 2T/(T_m + T)$, the latter accounting for effects arising from the fall in the heat of fusion. Use of this expression above $T_g + 100°$ ordinarily leads to acceptable estimates of K_g, and is convenient and often employed to good effect if Q_D^* is not known, but is not as accurate there as equations (27a), (29a), or (33a),

especially if Q_D^* is known. Equation (33d) often allows an excellent description of the growth rates at low temperatures, i.e. below the maximum that occurs in the growth rate[3]. The U^* and T_∞ of equation (33d) do not in our view correspond to those relevant to viscosity. The treatment outlined here implies that they are instead associated with forced reptational diffusion, including reptation of slack at low T_x. The forms of equations (27a), (29a), and (33a) with exp $(-Q_D^*/RT)$ are appropriate for melt-crystallized PE in regimes I and II and the upper part of regime III at all growth temperatures to be encountered in the analysis to be given later, since the T_x employed are far above $T_g + 100°$ where the Arrhenius form applies. Fortunately, Q_D^* for PE is known from independent studies (*Table 1*).

The onset of regime III is governed by the mean distance between primary nucleation sites. This is given by the relation

$$S_k = (2g/i)^{1/2} \tag{34}$$

With equations (6), (12), and (17) there is obtained the ratio

$$\frac{S_k}{a_0} = \left[\frac{8b_0 l_u \sigma}{kT}\right]^{1/2} \left(\frac{1}{C_0^{1/2}}\right) e^{-q/2kT} e^{K_{g(II)}/T(\Delta T)} \tag{35}$$

where a_0 is the width of one stem. The regime II $\rightarrow$ III transition occurs at the undercooling $\Delta T_{II \rightarrow III}$ where S_k/a_0 takes on a value of $n_{III} \cong 2.0$–2.5 stem widths. At the regime I $\rightarrow$ II transition where $G_I = G_{II}$, equation (34) gives $S_k/a_0 = n_L$ as required by the defining relations given in equations (26) and (28) for regimes I and II. A plot of S_k/a_0 vs. undercooling ΔT showing the onset of regime III will be given subsequently for PE, based on the C_0 value obtained from an analysis of regimes I and II. Equation (35) is more exact than that given[4] (see also refs 66 and 93) in the original theory for regime III.

The overall relationship between the regimes is shown in schematic plots of $\log G$ vs. T_x and of $\ln G + Q_D^*/RT$ vs $1/T(\Delta T)$ in *Figures 3b* and *c*.

There are some special features of regime III crystallization that require to be noted. Crystallization in this regime has both technical and scientific importance. From a technical standpoint, this is true because in processing, PE is frequently in effect 'quench-crystallized' which definitely invites crystallization in regime III. From a scientific viewpoint, the importance of regime III stems largely from the fact that neutron scattering and i.r. spectroscopic studies aimed at uncovering the chain morphology ('molecular trajectory') of melt-crystallized PE were carried out using PEH–PED mixtures which were of necessity crystallized as thin specimens that were cooled in air or by quenching—this again invites regime III crystallization. (Here PED means perdeuteropolyethylene and PEH refers to the ordinary protonated polymer.) The reason that this type of procedure had to be used was that PEH and PED molecules tend to segregate during slow crystallization as in regime I—thus rapid crystallization in regime III was the only route available to obtain specimens for study that exhibited minimum segregation. The segregation effect prevents the determination by neutron scattering of molecular trajectories for PEH–PED specimens crystallized from the subcooled melt in regime I or II. (The origin of the segregation effect was explained by Bates, Keith, and McWhan[96] as being a result of quite different melting points for PEH and PED caused by their differing molecular volumes and unequal molecular polarizabilities; an effort to eliminate the melting point difference and, thus, the segregation effect by the use of partly deuterated chains was not successful for specimens slow-cooled from the melt[97]. As will be noted shortly, problems involving segregation effects for PEH–PED single crystals formed from dilute solution well in regime II are mitigated to an extent that allows molecular trajectories to be determined[98].) Accordingly, the neutron scattering studies on specimens formed from the subcooled melt reflected the molecular morphology characteristic of regime III, which is clearly more disorganized than that of regimes II or I. We shall return to this point and show that kinetic data imply the presence of a relatively high degree of adjacency in PE fractions of moderate molecular weight crystallized from the melt in regime I, whereas the neutron scattering and i.r. studies for comparable molecular weights suggest considerably poorer adjacency for PE specimens crystallized in regime III (see Section VI).

One of the most interesting features of regime III is that, unlike regimes I and II, it has been predicted that deposition of stems with space filling can only occur if more than one lattice plane is involved. This was uncovered by Guttman and DiMarzio in their modelling of regimes I, II, and III behaviour by Monte Carlo techniques using a 'bricklayer' model[95]. It follows that more than one type of chain fold may well be present in PE crystallized in regime III as is shown schematically in *Figure 3a*. Accordingly, one might expect $K_{g(III)}$ to differ slightly from $K_{g(I)}$ or $2K_{g(II)}$.

The foregoing treatment refers to regime III as it would result from crystallization at large undercoolings in the intermediate molecular weight ranges B–B′ and C–C′, where interferences with the steady-state reptation process caused by multiple attachments of a molecule at the growth front are not severe. Here, regimes I, II, and III appear in succession with lowering T_x as in *Figure 3b*. There is another circumstance that can promote a tendency toward regime III-like growth. The main molecular characteristics of regime III growth are a very short 'substrate run'—not more than a few stems—and a transport mechanism that involves reptation of slack; when these features apply, one will approach the condition $G_{III} \propto i$. Thus, if some agency, such as chemical crosslinking or multiple attachments by a long molecule at separated sites on the growth front at high molecular weights, forces the substrate completion process to involve reptation of slack, a tendency toward a regime III-type of behaviour (denoted regime III-A) is to be anticipated. This begins to occur in PE as 'mixed' regime behaviour over a considerable range of undercooling at high molecular weights in range D–D′ and culminates in close to ideal regime III-A behaviour at ultra-high molecular weights in range E–E′. These effects, together with those of chemical crosslinking, are discussed in Section IV.

At this juncture it is useful to reflect on why, in the absence of significant isothermal thickening which involves longitudinal translation of crystalline stems, a new substrate layer will tend to maintain itself at a thickness close to l_g^* during its formation. In regime III (large ΔT) and in the main part of regime II (moderate

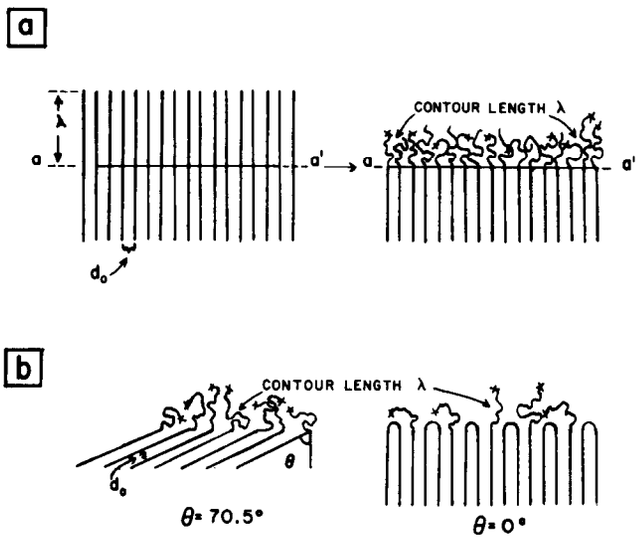

Figure 4 *The density anomaly and its resolution.* (a) Melting of an extended-chain crystal along plane a–a′ showing density anomaly for random coils at lamellar surface. (b) Resolution: tilting either by angle $\theta = 70.5°$ with no folding, or folding back two out of three stems for case $\theta = 0°$ removes the density anomaly. Actual PE lamellae exhibit angles of tilt between 19° and 45°, requiring substantial degree of 'tight' folding during crystallization to prevent the anomaly. See Gambler's Ruin expression, equation (36), and *Table 3.2*. The 'fringed-micelle' model and the random re-entry 'switchboard' model are eliminated for well-formed lamellae of large lateral extent by topological constraints

ΔT), multiple nucleation acts occur on the substrate of length L thus repeatedly re-establishing the initial lamellar thickness very near to l_g^* at close intervals. In regime I (low ΔT) only a single nucleus is involved in the length L, but here the LP fluctuation theory[10] shows that protruding folds incur an energy cost that tends to maintain the lamellar thickness close to l_g^* during substrate completion (Section III.J). In melt-crystallized PE, the induction period for the initial onset of isothermal thickening is longer the higher T_x, but once begun the thickening rate, which goes as $K \log t$ for a considerable residence time t, is higher with increasing T_x. Single PE crystals formed in dilute solution do not normally exhibit isothermal thickening at T_x.

I. The topological lower bound on the degree of tight folding and adjacent re-entry: also estimate of n_{III}

In dealing with the problem of chain folding in melt-crystallized lamellar PE it is essential to understand that there is in such systems a fundamental topological lower bound on the degree of 'tight' folding. This is especially relevant to crystallization in regime III, which will tend to have the minimum degree of 'tight' chain folding. For a flexible chain polymer such as PE, which has a marked natural tendency to form random coils in the melt phase, this minimum can be stated simply: as a lower bound, close to two out of every three emergent chains must re-enter the crystal nearby as first- or second-nearest neighbours with no significant amorphous character in the transit; the chains that do so form what we have earlier termed 'tight' folds. This applies specifically to the case of vertical stems, i.e. stems that are perpendicular to the fold plane. The remaining one-third of the emergent chains execute more distant re-entries as third- or greater nearest neighbours into the same lamella (or less often to a different lamella forming an interlamellar link), all these longer traverses having amorphous character. If more than one-third of the emergent stems are assumed to make these random-coil amorphous traverses, a region of excess density would have to appear in the vicinity of the lamellar surfaces, which is of course aphysical. This is the basic origin of the topological constraint. As shown below, this constraint can be relaxed to varying degrees if the stems are tilted at an angle that departs from the vertical to the plane of the chain folds.

Despite the mathematical complication involved in deriving it, the probability of 'tight' folding p_{tf}, which as noted in Section I is the sum of the probabilities of adjacent and next-nearest adjacent re-entry, p_{ar} and p_{aar}, can be stated in straightforward terms

$$p_{tf} \geq 1 - \left(\frac{\rho_a}{\rho_c}\frac{l_b}{l_u}\right)\frac{1}{3\cos\theta} \qquad (36)$$

Here ρ_a/ρ_c is the ratio of the amorphous and crystalline densities and θ is the angle of tilt as measured from the vertical. The quantity $\rho_a l_b/\rho_c l_u$ is close to 1.03 for PE.

Equation (36) was designed for a polymer with the chain flexibility of PE in mind, where it is reasonable to let both first- and second-nearest neighbour re-entries, i.e. p_{ar} and p_{aar}, represent basically non-amorphous excursions. The folds involving p_{ar} and p_{aar}, as well as the somewhat more distant nonadjacent traverses returning to the same lamella, occupy a relatively thin interfacial zone (see below). Adherence to equation (36) assures that no anomalous density excess will appear in the vicinity of the lamellar surface. Thus, if the actual p_{tf} is equal to or greater than the right-hand side, there is no density anomaly, but p_{tf} cannot go below the right-hand expression without incurring the unacceptable excess surface density. Equations of the general form of equation (36) were first derived for a cubic lattice[14] and the RIS model[15], the former using the mathematical framework of the Gambler's Ruin problem. The formula derived from the original Gambler's Ruin model for the cubic lattice case given in ref. 14 is $p_{tf} \geq 1 - (\rho_a/\rho_c)/(3\cos\theta)$. The 'real chain' RIS model calculation given in ref. 15 brings in the extra factor l_b/l_u. Only trivial approximations are involved in arriving at equation (36) from these treatments. Stated in direct terms, equation (36) eliminates pathological models that would put two or three objects (chain segments) in the same space at the same time in the interfacial zone of a PE system of intermediate molecular weight consisting of well-formed lamellae.

It is helpful for the reader unfamiliar with the problem to indicate the physical origin of the density anomaly at the interface when too many random coil chains are assumed to emanate from a plane surface. The simple illustrative example of the origin and resolution of the density anomaly given below is due to DiMarzio[99]. An illustration leading to similar conclusions was given by Frank[62]. Begin with an extended-chain crystal as shown in the left-hand diagram of *Figure 4a*. Now imagine the upper part of this crystal to be melted, with *all* the melted chains forming random coils; the interface between the melted part and the unmelted body of the crystal is taken to be at the plane a–a′. In viewing this figure it is well to remember that the chains in the random coil state have the same diameter as those in the crystal proper. It is readily seen in the right-hand diagram in *Figure 4a* that the random coil phase is much more dense than is the

body of the crystal—this is not a misleading optical illusion but rather a correct general representation of the impossibility of having random coils emanate from every surface site, these sites being confined to a plane normal to the chain axes in the crystal where the interfacial zone is relatively thin. (One can suppose here that, following Gibbs, the liquid-crystal boundary will be as thin as can be arranged even though in the present situation the concept is complicated by the presence of chain molecules in the interfacial zone.) There are two possible resolutions to this paradox, which are not mutually exclusive. One is to tilt the chains at an angle of $\cos^{-1}(1/3)$ or $\theta \cong 70.5°$ from the vertical, as illustrated in *Figure 4b*, which dilutes the existing chains sufficiently to prevent a density anomaly. The other resolution, which applies to the case $\theta = 0$ (vertical stems) is to fold two out of three of the emergent chains back into the crystal as either adjacent or 'tight' folds or a mixture thereof. The adjacent case is illustrated in *Figure 4b*. Here again the dilution of the emergent chains prevents a density excess at the interface. With the correction factor $(\rho_a/\rho_c)(l_b/l_u)$ for real polymer chains, equation (36) covers both of these effects and conformity to this expression prevents a physically inadmissible situation at the interface in chain-folded PE lamellae[100].

Since the earlier calculations referred to above, certain related problems have been worked out by Mansfield including: (i) details of the semi-ordered interfacial zone[19], (ii) the effect of the work of chain-folding, i.e. chain stiffness, on the probability of adjacent re-entry[19] as distinct from the rather higher degree of 'tight' folding, (iii) a continuum derivation[16] of the Gambler's Ruin problem, and (iv) the Gambler's Ruin problem for the case where the chain structure demands a regular up-down sequence for the stems, which replaces the factor $3\cos\theta$ in equation (36) by $6\cos\theta$, thus requiring a higher fraction of tight folds[17,18].

The calculations on the effect of the work of chain folding are of special interest. Mansfield showed by Metropolis Monte Carlo for the case $\theta = 0°$ that the work of chain folding disfavours strictly adjacent re-entry, reducing it from $p_{ar} \cong 0.7$ for a completely flexible chain to about 0.37 for chain energetics comparable to those appropriate to PE[19]. Virtually all of the adjacent re-entries in the p_{ar} of ~0.37 just cited involve sharp folds, i.e. folds formed in an adjacent position immediately after emergence as opposed to those where the emergent chain wanders about with a significant amorphous traverse before re-entering in an adjacent position. While p_{ar} is reduced by chain stiffness, p_{tf} is only slightly affected. For the PE chain non-amorphous traverses to second-nearest neighbours, i.e. p_{aar}, summed together with the p_{ar} of 0.37 brings p_{tf} up to ~0.62[19], which is close to the value of 0.66 required by equation (36) for $\theta = 0°$; this is significant because it provides independent evidence of the considerable accuracy of the Gambler's Ruin lower bound for p_{tf}. Employing a mean field approach, Kumar and Yoon[20] have arrived at results for p_{ar} as a function of chain stiffness similar to those found by Mansfield; also they found, as had Mansfield[19], that the interfacial zone thickened with increasing chain stiffness. The reason that the interfacial zone, which exhibits anisotropy, thickens with greater chain stiffness is that as the mean re-entry distance increases, thus lowering p_{ar}, the flights to nearby sites must project further above the crystal core, e.g. as a wicket-like transit to a third-nearest site over an existing fold. For the chain stiffness appropriate to PE, the anisotropy in the interfacial zone disappears 1 to 2 statistical steps away from the fold surface[101]. It has recently been demonstrated by Mansfield[101] that the Metropolis Monte Carlo results quoted above for the adjacency and 'tight' folding problems correspond to ergodic behaviour or the equivalent thereof. Accordingly, full reliance can be placed on the results.

It would appear that there is now a considerable degree of convergence of views concerning theoretical predictions of the degree of strict adjacency, the degree of 'tight' folding, and the existence of an interfacial zone with net chain orientation. While it might be possible in the future to improve these calculations, they clearly represent helpful and insightful theoretical benchmarks. In none of the above 'equilibrium' calculations (which reflect *lower bounds* for p_{ar} and p_{tf}—see below) do we see any reason to desist from presenting here a basically chain-folded model of melt-crystallization for PE, where p_{tf} is at worst 0.51 (for crystallization deep in regime III with a tilt angle of $\theta \cong 45°$) and considerably higher in regime I where θ is smaller, and where the overall average work of chain folding is defined as in the discussion associated with equation (14).

The foregoing leads to some observations that deserve emphasis:

(i) The random re-entry 'switchboard' model does not commend itself as appropriate for melt-crystallized PE specimens of intermediate molecular weight with well-formed lamellae with large lateral dimensions. If in the extreme case of 'switchboarding' one sets $p_{tf} = 0$ in equation (36), the angle of tilt has to be equal to or greater than 69.9°. No such large angle of tilt is known in melt-crystallized PE, a mean value of $\theta = 19°$ being typical for samples of low to near-moderate molecular weight crystallized at 130°C in regime I[78], and somewhat larger angles, commonly including 35°, at moderate molecular weights[78,102,103]. An angle of tilt of ~45° was found by Martinez-Salazar *et al.*[79] by a combination of longitudinal acoustic mode (LAM) and small-angle X-ray scattering (SAXS) measurements on hard-quenched small droplets of moderate molecular weight PE ($M_w = 32.1$ K). The crystallization in this case was undoubtedly deep in regime III and thus clearly represents a lower bound of p_{tf}. Even this rigorous treatment led to a degree of tight folding of a little over one-half (*Table 3*). The sources for the mean angle of tilt as a function of regime and molecular weight cited above and in *Table 3.2* were selected on the basis of investigations[78,102,103] that, in our judgement, reflect those angles typical of the interior of melt-crystallized specimens; results based on single monolayer crystals grown from the melt on a foreign substrate were not employed.

The interested reader will find examples in ref. 104 of the unacceptable density anomaly in the vicinity of the 'fold' surface (and in one case even the entire amorphous zone) incurred by assuming various forms of the 'switchboard' model. In brief, the 'switchboard' model visits too much of the disorder of the melt state upon the surface structure of a well-formed lamellar PE crystal of intermediate molecular weight thereby leading to a density anomaly and, in the process,

considerably undervalues the degree of 'tight' folding and by implication the degree of adjacent re-entry.

(ii) The Gambler's Ruin calculation as well as those involving chain stiffness give *lower bounds* for p_{tf} and p_{ar} for the cases considered and do not preclude higher values of these quantities from arising from kinetic reasons. This is already implied in the case of single crystals formed from dilute solution where the adjacent 'niche' in the substrate completion process is clearly a probable site for re-entry ('proximity' effect). Sadler[105] was able through neutron scattering studies to estimate that p_{ar} was ~0.75 for solution-grown PE single crystals, and this result is supported by other works. Based on i.r. studies of highly dilute PEH–PED specimens, Krimm and coworkers[106–108] have stated that adjacent re-entry is predominant in such crystals. In a recent book chapter Spells[98] has outlined a convincing treatment of i.r. and neutron scattering results for which segregation effects were minimal that strongly supports a p_{ar} of 0.75 for PE single crystals grown from xylene at 70°C[109]. (The T_x just cited suggests regime II crystallization which is consistent with the 'superfolding' phenomenon exhibited by the crystals.) These findings, taken together with recent atomic force microscopy (AFM) studies by Patil and Reneker[110] directly revealing a clearly recognizable if nominally imperfect {1 1 0} fold surface structure[111], render it certain that the probability of adjacent re-entry p_{ar} for solution-grown PE single crystals is well above the 'lower bound' calculations, with chain stiffness (fold energy) included, that centre around ~0.37 as given by Mansfield[19] (see also Kumar and Yoon[20]). (As will be brought out in Sections V and VI, the 'lower bound' calculations are actually applicable to melt-crystallization in regime III.) It is also evident that the probability of tight folding p_{tf}, which is quite generally somewhat greater than p_{ar}, exceeds the Gambler's Ruin lower bound of 0.58–0.64 for the low θ of solution-grown crystals (*Table 3*). Based on both the neutron scattering and i.r. results, Spells cites values of p_{ar} and p_{aar} for solution-grown PE single crystals that sum to a p_{tf} of 0.82. (Recent recomputation[114] of the neutron scattering results gives $p_{ar} = 0.75$ and $p_{tf} = 0.81$.) This high p_{tf}, which considerably exceeds the Gambler's Ruin lower bound, is clearly to be attributed to the 'proximity' effect, as is the high p_{ar}.

For PE fractions of low molecular weight crystallized from the melt in regime I, we shall show in Section V that the crystallization effects are 'quantized' and exhibit definite evidence for once-, twice-, and three-times folded structures. The implication in the case of the three-times folded quantized structures formed in regime I is that it is possible even in melt crystallization to obtain a high p_{ar} and to exceed the Gambler's Ruin lower bound for 'tight' folding because of kinetic effects associated with the 'niche' as a convenient site for re-entry. From a kinetic point of view we see regime I as providing the most regular folding and regime III the worst for a specified moderate molecular weight.

(iii) It is to be expected that crystallization from the melt in regime III will lead to structures consistent with the minimal p_{ar} and the lower bound of p_{tf} as expressed in equation (36). Noting that p_{tf} can be minimized by introducing an angle of tilt, one might expect a tendency for rather tilted structures to appear in regime III—see *Table 3* for typical values of the lower bound of p_{tf} for various assumed θ. The experimental results cited above imply that in at least the normal molecular weight range the angle of tilt in PE tends to be larger for regime III than for regime I. This type of result may not apply to other polymers where specific interactions between the stems favour a specific angle of tilt.

(iv) The Gambler's Ruin calculation provides an approximate guide for the value of n_{III}, which is the value that S_k/a_0 as given by equation (35) must attain in regime III. The basic concept is that the spaces between the primary nuclei injected at the rate i must be large enough for an emergent chain belonging to a primary stem to fold back frequently enough to be consistent with the prevailing degree of 'tight' folding. If n_{III} is 2.0, the mean distance separating nucleating stems is a_0. This allows only limited scope for adjacent re-entry and 'tight' folding but is, for instance, consistent with a mixture of singlets and adjacent re-entrant doublets interspersed with non-adjacent events corresponding to $p_{ar} \simeq 1/3$ and $p_{tf} \simeq 1/2$, the latter with equation (36) requiring an angle of tilt close to 45°. Meanwhile, if n_{III} is set at 2.5, the mean separation of primary stems is $1.5a_0$, which can accommodate a higher p_{ar} and a p_{tf} of 2/3, the latter being close to the Gambler's Ruin lower bound for $\theta = 0$, i.e. vertical stems. We surmise that an n_{III} close to 2.0 is appropriate for crystallization in regime III.

(v) It needs to be noted that equation (36), as well as the kinetic expressions given in this work, apply only where the polymer chain is flexible enough to permit some adjacent re-entry and tight folding. Beyond a certain chain stiffness, which is clearly well above that of PE, any semblance to regular folding will be remote as is likely the case for certain high melting semirigid chain polymers. Here, the interfacial zone is apt to be quite thick, and a mode of crystallization (though still likely involving nucleation) that differs in major respects from that treated here is to be anticipated.

(vi) The Gambler's Ruin calculation at its lower bound deals with the subject of interlamellar links ('tie chains') in a context that relates to regime III crystallization at intermediate molecular weights. Discussion of the tie molecule question is deferred to a later section where the molecular trajectories characteristic of regimes I and III are considered.

J. Summary

The present approach holds that: (i) even as a lower bound, the Gambler's Ruin topological effect requires a substantial degree of 'tight' folding with its concomitant modest adjacency in the relatively flexible chain PE system; (ii) consistent with the surface nucleation model, the 'proximity' effect under appropriate conditions can considerably enhance adjacency during the substrate completion process; and (iii) flux-based nucleation theory provides a basis for an understanding of not only the crystal growth rates in the various regimes but also the kinetic origin of the lamellar thickness and its variation with undercooling. We would propose that these effects, together with forced steady-state reptation or forced reptation of slack as the transport mechanism, go a long way toward explaining the generation of well-formed lamellar structures with a substantial degree of 'tight' chain folding in melt-crystallized PE of intermediate molecular weight. In what follows, a number of features of the theory are subjected to quantitative test.

III. APPLICATION TO MELT-CRYSTALLIZED PE: GROWTH RATES, LAMELLAR THICKNESS, AND MORPHOLOGY IN REGIMES I, II AND III FOR FRACTIONS OF INTERMEDIATE MOLECULAR WEIGHT (RANGES B–B′ AND C–C′)

A. Nature and preparation of samples

Although details concerning the linear PE fractions and the growth rate measurements to be discussed have been given in the original publication[77] (often referred to hereafter as HFRL), it is essential to highlight certain facts about their preparation for microscopy, since this has a bearing on the results. Specifically, steps were taken to assure that large spherulites and axialites could be formed without degrading the samples, and the lower extreme of the molecular weight distribution was removed.

The most important steps in the preparation of the fractions for microscopic observation to obtain growth rates were (i) a filtration from hot xylene solution that reduced the number of heterogeneities that initiated crystallites from 10^{10}–10^{13} to $\sim 10^4$ per cm^3, thereby allowing observation of large spherulites or axialites without resorting to high T_l (preheat) temperatures that could cause degradation and (ii) a subsequent crystallization from dilute xylene (85°C) step that removed any very low molecular weight component, which minimized effects resulting from rejection of short chain species during subsequent crystallization from the subcooled melt. (See papers by Gedde *et al.*[115] and Winram *et al.*[116] on rejection of short chain species.) Solution-formed crystals prepared as above were rigorously vacuum dried (50°C) and then melted between cover slips (specimen thickness $\sim 40\,\mu$m) for observation with a polarizing microscope using a hot stage (oxygen excluded) with temperature control of $\pm 0.01°$ for long periods of time. Attempts to inactivate most of the heterogeneous nuclei and thus reduce the number of spherulites (so that larger ones could be formed at T_x prior to impingement) by first heating the original (untreated) specimens to T_l values well in excess of 155°C led to degradation and spherulite morphologies that were not characteristic of the input molecular weight. When an initial heat temperature of $T_l = 155$°C was employed, the fractions never exhibited any signs of degradation in the volume element under study even after long runs at T_x for many weeks. With degradation avoided, variation of T_l did not alter spherulite or axialite growth rates on crystallization at a specified T_x.

At this point we mention how we have classified the fractions with respect to molecular weight as correlated with spherulite morphology, the nature of the reptation process, and the regime of crystallization. (Subsequently, the nucleation constants K_g and the degree of crystallinity will become part of the classification scheme.) For reasons based on the nature of the reptation process as expressed in equation (25), the molecular weight employed for certain plots for range B–B′ is $\bar{M}_{nw}$ which is defined as $(M_n \times M_w)^{1/2}$. Often we refer to the number of $-CH_2-$ groups in a fraction—in the case of $\bar{M}_{nw}$ this is denoted $\bar{n}_w$ which is calculated as $\bar{M}_{nw}/14$ as in equation (25). The 'z-average' molecular weight M_z is used in a few cases, the corresponding number of $-CH_2-$ groups being $n_z = M_z/14$. In quoting molecular weights, the symbol 'K' means 1000; thus, the notation $M = 11.0$K means $M = 11\,000$. The classifications are as follows:

(i) *Quantized chain-folding range, A–A′.* $\bar{M}_{nw} = 3.39$K, $\bar{n}_{nw} = 242$ to $\bar{M}_{nw} = 11.36$K, $\bar{n}_{nw} = 811.1$. All T_x correspond to regime I and only axialites were observed.

(ii) *Intermediate molecular weight ranges, B–B′ and C–C′.*

Range B–B′, near-ideal reptation, $\bar{M}_{nw} = 15.34$K, $n_{nw} = 1100$ to $\bar{M}_{nw} = 38.56$K, $\bar{n}_{nw} = 2755$. Axialites in regime I, non-banded spherulites in main body of regime II, but with coarse bands at the lowest T_x. Finely banded spherulites in regime III (quench, reptation of slack). Preliminary studies showed that fractions heated to a quite high T_l (i.e. degraded) tended to exhibit only ringed spherulites rather than the non-banded type everywhere in regime II.

Range C–C′, perturbed reptation, $\bar{M}_{nw} = 53.6$K, $\bar{n}_{nw} = 3830$ to $\bar{M}_{nw} = 90.6$K, $\bar{n}_{nw} = 6475$ or $M_z = 98.6$K, $n_z = 7030$ to $M_z = 204$K, $n_z = 14\,500$. Axialites in regime I, non-banded spherulites in main body of regime II, coarse bands at lowest T_x in this regime. Finely banded spherulites in regime III (quench, reptation of slack).

(iii) *High molecular weight range, D–D′.* $\bar{M}_{nw} = 103$K, $\bar{n}_{nw} = 7357$ to $\bar{M}_{nw} = 640$K, $\bar{n}_{nw} = 45\,700$. Irregular spherulites only and no I → II regime transition. 'Mixed' II and III-A regime behaviour.

(iv) *Ultrahigh molecular weight range, E–E′.* $M \geq \sim 10^6$. No objects of discernable morphology by optical microscopy. Regime III-A.

The emphasis in the present section is on ranges B–B′ and C–C′ where the regime I → II transition is clearly apparent in the experimental data and where the effects of 'quantized' chain folding at lower molecular weights have damped out. These are the fractions listed in *Table 2*.

It is convenient at this point to mention studies by others of the micromorphology of melt-crystallized PE fractions by electron microscopy that provided highly useful information on the lamellar structures formed, including the mean angle of tilt of the stems with respect to the fold surface. One of these is the work of Voigt-Martin, Fischer, and Mandelkern[78] (hereafter VMFM), which involved studies on PE fractions covering a wide range of molecular weight that were melt-crystallized under clearly specified conditions. Fortunately, the latter included crystallization at 130°C, which is well in regime I and which we accordingly found most helpful. A key point concerning the studies of VMFM is that they differentiated between the structures formed *at* the isothermal crystallization temperature T_x and those formed on subsequent cooling to room temperature when the electron microscope studies were carried out. The angles of tilt reported in the VMFM work were deduced from microtomed and stained sections, and we take these angles to be representative of the specimen interior. Another set of electron microscope studies by Bassett and coworkers[102,103], also on fractions crystallized from the melt under specified conditions, provided useful information on such subjects as the angle of tilt. These studies complemented the work of HFRL, which emphasized kinetics and the nature of fully developed axialites and spherulites.

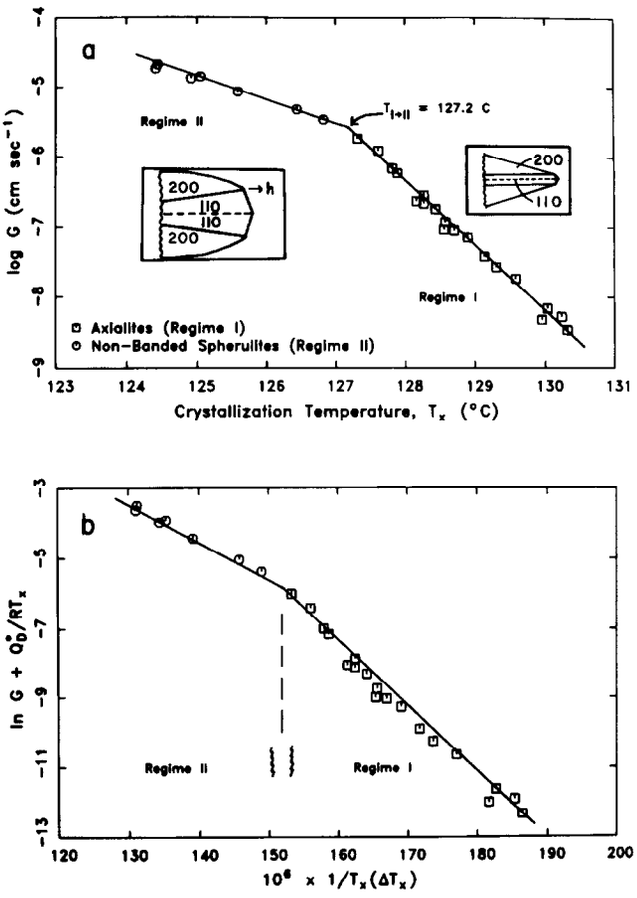

Figure 5 *Regime I and II behaviour in a typical PE fraction, MW range B–B′.* (a) Plot of $\log G$ vs. T_x for fraction 4, $\bar{M}_{nw} = 28.0$K, $\bar{n}_{nw} = 2000$. (b) Plot of $\ln G + Q_D^*/RT$ vs. $1/T(\Delta T)$ for same fraction with $Q_D^* = 5736\,\text{cal mol}^{-1}$ and $T_m = 143.61$°C. Solid lines drawn with slope change of exactly 2 at I → II regime transition. Data of HFRL[77]. Left-hand inset in (a) is schematic of sectors near growth tip in truncated lozenge typical of regime II in melt-formed crystals[27]; the {1 1 0} sectors have macroscopic growth fronts and the curved {2 0 0} sector edge is a section of an ellipse ('Mansfield crystal'[30]). Right-hand inset depicts corresponding situation for melt-formed lenticular crystal (regime I) after Toda[27,117]; the {2 0 0} sector edge is nearly straight near the growth tip ('Toda crystal'[118]). Note postulated narrow central strip with small {1 1 0} growth fronts. Lamellae arising from screw dislocations in such crystals are asymmetrical and exhibit only a single larger {1 1 0} growth front—see Section III.G. Solution-grown crystals are truncated lozenges with a macroscopic {1 1 0} front as in left-hand inset for both regimes I and II[32,83]

B. *Typical plot of* $\log G$ vs. T_x *and* $\ln G + Q_D^*/RT$ vs. $1/T(\Delta T)$ *showing nature of regime I → II transition*

Prior to analysing the growth rate data in *Table 2*, it is instructive to show an example of the actual growth rate data leading to our earlier (and present) conclusion that a regime I → II rate transition actually occurs. The plot of $\log G$ vs. T_x in *Figure 5a* depicts the actual growth rate measurements on sample 4 of *Table 2*, $\bar{n}_{nw} = 2000$, which is in molecular weight range B–B′. There is an unmistakable change of slope in the plot. Note that there is in this case a definite change of gross morphology in the general vicinity of the I → II transition—axialites form at temperatures beginning slightly above it and non-banded spherulites beginning slightly below. The transition between these two morphologies is not completely sharp, taking place over about 1° on either side of the observed rate transition. This change of gross morphology in the vicinity of the I → II rate transition is associated with the change of crystal type illustrated in the insets in *Figure 5a*[119]; as implied in Section II.H, no such change in crystal type is known with certainty to take place at this rate transition in other polymers. As will become evident, this situation in melt-crystallized PE still has the II → I rate transition resulting from a shift from multiple nucleation on a {1 1 0} substrate of length L in regime II to single nucleation on the {1 1 0} substrate of length L in regime I.

Though in most cases based on fewer data points, the I → II rate transition was clearly seen in plots such as those shown in *Figure 5a* for all the samples in molecular weight ranges B–B′ and C–C′ listed in *Table 2*, i.e. from $\bar{n}_{nw} = 1100$ all the way to $\bar{n}_{nw} = 6475$, $n_z = 14\,500$. At higher molecular weights, only irregular spherulites were found in the normal T_x range, and the I → II transition as a clearly defined phenomenon was lost (see later). Regime I persists down to $\bar{n}_{nw}$ values much lower than 1100, exhibiting 'quantized' chain folding beginning at $\bar{n}_{nw} = 242$. Growth in regime II could not be verified by HFRL below $\bar{n}_{nw} \cong 1100$ because of the rapidity of the crystallization in that regime; all growth rate measurements were restricted to $G \leq \sim 5 \times 10^{-5}\,\text{cm s}^{-1}$ to be certain to avoid self-heating effects and thus assure isothermal growth.

Figure 5b shows the corresponding plot of $\ln G + Q_D^*/RT$ vs. $1/T(\Delta T)$ for sample 4. The change of slope in the vicinity of the I → II transition is close to the factor of 2 suggested by regime theory—see equations (27) and (29) and *Figure 3c*. The solid lines representing regimes I and II in *Figure 5b* have been drawn as having exactly a slope change of 2. Values of $K_{g(I)}$ and $K_{g(II)}$ were readily obtained for all the fractions listed in *Table 2* from the actual slopes of plots similar to *Figure 5b*. The values of $K_{g(I)}$ and $K_{g(II)}$ listed in *Table 1* are representative of all the specimens listed in *Table 2* within an error of 10% or less. The relation $2K_{g(II)} = K_{g(I)}$ given by theory is thus closely obeyed for all the samples listed in *Table 2*. This result is relatively insensitive to variations in Q_D^*, which is in any case independently known.

In the original work by HFRL a Flory–Vrij[76] type of expression based on $T_m^0 = 146.5$°C was employed to calculate T_m values for the various fractions. Flory and Vrij gave T_m^0 as 145.5 ± 1°C. In the present and certain recent analyses, an expression based on the central value of T_m^0 of 145.5°C for $n \to \infty$ was employed to calculate T_m for each specimen—see numerical formula for T_m in footnote of *Table 2*. This lowered the undercoolings ΔT slightly and, therefore, also the $K_{g(I)}$ and $K_{g(II)}$ values to those listed in *Table 1*. Because of the lower T_m^0, each K_g and $\sigma\sigma_e$ employed here and quoted later in this work is a factor of 0.86 of that listed in HFRL.

There is recent confirmation that the melting point expression based on the T_m^0 of 145.5°C that has been employed here to estimate T_m values at lower molecular weights is of adequate accuracy. Barham[120] has generated both T_m' vs. T_x and T_m' vs. $1/l$ plots for a melt-crystallized PE fraction $M_w = 32.1$ K (NBS standard fraction) by measuring the lamellar thickness l_{obs} in real-time SAXS studies with synchrotron radiation (sweep time 1 s), so they are believed by us to be relatively free of the effects of isothermal thickening[121]. The T_m' vs. T_x plot[59] gave $T_m = 144.15 \pm 0.1$°C and the T_m' vs. $1/l$ plot based on equation (7a) yielded $T_m = 144.2 \pm 0.4$°C (orthorhombic form). The melting point from the form

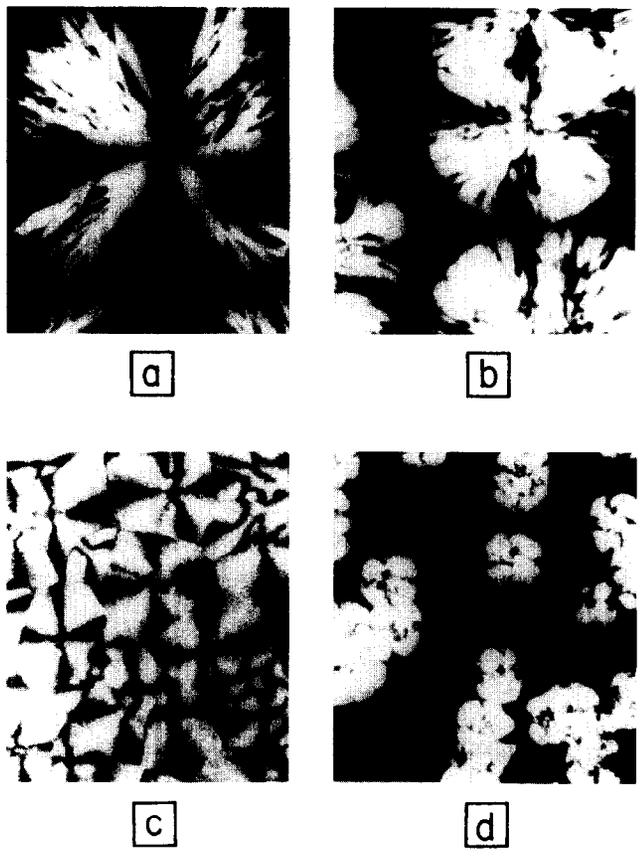

Figure 6 *Spherulites and axialites in melt-crystallized PE as a function of regime and molecular weight.* Optical micrographs (crossed polarizers) from HFRL study. Width of each illustration corresponds to ~200 μm. (a) Molecular weight range B–B′: $\bar{M}_{nw} = 28\,000$, axialites, regime I, $T_x = 128.55°C$, $\Delta T = 15.06°$; (b) $\bar{M}_{nw} = 28\,000$, non-banded spherulites, regime II, $T_x = 125.54°C$, $\Delta T = 18.07°$; (c) $\bar{M}_{nw} = 28\,000$, banded spherulites, quenched, regime III; (d) Molecular weight range D–D′: $\bar{M}_{nw} = 255\,000$, irregular spherulites, 'mixed' regime II and III-A (mostly III-A), $T_x = 125.54°C$, $\Delta T = 19.74°$

of the Flory–Vrij expression employed here that is based on $T_m^0 = 145.5°C$, is $T_m = 143.6°C$ for $M_w = 32.1K$, which is in satisfactory agreement with those from the T_m' vs. T_x and T_m' vs $1/l$ plots. Additional benefits of this work are that: (i) the T_m' vs. $1/l$ plot yielded $\sigma_e = 89.3\,erg\,cm^{-2}$ in excellent accord with that given in *Table 1*, and (ii) an estimate of $C_2 \cong 43\,Å$ in the expression for the initial lamellar thickness $l_{obs} = C_1/\Delta T + C_2$ was found. This value of C_2 will prove to be of considerable importance. The value of C_1 leads to a σ_e close to $90\,erg\,cm^{-2}$ (Section III.I).

Assuming a constant substrate length L at the I → II regime transition, the theory calls for $\Delta T_{I\to II}$ to have close to a fixed value with increasing molecular weight despite the corresponding increase in T_m. The $\Delta T_{I\to II}$ values were estimated by inspection of $\log G$ vs. T_x plots. The mean value of $\Delta T_{I\to II}$ of $16.37 \pm 0.50°$ noted in *Table 2* is sufficient to support the concept of L at the I → II transition being essentially constant with changing molecular weight in ranges B–B′ and C–C′; the assumption that $T_{I\to II}$ rather than $\Delta T_{I\to II}$ is constant in these ranges fails in comparison.

We draw attention to the fact that the existence of the I → II rate transition effect in melt-crystallized PE does *not* depend solely on plots of $\ln G + Q_D^*/RT$ vs. $1/T(\Delta T)$ of the type shown in *Figure 5b*—the regime I → II effect is clearly apparent in straightforward plots of $\log G$ vs. T_x such as that depicted in *Figure 5a*, which in no way depend on the undercooling, i.e. the choice of T_m. We mention this because it is possible for a given set of growth rate data with an arbitrarily chosen T_m (which is seriously wrong by, say, 5–10°) to generate in a $\ln G + Q_D^*/RT$ vs. $1/T(\Delta T)$ plot an apparent 'I → II' transition when in fact there is none and, conversely, to remove a real I → II transition where such actually exists. *Example*: for fraction 4 in *Table 2* whose true T_m for the orthorhombic form is close to 143.6°C, the (deliberately incorrect) assumption $T_m \cong 137°C$ will apparently remove the I → II transition in a plot of $\ln G + Q_D^*/RT$ vs. $1/T(\Delta T)$; however, the resultant single 'straight' line is actually rather 'S'-shaped, the scatter of data points around the line decidedly non-random, and the standard deviation notably inferior to that obtained with the correct T_m which exhibits the I → II transition with close to the theoretically predicted slope change of 2. Note that the incorrect melting point does nothing to erase the obvious I → II transition in the $\log G$ vs. T_x plot.

The example just given highlights the importance of having available an accurate T_m value for use in a regime analysis and the determination of K_g. Considering that our T_m values are independently supportable well within limits that do not admit of a spurious I → II transition and that the I → II regime rate transition effect appears in plots of $\log G$ vs. T_x, it is evident that both regimes do actually occur in melt-crystallized PE and that the K_g values are meaningful as well. Readers will find in HFRL detailed plots of $\log G$ vs. T_x and the corresponding plots involving $1/T(\Delta T)$ showing all the growth rate data points for fractions 1, 4, and 9 of *Table 2*.

The definite I → II rate transitions found by HFRL and others[77,83,117,122] in PE raise serious questions about the contention[123] that this transition does not, or should not, exist. A list of other polymers exhibiting the I → II effect is available[91].

C. *Spherulitic, axialitic, and microlamellar morphologies as a function of molecular weight and undercooling*

Four different morphological structures were encountered with the fractions and methods just described. A description follows:

(1) *Axialites*, typified by those shown in *Figure 6a* were seen in regime I, i.e. at undercoolings normally less than 16 to 16.8° from very low molecular weights beginning at $\bar{M}_{nw} = 3.39K$ on up to $\bar{M}_{nw} \cong 90.6K$, $M_z = 204K$. This covers molecular weight ranges A–A′, B–B′, and C–C′ in *Figure 7*.

(2) *Non-banded spherulites*, generally similar to those shown in *Figure 6b*, form in the main body of regime II, normally at undercoolings larger than 16.0 to 16.8°, beginning at $\bar{M}_{nw} = 15.3K$ and on up to $\bar{M}_{nw} = 90.6K$, $M_z = 204K$. This defines ranges B–B′ and C–C′ in *Figure 7*. The spherulites tended to exhibit coarse bands at the largest undercoolings still corresponding to isothermal growth in regime II. Thus, beginning at a T_x just below the I → II transition, the spherulites in range B–B′ and C–C′ were unbanded but at low T_x in regime II they tended to develop coarse bands. (The absence of bands may have a connection with the minimal low MW component in the fractions; recall also that banded spherulites tend to appear in degraded or oxidized specimens.) At very low T_x, as

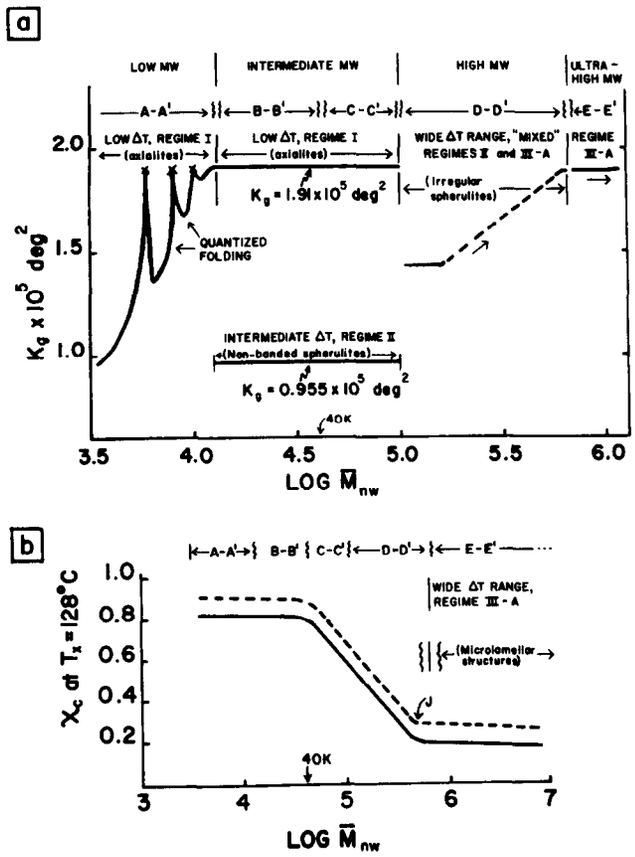

Figure 7 *Nucleation constant K_g, morphological type, and degree of crystallinity χ_c at near-completion for $T_x = 128°C$ as function of molecular weight.* The K_g data in (a) are from HFRL[77] up through range D–D′ and the degree of crystallinity curve (solid line in b) is from Mandelkern *et al.*[124]. See text for definition of χ_c. The K_g for range E–E′ as noted in the text was derived from the dilatometric data of Ergoz *et al.*[125]. Regime III effect at large ΔT, $K_g \cong 1.91 \times 10^5 K^2$, in ranges B–B′ and C–C′, finely banded spherulites, omitted for reasons of clarity

in regime III (see below), the bands were tightly spaced. This shrinkage of the band spacing with lowering T_x is the norm for many polymers, and the HFRL study of melt-crystallized PE fractions in no manner contradicts this general theme.

(3) *Highly banded spherulites* were readily formed by quenching thin specimens of fractions in the intermediate molecular weight range in ice water. A typical example is shown in *Figure 6c*. These are representative of crystallization deep in regime III in this general molecular weight range.

(4) *Irregular spherulites*, with the highly characteristic appearance shown in the optical micrograph in *Figure 6d*, were found for seven fractions over a considerable range of undercoolings corresponding to isothermal T_x (typically $\Delta T = 15.6–16.8°$ to $19.7–22.8°$) at moderately high to high molecular weight beginning near $\bar{M}_{nw} \cong 103K$ and ending near $\bar{M}_{nw} = 640K$. [Irregular coarse bands were seen in some specimens at the larger undercoolings (not shown).] This is molecular weight range D–D′ in *Figure 7*. The regime I → II transition was absent in this molecular weight range, being replaced by linear plots of $\ln G + Q_D^*/RT$ vs. $1/T(\Delta T)$ that led to 'K_g' values midway between $K_{g(II)}$ and $K_{g(III)}$ at lower M and then tending to exhibit sporadic values including some of a $K_{g(III)}$ magnitude at higher M. The reason for the appearance of a regime III type of behaviour, later denoted III-A as in *Figure 7b*, over a wide range of undercoolings at higher molecular weights is discussed in Section IV.

Special attention is drawn to the irregular spherulites that appear in range D–D′ in the work of HFRL (see *Figures 6d* and *7a*). Until recently, such structures have apparently not been reported by others. A recent study based on a PE fraction $M \simeq 350K$ that was treated in a manner similar to that used by HFRL confirms the existence of irregular spherulites in range D–D′, including the presence of coarse irregular bands at low T_x[126]. In the event, we believe that the HFRL results to be employed in the present work accurately reflect the gross morphologies and growth rates indigenous to undegraded fractions of linear chain PE from which solvent was fully removed and that had a minimal content of extraneous short chain species.

Figure 7a shows for the PE fractions in schematic form the relationship between molecular weight, on the one hand, and the nucleation constant K_g and spherulite or axialite morphology, on the other. In the appropriate undercooling range, regime I is seen through molecular weight range A–A′, B–B′, and C–C′, and both regimes I and II are observed in molecular weight ranges B–B′ and C–C′. Irregular spherulites with no I → II transition occur in the range D–D′ as noted above.

During the original work, which was carried out in the years 1973 to 1975, HFRL were concerned whether the structures were lamellar or not. SAXS studies on isothermally crystallized fractions with $\bar{M}_{nw} = 11.35K$, 28K, and 396K all exhibited primary SAXS spacings in the range ~180 Å to ~225 Å, which implied that lamellar structures were present. Subsequent work on melt-crystallized PE fractions by others, notably VMFM[78] and Bassett and coworkers[102,103,127,128], has shown in considerable detail by electron microscopy that the morphology in melt-crystallized PE is lamellar over a wide range of molecular weight. It has been reported, however, that the lamellae in the ultra-high molecular weight range are rather ill-formed and of limited lateral extent (VMFM).

D. Analysis of growth rates in regimes I and II involving near-ideal forced reptation in molecular weight range B–B′, $\bar{M}_{nw} = 15.34K$ to $\bar{M}_{nw} = 38.6K$. Also kinetic estimate of substrate length L

This set of samples, numbered 1–7 in *Table 2*, will be employed to test and evaluate numerical constants of interest for the near-ideal forced reptation model. Specimens of significantly lower molecular weight (range A–A′) exhibit 'quantized' chain folding (see later) and cannot be used for this purpose, and fractions with a somewhat higher molecular weight (range C–C′) obey a $G \propto 1/n_z$ rather than a $G \propto 1/\bar{n}_{nw}$ law at constant ΔT that will be dealt with subsequently. It is our intent here to evaluate the mean values of the pre-exponential constants $\bar{C}_I$ and $\bar{C}_{II}$, and thence obtain estimates of n_L, L, and C_0 for range B–B′. A close estimate of C_0 is required for the accurate prediction of the onset of regime III through equation (35).

The analysis to obtain $\bar{C}_I$ for regime I in range B–B′ utilizes equation (27a) for the growth rate of the {1 1 0} front, which we write in the numerical form

$$G_I = [C_I/(2/3)\bar{n}_{nw}]\, e^{-5736/RT_x}\, e^{-1.91\times10^5/T_x(\Delta T_x)} \quad (37)$$

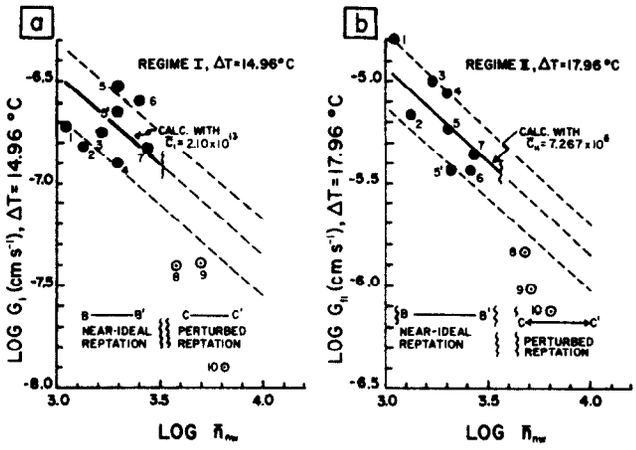

Figure 8 *Plots of* $\log G$ *for regimes I and II as a function of* $\bar{n}_{nw}$ *at constant undercooling for fractions 1–10 in Table 2.* Numbers near each data point indicate fraction designation in *Table 2*. Solid line in each $\log G$ vs. $\bar{n}_{nw}$ plot corresponds to theoretical $G \propto 1/\bar{n}_{nw}$ law for near-ideal forced reptation. Dashed lines show error of factor of 1.5 from mean; fractions 8–10 fall well below error limit indicating perturbed reptation

where $Q_D^* = 5736\,\text{cal mol}^{-1}$ and $K_{g(I)} = 1.91 \times 10^5$ (*Table 1*). Values of the growth rates G_I for fractions 1–7 at $\Delta T_x = 14.96°$ are given in *Table 2*; this is about 1.5° above $T_{I\to II}$ (see heavy dots, *Figure 3b*) and are all solidly in regime I. Computation of C_I with equation (37) for each fraction was carried out using $\Delta T = 14.96°$ and the T_x corresponding: $T_x = T_m - 14.96$. The mean value for all the specimens 1–7 is $\bar{C}_I = 2.100 \pm 0.720 \times 10^{13}\,\text{cm s}^{-1}$ (*Table 3*). A similar procedure was employed for the same specimens in the calculation of C_{II} for regime II using the data in *Table 2* for G_{II} using $\Delta T = 17.96°$; the latter corresponds to a growth temperature that is about 1.5° below $T_{I\to II}$ and is well within regime II. Thus, for the growth rate of the {1 1 0} growth front in regime II, we employ the expression

$$G_{II} = [C_{II}/(2/3)\bar{n}_{nw}]\, e^{-5736/RT_x}\, e^{-0.955\times10^5/T_x(\Delta T_x)} \quad (38)$$

in finding C_{II}. The result is $\bar{C}_{II} = 7.267 \pm 2.530 \times 10^6\,\text{cm s}^{-1}$ (*Table 3*). The growth rate data on which $\bar{C}_I$ and $\bar{C}_{II}$ for range B–B′ are based are exhibited in *Figure 8*.

Prior to calculating n_L from equation (30), which involves $\bar{C}_I/\bar{C}_{II}^2$, we first test the values of $\bar{C}_I$ and $\bar{C}_{II}$ to determine if they give a consistent value of $\overline{\Delta T}_{I\to II}$ that falls within the experimentally-determined range (*Table 2*). This is accomplished by setting the expressions for G_I and G_{II}, equations (37) and (38), respectively, equal to each other to obtain

$$T_x(\overline{\Delta T}) = K_{g(II)}/\ln(\bar{C}_I/\bar{C}_{II}) = 6419.42K^2 \quad (39)$$

With the melting point for fraction 4 this yields $\overline{\Delta T}_{I\to II} = 16.02°$. The average value of $\overline{\Delta T}_{I\to II}$ found in this way for fractions 1–7 is $16.04 \pm 0.03°$, which falls within the experimental range of $16.37 \pm 0.50°$ given in *Table 2*.

Despite the great care taken in the experiments, there is considerable scatter in the individual C_I and C_{II} values for fractions 1–7. Here, as in rate experiments generally, pre-exponential factors are difficult to estimate with high accuracy. Nevertheless, it is evident that the *averages* $\bar{C}_I$ and $\bar{C}_{II}$ for fractions 1–7, through equation (39), closely reproduce the mean value of $\overline{\Delta T}_{I\to II}$. Accordingly, it is reasonable to rely on quantities derived from these averages. On this basis we may proceed to estimate n_L (and L), which involves the ratio $\bar{C}_I/\bar{C}_{II}^2$.

To estimate n_L, we employ the melting point of sample 4 as being typical of the fractions 1–7 and calculate n_L with equation (30) using $T_m = 416.81\,\text{K}$, $\overline{\Delta T}_{I\to II} = 16.37°$, and $\bar{C}_I/\bar{C}_{II}^2 = 0.3977$, which with the other necessary input data in *Table 1* yields $n_L = 246.9\kappa$; with $\kappa = 0.77$ from equation (22) this gives

$$n_L \cong 190 \quad (40a)$$

Then, with $L = n_L a_0$, one has

$$L \cong 865\,\text{Å} \quad (40b)$$

These results apply in the near-ideal reptation region B–B′ in *Figure 8*. Our estimate of the error in n_L and L, which we deem partly a result of the uncertainty in κ and partly that of $\bar{C}_I/\bar{C}_{II}^2$, is such that n_L is unlikely to be in error by more than a factor of ~1.5 with a corresponding limit for L (*Table 3*). This 'kinetic' value of L for the {1 0 0} growth front holds at the T_x corresponding to the I → II transition but may differ somewhat at a T_x removed from the transition. The ratio $\bar{C}_I/\bar{C}_{II}^2$ for range C C′ leads to similar but less accurate n_L and L values than those just given for range B–B′. Accordingly, we do not suggest that L for C–C′ differs substantially from that of B–B′.

The authors believe that the estimates of n_L and L above are more firm than earlier ones[6,7,91] based on the same growth rate data, but with a greater error in κ and a less exact theoretical framework. The present kinetically-based estimate of L will be discussed subsequently in terms of its relation to the range of lattice coherence.

With n_L now being known, a straightforward calculation of $C_0\kappa$ at $\bar{T}_x = 400.44\,\text{K}$ as for fraction 4 and $\overline{\Delta T}_{I\to II} = 16.37°$ can be effective through the use of equation (27b). The result is $C_0\kappa = 5.725 \times 10^5$. Then with κ set at 0.77 as before, one has

$$C_0 = 4.408 \times 10^5, \qquad C_0^{1/2} = 664 \quad (40c)$$

A parallel calculation with equation (29b) yields an identical result for $C_0^{1/2}$. This value of C_0 will play a crucial role in predicting the onset of regime III. The results for n_L, L, and C_0 given above may be taken as typical of the specimens in the range B–B′.

With 'best' mean values for κ and C_0 now being known for range B–B′, fractions 1–7, it is convenient to give numerical estimates of g and i. Besides being of general interest, these expressions are useful in the discussion to follow of the Lauritzen Z_L factor[86], which deals with the rapidity of the crossover between regimes I and II. Employing equation (17) with $\kappa = 0.77$ and noting equation (25) for the form of n, one finds with the additional input data in *Table 1* that the substrate completion rate on the {1 1 0} growth front is

$$g\,(\text{cm s}^{-1}) = \frac{1.182 \times 10^4}{\bar{n}_{nw}}\left[\frac{T_x(\Delta T)}{T_m}\right] e^{-10\,636/RT_x} \quad (41a)$$

where the factor 2/3 multiplying $\bar{n}_{nw}$ has been subsumed as a factor of 1.5 in the numerical pre-exponential factor, and where the number in the exponent is $Q_D^* + q$ in kcal mol^{-1}. This expression is valid only in regimes I and II where substrate completion involves successive addition of a number of stems. The steady-state 'reeling in' rate $\bar{r}$ in these regimes is given by $g(l_g^*/a_0)$ and exhibits little variation with T_x. As

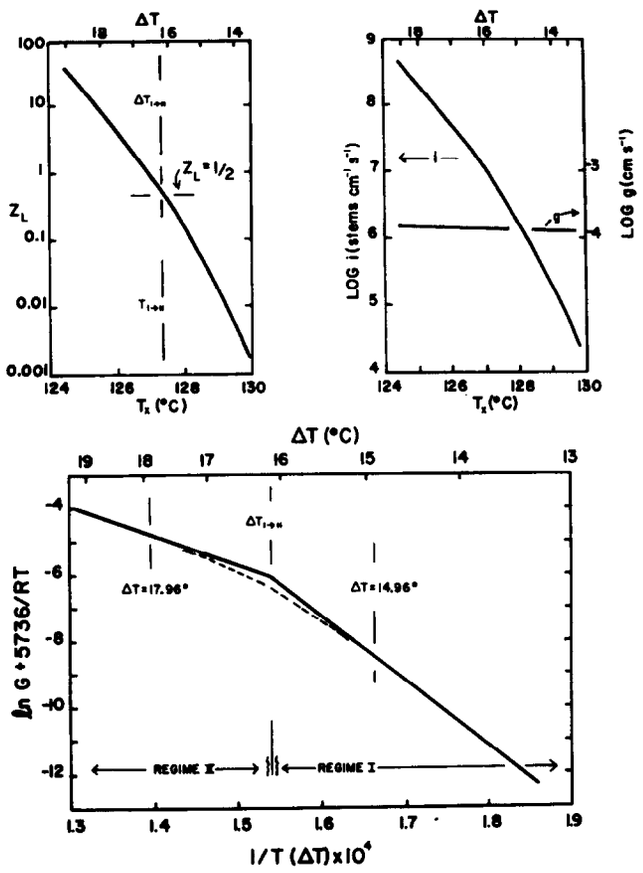

Figure 9 *Behaviour of Z_L, i, and g as a function of ΔT; also* $\ln G + Q_D^*/RT$ vs. $1/T(\Delta T)$ *(theoretical).* Calculated for $\bar{n}_{nw} = 2000$, range B–B′, for $T_m = 416.8$ K with $Q_D^* = 5736$ cal mol^{-1}, and $q = 4900$ cal mol^{-1}. Dashed line in lower plot shows calculated deviation from straight line behaviour near I → II transition. Compare bottom plot with *Figure 5b*

estimated with $l_g^*(\text{Å}) = 2680/\Delta T + 43$ (see later) for the case $\bar{n}_{nw} = 2000$, $\bar{r}$ is 7.1×10^{-3} cm s^{-1} at $\Delta T = 13.3°$ and 5.5×10^{-3} cm s^{-1} at $\Delta T = 24.4°$, the latter being at the low temperature extreme of regime II where $g = G_{II} = 1.617 \times 10^{-4}$ cm s^{-1}. As noted in Section II.G, the reeling rate in regime III is given by $\bar{r}_{III} \simeq a_0 i l_g^*$. For $\bar{n}_{nw} = 2000$, this yields $\bar{r}_{III} = 5.9 \times 10^{-3}$ cm s^{-1} at $\Delta T = 24.4°$, which closely matches the regime II result based on $\bar{r} = g(l_g^*/a_0)$ at the same ΔT as is required. However, at larger undercoolings rapidly increasing values of $\bar{r}_{III}$ are found which imply that crystallization in the body of regime III must begin to involve reptation of slack—see Section III.H where the extremely high $\bar{r}_{III}$ values required to facilitate crystallization deep in this regime are treated.

With $\kappa = 0.77$ and the value of C_0 given above, equation (6) for the surface nucleation rate i for the {1 1 0} growth front in numerical terms comes to

$$i\,(\text{stems s}^{-1}\,\text{cm}^{-1}) = \frac{1.39 \times 10^{22}}{\bar{n}_{nw}}\left[\frac{T_x^2(\Delta T)}{T_m}\right] \times e^{-5736/RT_x}\, e^{-1.91\times10^5/T_x(\Delta T)} \quad (41b)$$

The 2/3 factor multiplying $\bar{n}_{nw}$ is included as a factor of 1.5 in the numerical pre-exponential factor.

The above expression holds in regimes I and II in range B–B′, but some deviation may appear in the body of regime III owing to the long extrapolation. The mean delay time τ_{nuc} between nucleation acts on a substrate of length L is given by $1/iL$. This comes to 1.6×10^{-2} s at $\Delta T_{I\to II} = 16.37°$ for $\bar{n}_{nw} = 2000$.

The crossover from regime I to regime II is not completely abrupt but is commonly believed to occur over a relatively narrow range of temperature. That the crossover is not completely abrupt is already implied by the fact that the change from strictly axialitic structures to normal spherulitic ones occurs over about a 2° range of temperature[3]. The dimensionless parameter $Z_L = iL^2/4g$ devised by Lauritzen[50,86] provides a measure of the degree of conformity to the idealized 'straight line' representation of the Regime I → II effect. With the expressions given above for i, g, and L, there is obtained

$$Z_L \equiv iL^2/4g = 2.20 \times 10^7 T_x\, e^{4900/RT_x}\, e^{-1.91\times10^5/T_x(\Delta T)} \cong 8.81 \times 10^9\, e^{4900/RT_x}\, e^{-1.91\times10^5/T_x(\Delta T)} \quad (41c)$$

where 4900 cal mol^{-1} is the work of chain folding q. The approximation applies near a nominal transition temperature $T_{I\to II}$ of 400.4 K.

Based on Frank's treatment[84] of the crossover between regimes I and II, which is of a 'mean field' character, Mansfield[129] has developed a master plot giving the fractional deviation from idealized 'straight line' behaviour as a function of Z_L. [By 'straight line' behaviour we mean the representation of the I → II effect as two straight lines that intersect at $T_{I\to II}$ which have a slope change of 2 at that temperature in plots of $\ln G + Q_D^*/RT_x$ vs. $1/T(\Delta T)$.] The maximum deviation from straight line behaviour is only a factor of 1.326 in G at $Z_L = 1/2$, which is at $T_{I\to II}$. If $Z_L = 3.2$, the growth rate G_{II} falls just 10% below the idealized 'straight line' representation for regime II, and if $Z_L = 0.095$, G_I falls just 10% below the corresponding growth rate for regime I. Straightforward calculations with equation (41c) show that this close approach to idealized behaviour occurs only 0.90° above $T_{I\to II}$ for regime I and only 1.14° below $T_{I\to II}$ for regime II. These figures appear to correlate with the range of temperature of ~2° over which the axialite → spherulite morphology transformation takes place in PE. At ~1.5° away from the transition, which corresponds to the G_I and G_{II} data in *Table 2*, idealized straight line behaviour is even more closely approached in both regimes.

Figure 9 gives a plot of Z_L as a function of T_x and ΔT according to equation (41c) for melt-crystallized PE, range B–B′. Also shown is a plot of $\ln G + Q_D^*/RT_x$ vs. $1/T(\Delta T)$ calculated according to equations (37) and (38) using $T_m = 416.81$ K and $\bar{n}_{nw} = 2000$ with the values of C_I and C_{II} listed in *Table 3*; the calculated deviation from idealized 'straight line' behaviour in the crossover region between regimes I and II derived from Mansfield's master plot is shown as a dashed line. Since the repeatability of the data for G at a fixed ΔT has an estimated error of a factor of ~1.3 in regime II and somewhat larger in regime I (see repeat runs for fraction 5 in *Table 2*) it is not possible to be certain of the presence or absence of the predicted curvature in the transition region. Should future studies of high accuracy indeed show that the I → II rate transition is actually sharper in melt-crystallized PE than predicted by Frank's treatment, the cause of the sharpness is likely to be found in the strain-induced behaviour of $g_{200}(T_x)$ to be noted subsequently that causes a change of crystal type at or

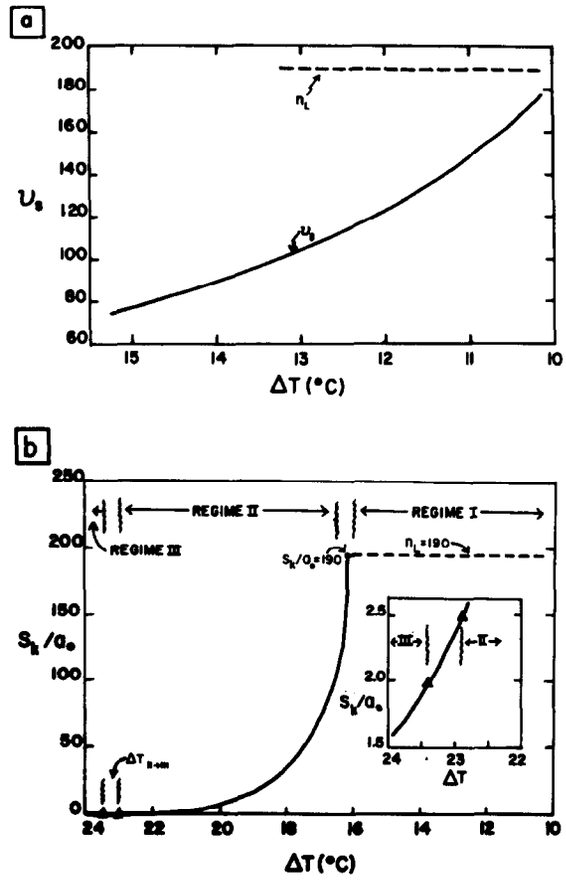

Figure 10 *Details of substrate completion process, MW ranges B–B′ and C–C′.* (a) Plot of number of stems ν_s required to form just stable surface nucleus as a function of ΔT *via* equation (42) showing that $n_L > \nu_s$ in regime I up to ΔT_{cutoff}. Normal regime I growth will occur at all ΔT larger than ΔT_{cutoff} until regime II is entered. (b) Plot of mean separation of primary nuclei on substrate in stem units S_k/a_0 as function of undercooling *via* equation (43) in regimes I, II, and III. Regime III begins at the undercooling where the primary nuclei have a separation S_k/a_0 of 2–2.5 stem widths (see inset)

very near the transition. Even so, the regime I and regime II concepts would remain intact since a {1 1 0} growth front is still present in both regimes.

For completeness, *Figure 9* illustrates the variation of i and g as a function of T_x and ΔT for $\bar{n}_{nw} = 2000$ according to equations (41a) and (41b). The substrate completion rate g exhibits but little variation in the entirety of regimes I and II—the ratio $g(\Delta T = 24.4°)/g(\Delta T = 13.3°)$ is only 1.23. In contrast, the surface nucleation rate i exhibits a very large change in these regimes, mainly because of the factor $\exp[-K_{g(I)}/T(\Delta T)]$; here $i(\Delta T = 24.4°)/i(\Delta T = 13.3°) = 8.80 \times 10^6$. *Figure 9* shows in explicit numerical terms why the variation of G_I and G_{II} with T_x tends to be dominated by i and $i^{1/2}$, respectively, rather than being seriously influenced by changes in g.

The numerical expressions for i and g given above can be employed to construct a plot (not shown) of $\log G$ vs. T_x through the relationships $G_I = b_0 iL$ and $G_{II} = b_0(2ig)^{1/2}$. Since this formulation accounts for the temperature-dependence of the pre-exponential factors, it leads to a slightly different prediction of the detailed shape of the $\log G$ vs. T_x curves than those based on $\bar{C}_I$ and $\bar{C}_{II}$. However, the differences are well within experimental error.

Before proceeding further, it is required to determine through the use of equation (31) if $n_L \geq \nu_s$ even at the lowest ΔT employed in measuring the growth rate G_I in regime I. This condition must hold for the L characteristic of the 'leading' {1 1 0} growth tips that control the observed growth rate of the axialites in regime I; recall, however, that this condition need not hold for slower growing lamellae with a growth tip that is smaller than the range of lattice coherence.

To test whether the condition $n_L \geq \nu_s$ holds, equation (31) may be written in the numerical form

$$\nu_s = \frac{19\,630}{(\Delta T)^2} - \frac{176.8}{(\Delta T)} \qquad (42)$$

where δ is taken to be 10.55×10^{-8} cm according to the exact form for this quantity as given in equation (8b). This value of δ holds well for the low ΔT of 13.3°, which corresponds to the lowest ΔT ever employed in the HFRL growth rate studies (highest temperature point for fraction 4 in *Figure 5a*). Though calculated with the T_m of fraction 4 to find ΔT, the above expression holds with good accuracy for any of the fractions in *Table 2*. A calculation with equation (42) shows that ΔT_{cutoff}, which is where $n_L \simeq \nu_s$, would be 9.7° if n_L had its central value of ~190 as calculated with $\bar{C}_I/\bar{C}_{II}^2$ in equation (30)—see *Figure 10a* which shows a plot of ν_s vs. ΔT in comparison with $n_L = 190$. Although the C_I and C_{II} values for individual fractions lead to scattered n_L values, we adhere in this discussion to the mean n_L of 190 based on $\bar{C}_I/\bar{C}_{II}^2$. Noting that regime I theory is valid when $n_L > \nu_s$ and recalling further that the lowest ΔT employed was 13.3°, it is evident from *Figure 10a* that this condition has been met for fractions 1–10 since $\Delta T \geq 13.3°$ for all of them. From the above considerations it follows that the theory for regime I has been applied here in a temperature range where it was fully valid.

An erroneous assertion[89] to the effect that the regime I concept was generally invalid because n_L was presumed to be always less than ν_s arose in part from the inappropriate use of a δ of $kT/2b_0\sigma$ rather than $kT/b_0\sigma$ [or the exact δ of equation (7b)] in equation (30) to get a ν_s about twice too large. As pointed out by us[91], the smaller δ might occur if the backward reactions B and B_1 were inactive (as may conceivably occur deep in regime III) but equation (7b) or (8b) is the correct δ for the basic LH model in regime I.

E. Growth rates in regimes I and II for perturbed reptation, molecular weight range C–C′, $\bar{M}_{nw}$ = 53.63K, M_z = 98.6K to M_{nw} = 90.6K, M_z = 204K

The treatment in Section II has G in both regimes varying generally as $1/n$ at constant ΔT because of retardations associated with reptation in the subcooled melt. As shown in *Figure 8b*, there is a general downward trend of the growth rate at constant ΔT in regime II in range B B′ with increasing $\bar{n}_{nw}$—a fit of the data in this 'near ideal' reptation range yields $G_{II} \propto 1/\bar{n}_{nw}^{1.39 \pm 0.42}$ (±0.42 = standard error), which is in at least fair accord with the predicted $G \propto 1/\bar{n}_{nw}$ law (see also ref. 7). However, it is seen in *Figure 8a* that the scatter of the data precludes any estimate of the corresponding slope for regime I in range B–B′. The situation for both regimes can be clarified further by considering the data for molecular weight range C–C′ where definite perturbations of the reptation process enter the picture

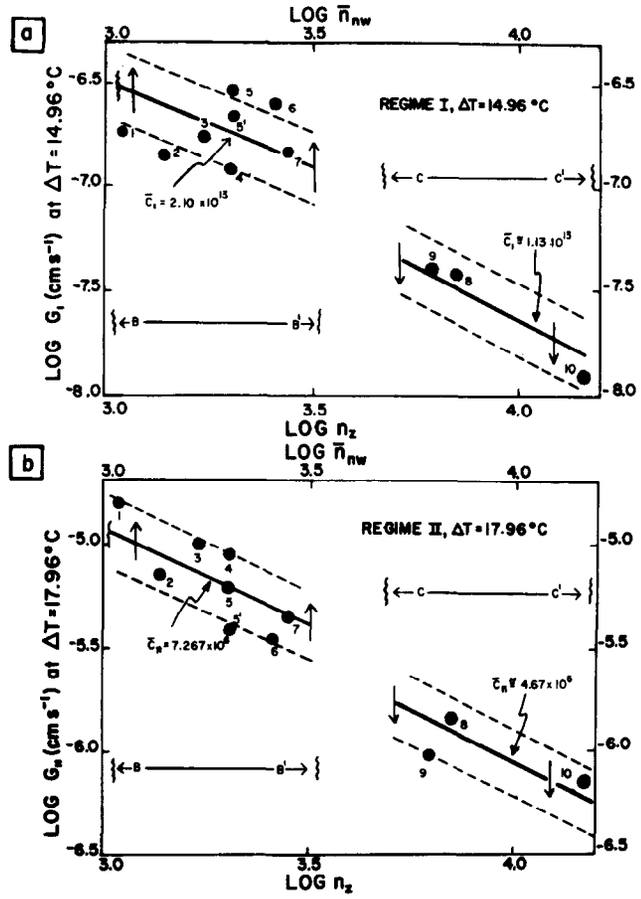

Figure 11 *Master plots of* $\log G$ *at a constant undercooling in regimes I and II as a function of* $\log \bar{n}_{nw}$ *(near-ideal forced reptation) or* $\log n_z$ *(perturbed reptation).* Solid lines are based on $\bar{C}_I$ and $\bar{C}_{II}$ values shown. Up arrows (↑), read $\log \bar{n}_{nw}$ scale; down arrows (↓), read $\log n_z$ scale. Plots show that general $G \propto 1/n$ at constant ΔT law (heavy solid lines) prevails in both regimes I and II in MW ranges B–B′ and C–C′. Note that onset of the $G \propto 1/n_z$ law corresponds to a fall in the degree of crystallinity χ_c as shown in *Figure 7b* for range C–C′

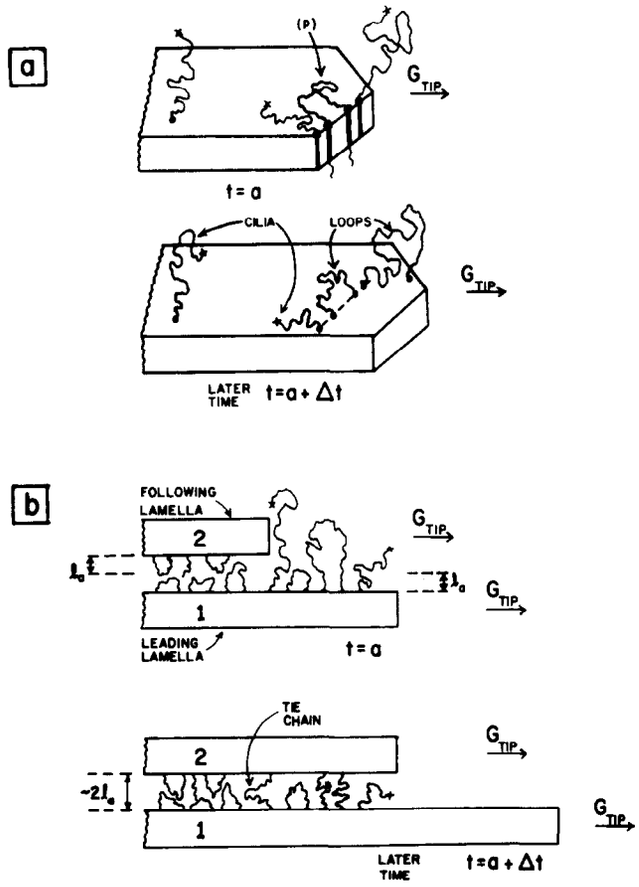

Figure 12 *Non-adjacent structures that impede nucleation and growth and lower degree of crystallinity: also tie chain formation (schematic).* (a) Incorporation of long cilia and loops on lamellar surface during growth at higher molecular weights in upper part of range C–C′ and all of D–D′ and E–E′. Multiple attachment at growth front (*p*) lowers growth rate and creates loops that persist behind front. Trapped cilia also formed. (b) Formation of tie chains by 'following' lamella (2) incorporating portions of longest cilia and largest loops emanating from surface of 'leading' lamella (1)

because of multiple attachment events on the growth front. With this, a better overall picture of the $G \propto 1/n$ law is obtained.

Range C–C′ consists of fractions 8–10 in *Table 2* where the *z*-average molecular weights are as noted above, with the corresponding n_z values going from $n_z = 7030$ to $n_z = 14\,500$. All these fractions exhibit clear-cut regime I → II transitions and are therefore subject to the same type of analysis as fractions 1–7. However, fractions 8–10 do not follow the $G \propto 1/\bar{n}_{nw}$ law at constant ΔT as is evident from *Figures 8a* and *b*.

On an empirical basis, it was found that fractions 8–10 obeyed approximately a $G \propto 1/n_z$ law in both regimes. This is illustrated in the master plot given as *Figure 11*. In this graph, $\log G_I$ and $\log G_{II}$ are plotted as a function of $\log \bar{n}_{nw}$ at the constant ΔT values noted for samples 1–7 (upper scale) and as a function of $\log n_z$, again for the constant ΔT's noted, for fractions 8–10 (lower scale). This plot implies that a $G \propto 1/n$ reptation-based law holds from $M_{nw} = 15.34$K, $\bar{n}_{nw} = 1100$ all the way to $M_z = 204$K, $n_z = 14\,500$, but with the proviso that n changes from $\bar{n}_{nw}$ to n_z in the process.

We believe that the reason for the shift from near-ideal forced reptation (range B–B′) to what we have designated 'perturbed' forced reptation (range C–C′) is related to the advent of multiple attachment acts by a given long molecule on the growth front forming temporary doubly-pinned or multiply-pinned loops. The probability of such nonadjacent re-entry events (some at widely separated sites) will increase with increasing chain length. For the force of crystallization to reptate (in the steady-state mode) such a molecule on to the growth front to form a crystalline stem will require one of the points of contact with that front to be broken, which has the effect of making the section of molecule involved act as if it had a higher than normal friction coefficient. [A molecule of this type is depicted on the growth front in *Figure 12a* at point (*p*).] In this situation, the longer molecules in the distribution represented by M_z will tend to dominate the now perturbed reptational transport mechanism, leading to the shift from the $1/\bar{n}_{nw}$ to the $1/n_z$ law as one goes from range B–B′ to C–C′. It follows also that these multiple attachment acts by the longer molecules will cause the nucleation and substrate completion processes, and thence the growth rate, to be slower as is observed (see later). Some of the nonadjacent events will survive behind the growth front as long-lived, once-pinned, random coil cilia and doubly- or even multiply-pinned long loops, causing a relatively thick, near-normal amorphous phase to be associated with each fold surface (*Figure 12a*). Accordingly, one must expect a fall in the degree of crystallinity to accompany

the perturbation of the reptation process leading to $G \propto 1/n_z$ and the corresponding reduction in the growth rate. To show the fall in crystallinity, it is required to introduce an appropriate degree of crystallinity–molecular weight scale. This is outlined below.

Figure 7b shows the estimated degree of crystallinity χ_c of PE fractions as it develops to near-completion at $T_x = 128°C$ as a function of $\bar{M}_{nw}$. It is to be emphasized that χ_c here refers to the χ that appears *at* T_x at near-completion and not the considerably increased χ that develops at each molecular weight on cooling to room temperature, the latter exhibiting the additional formation of thin lamellae in the amorphous phase between the original thicker lamellae formed at T_x. Thus by 'χ at near-completion' we mean to refer to the value of χ, namely χ_c, that appears at T_x near the end of stage 1 crystallization. A specific example is helpful here. For the case of bulk crystallization involving growth of spheres born at the same time, χ_c appears directly in the modified Avrami expression for stage 1:

$$\chi(t) = \chi_c\{1 - \exp[-(4\pi/3)\nu_0 G^3 t^3]\} \qquad (43a)$$

Here t = elapsed time and ν_0 = number of heterogeneous nuclei per unit volume. After χ_c is attained, a very slow increase of χ still takes place (stage 2) which goes for long periods approximately as $\log t$: this is likely a result of lamellar thickening accompanied by tie chains and other components of the amorphous phase between the lamellae being slowly drawn into the lamellae. Examples of the estimation of χ_c from bulk crystallization isotherms based on specific volume data for poly(chlorotrifluoroethylene) using equation (43a) can be found in a paper by Hoffman and Weeks[48,130]. This work illustrates the meaning of stage 1 according to $\chi(t)$ above and the ensuing slow stage 2 process which varies as $\log t$. Equation (43a) applies specifically to the case of spherical growth corresponding to an Avrami exponent of 3. Similar expressions with the prefactor χ_c are readily devised for needles and discs born at $t = 0$ that correspond to Avrami exponents of 1 and 2, respectively. (Sporadic initiation can also be brought into the scheme). In each case, irrespective of the Avrami exponent, χ_c has the same meaning as described above for spherical growth, i.e. it represents the limiting degree of crystallinity at T_x at the end of stage 1 crystallization.

The solid line in *Figure 7b* is from the heat of fusion data of Mandelkern *et al.*[124] for $T_x = 128°C$, regime I. Their curve for $T_x = 122°C$ (regime II) is very similar, so the result shown in *Figure 7b* is basically the same for regimes I and II up to molecular weights where these regimes still appear. There is some uncertainty in the absolute value of χ_c—in another place VMFM gave the crystallinity as ~0.3 at $M_\eta \cong 8 \times 10^6$ rather than ~0.20 as in *Figure 7b*—accordingly we have introduced the dashed curve in *Figure 7b* to represent a reasonable approximate upper bound for χ_c. Whatever the modest uncertainties in the absolute χ_c scale for near-completion at T_x in *Figure 7b*, the trends depicted may be taken as fully reliable.

It is advantageous at this point to introduce in brief form some of the notation and concepts concerned with the relationship between χ_c and the relatively normal amorphous phase associated with large scale non-adjacent events that lead to the notable fall of χ_c beginning in molecular weight range C–C′. Here each 'leading' lamella, viewed initially as an isolated entity, is assumed to have a crystalline core of thickness l_{core} and a layer of amorphous material consisting of long loops and cilia of thickness l_a associated with each 'fold' surface. A contiguous 'following' lamella is assumed to have the same l_{core} and a similar l_a associated with each 'fold' surface but with some of the longer cilia and loops from the 'leading' lamella being incorporated in it thus forming tie chains between the lamellae (*Figure 12b*). Then, the total thickness of the relatively normal amorphous polymer between the lamellae, l_{amorph} may be taken as approximately equal to $2l_a$. Setting aside density differences, this model leads to the simple relationship

$$1 - \chi_c = \phi_a \cong \frac{l_{amorph}}{l_{core} + l_{amorph}} \cong \frac{2l_a}{l_{core} + 2l_a} \qquad (43b)$$

where ϕ_a is the fraction of amorphous material. In range B–B′ where ϕ_a (and thus l_a) is small, we take l_a to be associated with the relatively short non-adjacent traverses back to the lamella of origin in the thin interfacial zone; here there are virtually no tie chains, large loops, or long cilia. Accordingly, we shall later denote the small l_a characteristic of range B–B′ as d_a to highlight its short-range origin and confinement mostly to the semi-oriented interfacial zone as contrasted with the much longer range traverses that constitute the bulk of l_a at higher molecular weights. Thus, in C–C′ and higher molecular weight ranges where ϕ_a and hence l_a become progressively larger, the bulk of the increase in l_{amorph} is attributed to the presence of large loops, tie chains, and cilia of dimensions sufficient to exhibit relatively normal random-coil amorphous behaviour. A number of points raised above will be discussed in more detail later in this work.

Returning to the issues at hand, the point to notice in *Figure 7b* is that a definite fall in χ_c begins just after range C–C′ is entered at $\bar{M}_{nw} = 50–55K$. We take this fall as indicative of the advent of excess amorphous material between the lamellae corresponding to l_a that consists of tie chains, long loops, and some once-pinned long cilia. The implication is clear from this that a significant number of nonadjacent re-entries, some at distant sites for a given molecule, have begun to occur on the growth front and then become incorporated in the lamellae (*Figure 12a*). In the same general molecular weight range, nonadjacent events involving a specified long molecule at the growth front, through formation of a (temporarily) pinned loop (or loops) on that front, have interfered with the near-ideal steady-state reptation mechanism (*Figure 12a*). This causes the shift from the $G \propto 1/\bar{n}_{nw}$ to $G \propto 1/n_z$ (*Figure 11*). (The normal reptation process in the true melt is known through conformity to the $D_{CM} = D_0/M^2$ law to hold for molecular weights up to ~200K[70].) The prediction that at equivalent undercoolings the growth rates in range C–C′ are slower than in B–B′ is readily verified by inspection of the pre-exponential factors $\bar{C}_I$ and $\bar{C}_{II}$ in *Figure 11*, which are lower at the higher molecular weights.

Considering the sum of the above, it is reasonable to conclude that at the onset of range C–C′, nonadjacent events in the form of a specified long molecule engaging in multiple temporary attachments with an intervening loop (or loops) on the growth front are beginning to obstruct the steady-state reptation process. This reduces

the growth rate relative to range B–B′ and changes the growth rate law at constant ΔT from $G \propto 1/n_{nw}$ to $G \propto 1/n_z$. Simultaneously, the same class of events begins on entering range C–C′ to cause the surface of the lamella behind the growth front to possess some surviving long pinned loops and trapped cilia, the latter setting the stage for formation of tie chains, all of which depress the degree of crystallinity (*Figure 7b*).

The postulate that multiple attachment with intervening loops of a long chain on the growth front perturbs the local reptation process to an increasing extent with increasing molecular weight is further supported by the fact that regime I → II transitions with clear-cut slope changes close to 2 in plots involving $1/T(\Delta T)$ disappear somewhat above $\bar{M}_{nw} \cong 90.6$K, i.e. after range C–C′ comes to an end. At and above $\bar{M}_{nw} \cong 103$K, i.e. in range D–D′, only irregular spherulites are formed and the observed K_g tends to exhibit a 'mixed' value intermediate between $K_{g(II)} = 0.955 \times 10^5$ deg^2 as for regime II and a modified form of regime III denoted III-A ($K_{g(III\text{-}A)} \cong 1.9 \times 10^5$ deg^2)—see *Figure 7a*, range D–D′ and discussion in Section IV. The disappearance of clear-cut regime I → II transitions is seen in *Figure 7b* to be accompanied by a significantly lowered degree of crystallinity. From a theoretical standpoint, the occurrence of a clearly recognizable regime I → II transition depends critically on the crystal substrate having reasonably free access to molecules capable of steady-state reptation that can be drawn onto it by the force of crystallization. When this access is seriously interrupted by multiply-attached loops on the growth front, the crystallinity will fall sharply and the I → II rate transition will become highly diffuse and/or disappear as is observed (*Figure 7*).

Even a glance at the net overall decline of the growth rates in both regimes I and II with increasing $\bar{n}_{nw}$ and n_z at constant ΔT in the master plots in *Figure 11* allows one to literally visualize the effect of the retardation to crystal growth caused by forced steady-state reptation in the subcooled melt. The constant ΔT leads to a constant average force urging the pendant molecules in the subcooled melt onto the growth front, and at the same time mutes any variation of the growth rate by the nucleation factor $\exp[-K_g/T(\Delta T)]$. Then, only the length of the pendant molecules in the subcooled melt can materially affect the growth rate, which permits a law of the general type $G \propto 1/n$ that is characteristic of forced steady-state reptation to appear. Even though all the specimens in *Figure 11* had a molecular weight far above M_e, there is no indication whatsoever that G_I or G_{II} at constant ΔT varies as $1/M^{3.4}$. This counters the once-held concept that G at constant ΔT varies as the reciprocal of the melt viscosity η.

It is reasonable to conclude from the foregoing that the steady-state forced reptation concept provides at least an approximate explanation of the dependence of the growth rates on molecular weight at constant ΔT in regimes I and II for the PE fractions listed in *Table 2*. An improved treatment might, for example, consider the Rouse modes generated in the chain being reeled through the reptation tube of the type found[132] for DNA. Notwithstanding the possible modifications of the currently adequate $G \propto 1/n$ law, what we see as most important from the standpoint of crystallization is that the steady-state reptation process will begin to give way to the reptation of slack in regime III. Reptation of slack will be discussed after regime III crystallization is verified for PE.

F. Origin and magnitude of the substrate length L: correlation with range of lattice coherence

The proposal by Frank[84] that the substrate length L might be associated with the range of lattice coherence is now examined in the light of our estimate based in part on kinetics that L for the {1 1 0} growth front is within a factor of ~1.5 of 865 Å for melt-crystallized PE. [Recall here that L is based on $\bar{C}_I/\bar{C}_{II}^2$ from kinetics and the value of κ based on ξ_0—see equation (30).] In the discussion to follow, it is assumed that the L for PE single crystals formed from solution is of the same order. This is suggested by the fact that the undercooling $\Delta T_{I \to II}$ at which the I → II transition takes place is only slightly larger[32,83] for solution-grown crystals than for those grown from the melt. The characteristic length D_{110} determined from X-ray line width studies is taken to be a measure of the range of lattice coherence for the {1 1 0} sector.

Typical D_{110} values for solution-grown PE crystals (85°C in 0.05% xylene) run from ~600 Å and 900–1000 Å up to ~1200 Å[133], the last for a preparation subsequently annealed at 124°C. These results suggest an approximate correlation of L from kinetics with D_{110}. Recalling that the solution-grown truncated lozenges have a macroscopic {1 1 0} growth front (*Figure 5a*, left-hand inset) both above and below the I → II transition, it is plausible that this front is divided into sections of mean length L according to the range of lattice coherence. Accepting this, one has a natural explanation for the presence of the I → II rate transition in this system where there is *no* change of crystal type and in which the overall {1 1 0} growth front is always macroscopic.

In assigning D_{110} for melt-crystallized PE, we concentrate on bulk specimens annealed or crystallized at high temperatures corresponding to regime I. This leads to two results: (i) a specimen annealed at 140°C for 29 days[134] giving a D_{110} of ~720 Å and (ii) a specimen crystallized from the melt at low ΔT corresponding to regime I[135] giving a D_{110} of ~390 Å[136]. The first result is close to the L of ~865 Å derived from kinetics, but the second falls somewhat below the anticipated lower bound of ~430 Å. Nevertheless, the sum of the D_{110} results cited above implies that an approximate correlation exists between the L consistent with crystallization kinetics and the range of lattice coherence for both melt- and solution-crystallized PE.

In the case of melt crystallization, one recalls that there is a rather abrupt change of crystal type at the II → I transition, i.e. (truncated crystal, regime II) → (lenticular crystal, regime I) as depicted schematically in *Figure 5a*, left-hand and right-hand insets. As indicated in *Figure 5a*, the lenticular crystal is presumed to have a thin {1 1 0} strip and a very small {1 1 0} growth front[27]. At this writing, the proposed thin {1 1 0} strip in the lenticular crystal has not to our knowledge been observed directly, but there is evidence consistent with the existence of a {1 1 0} growth front of appropriate dimensions. Despite the harsh measures required to isolate single crystals from the melt-crystallized specimens, a *single* bevelled growth front ~1000 Å long, which we take to be the most densely packed, i.e. {1 1 0}, evidently survived for a derivative asymmetrical

lenticular crystal—see bevelled tip in electron micrograph in *Figure 2a* of Toda and Keller[26] for a PE fraction $M_w = 32.1$K crystallized in regime I at 130°C. The clear-cut single growth front just described is typical of what is expected for a crystal deriving at an early stage from a screw dislocation in a parent lenticular crystal of the symmetrical type with two small fronts depicted in the right-hand inset in *Figure 5a*[137]. The asymmetrical derivative 'lenticular' crystal with the single front ~1000 Å long, which one notes is on the order of the range of lattice coherence D_{110} as well as our 'kinetic' estimate of L, may well be a contributing or even the principal 'leading' {1 1 0} growth front for PE crystallized from the subcooled melt in regime I. The condition $n_L > \nu_s$ is handily met, and the substrate is large enough to sustain steady-state growth in regime I up to high T_x as is observed. (That a screw dislocation could occur in a symmetrical lenticular crystal formed in the melt in regime I leading to an asymmetrical derivative crystal with a large growth front had been shown previously by Bassett *et al.*[25]). The growth tips on the symmetrical lenticular single crystals derived from the melt, i.e. those without screw dislocations, appear to be considerably smaller than ~1000 Å and may represent a species of slower growing crystals according to the discussion following equation (31) in Section II.H. Should such a fine-tipped lenticular crystal develop a screw dislocation with a larger growth front, an abrupt increase in G_I could occur. While not treated, it has occurred to the authors that the {2 0 0} sectors in the regime I symmetrical lenticular crystals may conceivably be subject to *cumulative* strain, which would begin to limit their size and at the same time promote their tendency to develop screw dislocations.

G. Change of crystal type and curved {2 0 0} edges: dominance of the {1 1 0} growth front in regime I and II kinetics

The particular crystal type (truncated lozenge or lenticular) that appears in melt-crystallized PE of intermediate molecular weight is determined by magnitude of the velocity of advance h as defined in *Figure 5a* as it relates to the substrate completion rate g_{200} of the {2 0 0} sector. Important calculations by Mansfield[30,88] and by Toda[118] have shed light on the {2 0 0} curved edge and overall crystal shape problems. Mansfield solved the Seto–Frank differential equations (moving boundary condition) for the situation where h was *less* than g_{200}. The result was a truncated lozenge with macroscopic {1 1 0} faces and a curved {2 0 0} edge which was the section of an ellipse. Subsequently, Toda solved the Seto–Frank equations with the moving boundary condition for the case where h was *greater* than g_{200}; the result corresponded to a lenticular crystal where the {2 0 0} edge was almost straight near the very small {1 1 0} growth tips, but more curved away from the tips. Thus, the formation of a truncated lozenge depends on the condition $h < g_{200}$ and that of a lenticular crystal on the condition $h > g_{200}$. The transition of crystal type occurs when $h = g_{200}$. As implied earlier, the rather abrupt change of crystal type predicted to occur at $h = g_{200}$ could be implicated in the melt-crystallized PE case in causing the I → II rate transition to appear to be sharper than is predicted by Frank's treatment. While the actual sharpness of this transition is experimentally somewhat uncertain, it is evident that virtually pure regime I and regime II behaviour obtains within ~1° or so on either side of the transition region.

The velocity h depends mainly on G_{110}, and it emerges that g_{200} must not only be small to meet the condition $h \simeq g_{200}$, but must also fall markedly with increasing T_x to effect the rather abrupt change of type (truncated lozenge) → (lenticular crystal) that is observed in melt-crystallized PE. An expression of the conventional form $\exp(-Q_D^*/RT) \times \exp(-q_{200}/kT)$ is unable to reproduce the g_{200} required to predict the change of crystal type or the shape of the {2 0 0} edges. It is evident that an additional factor is present that further retards g_{200}. Thus, the substrate completion rates on the {1 1 0} and {2 0 0} growth fronts behave very differently. One notes also that the regime of growth can be different on these two growth fronts[32].

In treating the case of truncated lozenge with curved {2 0 0} edges formed in dilute solution, Miller and Hoffman[32] (hereafter MH) proposed that lattice strain resulting from mutual repulsion of the folds in the {2 0 0} sectors was a major source of the additional retardation of g_{200}. The lattice strain effect was embodied in the parameter σ_s, which appeared in the additional retarding factor that allowed the 'experimental' g_{200} to be closely reproduced. (The 'experimental' g_{200} was obtained from the growth rate and crystal shape data of Organ and Keller[83] as treated with Mansfield's solution[30,88] for $h < g_{200}$.) A value of σ_s on the order of 1.2–1.7 erg cm^{-2} gave not only $g_{200}(T_x)$ but also a good account of the change of overall shape with T_x of the truncated lozenges including that of the elliptical-section {2 0 0} edges. The treatment also predicted that the melting point for the {2 0 0} sector was below that of the {1 1 0} sector (see later). Significantly, the applicability of the MH treatment came to an end well above the I → II transition at a T_x that was very slightly below that where g_{200} was equal to h, implying that another crystal type might prevail at higher T_x where $h > g_{200}$. It is now understood through the subsequent work of Toda[118] that this latter condition leads to a lenticular crystal. The Organ and Keller experiments did not cover this higher T_x range. There is no 'δ catastrophe' associated with either the {1 1 0} or {2 0 0} growth fronts in the MH treatment.

Additional features of interest derive from the MH analysis. Among these is information on the fold energies that relate to the dominance of the {1 1 0} growth face in PE crystallization. The work of chain folding, q_{200}, for an isolated {2 0 0} fold was found to be 4.1 ± 0.5 kcal mol^{-1}. However, the *total* work of chain folding, W_{200}, which included effects expressed in terms of σ_s arising from fold–fold repulsions in a {2 0 0} sector that expanded and thus strained the underlying lattice, came to 7.3 ± 0.3 kcal mol^{-1}. This is larger than the work of chain folding, $q_{110} = 4.9$ kcal mol^{-1}, for the relatively unstrained {1 1 0} sector. The finding that $W_{200} > q_{110}$ provides a simple rationale for the kinetic dominance of the {1 1 0} growth front in crystallization of PE.

Another feature of the MH analysis was that the lateral surface free energy σ was smaller for crystallization from solution (5.8–7.4 erg cm^{-2}) than that from the melt (11.8 erg cm^{-2}). The solution data obeyed the relation $K_{g(I)} \simeq 2K_{g(II)}$, but the K_g's were both smaller than those for melt crystallization thus leading to the smaller σ values. Modification of equation (1), which applies only under 'theta' conditions, is evidently required if σ is to be predicted for crystallization from

dilute solution. The lessening of σ with increasing dilution has been seen in PPVL/PVF_2 blends, and tentative reasons for this effect have been discussed[138].

The concept of lattice strain in the {200} sector has independent support. First, as discussed by Marand[139], there is clear experimental evidence[140] for lattice strain in the {200} sector—the orthorhombic lattice in this sector is distorted and expanded relative to that of the {110}. This effect is logically assigned to mutual repulsion of the {200} folds. Second, based on the observed lattice expansion in the {200} sector, Marand has by molecular energy calculations[139] estimated *a priori* a value of the lattice strain parameter σ_s which coincides rather well with that which fits the growth rate data and allows prediction of the curved {200} edge and the change of shape of the truncated lozenge crystals as a function of T_x. Thirdly, we note that the MH finding that $W_{200} > q_{110}$ does not stand in isolation. Recent molecular energy calculations by Schmieg *et al.*[141] for an *array* of {200} folds, including the fold energy itself plus contributions from fold–fold repulsion as well as stem effects, indicated that $W_{200} > q_{110}$. The opposite result was obtained for an isolated {200} fold, but this does not correspond to the real crystal. Lastly, we note that Bassett *et al.*[142,143] and Harrison[144] established that the {200} sectors in truncated lozenges melted lower than did the {110} sectors—an indication of a difference in 'perfection' of the sectors in general accord with our predictions. The results of Organ and Keller[145] indicate that the melting point difference between the {110} sector and the {200} sector is subdued for lozenges formed at high T_x where the crystals are thicker. This implies that σ_s decreases somewhat with increasing lamellar thickness as predicted by the molecular energy calculations of Marand[139]. The MH model can be extended to include the situation where the {200} growth face is no longer ideally serrated so that a small σ effect appears for the first stem in addition to the σ_s term. With this, the barrier for the first stem can, if required, be more firmly differentiated from that associated with a stem involved in substrate completion.

The lattice strain approach to the curved {200} edge problem in folded chain PE lamellae has been criticized[27,119,146]. While we shall deal with one of these elsewhere, it is useful here to comment on the other. In this case[27,119], the objection begins with the undoubted fact that extended-chain PE crystals can also exhibit curved {200} sectors. It is then argued that with no folds present, extended chain systems have no source of lattice strain so that some other molecular mechanism must be the cause of the retardation of g_{200} in the extended-chain case; this is then taken to render doubtful the lattice strain approach for folded systems. While we do not discount the possibility of a different mechanism for the origin of curvature in extended-chain crystals, we do note that such crystals are (weakly) sectored[147] and exhibit small, though definite, lattice expansion effects attributable to repulsion of the $-CH_3-$ end groups[140] which are, of course, larger than is a $-CH_2-$ group. Whatever the cause of curved edges in extended-chain systems, significant lattice strain is undeniably present in the {200} sector in chain folded PE lamellae and the authors know of no basic objection to taking this into account in nucleation theory. While extensions are clearly possible along the lines already noted, the authors believe that the MH treatment as it stands brings out within the framework of surface nucleation concepts the important elements of how this strain causes major differences in the crystallization behaviour and shape of the {200} sector as compared with that of the relatively unstrained {110} sector.

H. Prediction and verification of regime III behaviour in melt-crystallized PE: reptation of slack

Having established a reliable value of $C_0^{1/2} \cong 664$ for use in equation (35) for the function S_k/a_0 from the analysis of regimes I and II, it is readily determined with the data in *Table 1* that S_k/a_0 takes the numerical form

$$S_k/a_0 = 2.863 \times 10^{-2} T^{-1/2} e^{-1233/T} e^{+0.955\times10^5/T(\Delta T)} \tag{44}$$

This expression, which reflects the mean distance between primary nuclei on the substrate, is valid for range B–B′ and probably holds with reasonable accuracy for somewhat higher molecular weights.

Barham[121] and Martinez-Salazar, Barham, and Keller[79] have given values of G at low T_x in regime III using a special optical technique involving micron-sized droplets for a PE fraction very close in molecular weight (NBS standard fraction $M_w = 32.1$K) to our fraction 4. Accordingly, we calculate S_k/a_0 employing ΔT as measured from $T_m = 416.81$ K for fraction 4 and consider these samples together. The result is shown in *Figure 10b*. Note that, as required, S_k/a_0 is exactly equal to n_L at $\Delta T_{I\to II} = 16.02°$, both being 190. The quantity S_k/a_0 falls rapidly and attains the value $S_k/a_0 = n_{III} = 2.5$ at $\Delta T_{II\to III} = 22.9°$, $T_{II\to III} = 120.7°$C, and $S_k/a_0 = n_{III} = 2.0$ at $\Delta T_{II\to III} = 23.4°$, $T_{II\to III} = 120.2°$C.

With a theoretical estimate of $\Delta T_{II\to III}$ in hand, the numerical expression for G_{III} can be generated. First we recognize that $K_{g(III)}$ is close to, but perhaps not precisely equal to, $K_{g(I)} = 1.91 \times 10^5$ deg^2. (Recall here that because chain folds in more than one lattice plane are likely involved in regime III, $K_{g(III)}$ may not be exactly the same as $K_{g(I)}$.) Next it is noted that at $T_{II\to III}$, $\Delta T_{II\to III}$, G_{II} must be equal to G_{III}. Constructing this equality with the help of equations (29a) and (33a), it is found that the pre-exponential factor for regime III comes to

$$C_{III} = C_{II} e^{K_{g(II)}/T_{II\to III}(\Delta T_{II\to III})} = 2.326 \times 10^{11} \text{ cm s}^{-1} \tag{45}$$

for the case $S_k/a_0 = n_{III} = 2.0$. The pre-exponential factor C_{III} is 2.88×10^{11} cm s^{-1} for $S_k/a_0 = n_{III} = 2.5$. For $S_k/a_0 = 2.0$, the theoretically derived expression for G_{III} valid at $T_x \leq 120.2°$C in numerical terms is

$$G_{III}(\text{cm s}^{-1}) \cong 1.745 \times 10^8 e^{-5736/RT_x} e^{-1.91\times10^5/T_x(\Delta T)} \tag{46}$$

where the pre-exponential $C_{III}/(2/3)\bar{n}_{nw} = 1.745 \times 10^8$ cm s^{-1} is for the case where $\bar{n}_{nw}$ is 2000 as for fraction 4. Note that C_{III} and $K_{g(III)}$ in the above expressions are based entirely on numerical values of properties such as $K_{g(I)}$, $K_{g(II)}$, C_{II}, and $C_0^{1/2}$ derived from our analysis of regimes I and II. Though the first theoretical estimate[4] of $T_{II\to III}$ and G_{III} for PE was based on a similar physical approach, it contained certain arbitrary parameters which are replaced in the present treatment by the definite quantity $C_0^{1/2}$. Nevertheless, the first estimate of $T_{II\to III}$ was within 1°C of that given here.

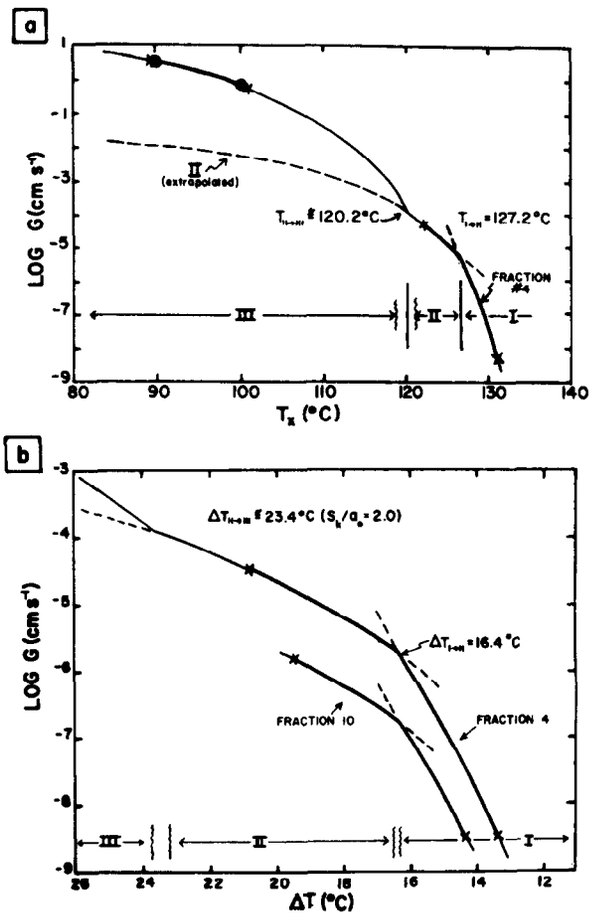

Figure 13 *Regime III crystallization in melt-crystallized PE fractions and relationship to regimes I and II.* (a) Log G vs. T_x for fraction 4 ($M_w = 30.6$K) showing fit of predicted regime III behaviour with growth rate data of Barham[121] for $M_w = 32.1$K fraction at 90° and 100°C. Heavy solid lines between '×' marks refer to range where growth rate data are known from experiment; thin lines theoretical (see text). (b) Detail of log G vs. ΔT for fractions 4 and 10 showing effect of molecular weight in regimes I and II and onset of regime III (cf. *Figure 3b*). Heavy solid lines and thin lines have same meaning as above

Figure 13a gives a plot of log G vs. T_x for fraction 4 showing regimes I and II, together with the growth rate in regime III beginning at 120.2°C predicted with equation (46) for $S_k/a_0 = 2.0$. The data points obtained at 90°C and 100°C in droplet experiments[121] are both matched to within 11% or better (*Table 3*). Because the error inherent in the data points is about a factor of 2–3, this does not uniquely determine S_k/a_0, but it is still reasonable to believe that the true value is close to 2.0 at $\Delta T_{II \rightarrow III}$. The dashed line beginning at $T_x = 120.2$°C is that calculated for regime II as extrapolated to lower temperatures—it misses the data point at 90°C by more than two orders of magnitude and that at 100°C by almost as much. Confronted by the decidedly superior fit of the low temperature results by the predicted regime III curve, one is assured that regime III crystallization occurs in melt-crystallized PE. The recent thermal bulk rate data on specimens of PE fractions with the mass of a few milligrams corresponding to molecular weight range B–B′ carried out by Fatou *et al.*[148] actually closely traverse the transition region and directly indicate the presence of a change of slope in the growth rate of the predicted type in the II → III transition region. This work also shows that $T_{II \rightarrow III}$ is close to that predicted earlier[4] as well as here for a fraction in the range 30–32 K. Considerations based on the data fit at low T_x depicted in *Figure 13a* plus the results of Fatou *et al.* imply that the overall slope change in a plot of $\ln G + Q_D^*/RT$ vs. $1/T\Delta T$ for this transition is close to 2. For PE fractions $M_w = 32.1$K and 74.4K, clear evidence of the II → III transition recently has been found by optical microscopy wherein spherulite growth rates were observed at temperatures down to as low as 114–115°C (J. P. Armistead, to be submitted). In sum, it is evident that a regime II → III rate transition exhibiting the behaviour originally predicted for it occurs in PE fractions of intermediate molecular weight.

A significant feature of the surface nucleation model depicted in *Figures 1* and *3* is that it leads in a straightforward manner to the II → III transition as well as the I → II transition. The C_0 and $K_{g(II)}$ values derived from the analysis of the I → II transition, through application of equation (44) for S_k/a_0, give a satisfactory prediction of the onset and general aspects of the II → III rate transition. The treatments of the I → II and II → III rate transitions are interdependent and mutually consistent, arising as they do in a direct way from the same surface nucleation model.

The alternative 'entropic barrier' models featuring surface roughening noted earlier in Section II.B[42–45], which set aside the concept of a surface nucleus of the type employed here, appear to be incomplete in some important aspects. They are able to give some account of the temperature dependence of the lamellar thickness[44,45], but do not for example cover the effect of changing molecular weight and currently seem to be unable to describe clearly the regime transition sequence I → II and II → III with increasing ΔT that is such a prominent feature of the growth rate behaviour of PE. As treated here, surface nucleation theory deals quantitatively with these effects and, as will be seen shortly, it leads to a quantitative description of the behaviour of the initial lamellar thickness as well.

Observe in *Figure 13a* that, counting the data point at $T_x = 90$°C ($G_{III} \cong 3.5\,\text{cm s}^{-1}$) obtained with droplet experiments, the growth rate of melt-crystallized PE for specimens similar to fraction 4 are known for nine decades in G. The growth rate at the highest T_x (130.3°C) employed for fraction 4 was $G_I \cong 3.5 \times 10^{-9}\,\text{cm s}^{-1}$. The existence of all three regimes in the molecular weight range involved is assured and the theory presented here covers them all. Note that the temperature range where regime II occurs in melt-crystallized PE is only about 7° long.

Figure 13b gives log G vs. ΔT for fraction 4 showing regimes I and II, together with the predicted onset of regime III for $S_k/a_0 = 2.0$ in some detail. To illustrate the effect of increasing molecular weight, fraction 10 is also included. In each case, the thin solid lines are calculated from the theoretical expressions for G_I, G_{II}, and G_{III}, as are the $T_{I \rightarrow II}$ and $\Delta T_{II \rightarrow III}$ values. The heavy solid lines in regimes I and II indicate the temperature range covered by the original growth rate data of HFRL[77].

The regime II → III transition has been seen in a considerable number of melt-crystallized polymers, including poly(oxymethylene), POM[4], poly(pivalolactone), PPVL[149], *st*-poly(propylene), *st*-PP[150], and *it*-poly(propylene), *it*-PP[151], the latter summarizing the results of many investigations and employing a T_m in the analysis to obtain $K_{g(II)}$ and $K_{g(III)}$ that was within 1° of

that subsequently verified by others[152]. All three regimes have been shown to be present in polymers other than PE. Early examples include *cis*-1,4-polyisoprene, natural rubber, by Phillips and Vantansever[153] and poly(3,3′-dimethylthietane) by Lazcano *et al.*[154], the latter being supported by many data points in a plot of $\ln \tau_{1/2}^{-1}$ vs. $1/T(\Delta T)$. Here, $\tau_{1/2}$ is the time required for one-half of the crystallinity to be attained. Recently, all three regimes were identified in poly(ethylene oxide), PEO, by Cheng *et al.*[155,156]. In some of the above cases, the authors have in addition to the customary plots involving $1/T(\Delta T)$ [or $1/T(\Delta T)f$] also emphasized the reality of the II → III rate transition by direct plots of $\log G$ vs. T_x as has been done here for PE. Use of both types of representation is a safeguard against incorrectly claiming a I → II or II → III transition based solely on a $\ln G + Q_D^*/RT$ vs. $1/T(\Delta T)$ or $1/T(\Delta T)f$ plot that happens to be based on an erroneous melting point and thus an incorrect ΔT scale—the transition should be evident in a $\log G$ vs. T_x graph as well as one involving the reciprocal of the undercooling. The II → III transition can, in principle, occur near the maximum in the growth rate and, in such cases, it can be more difficult to be certain of its presence because of possible uncertainties in the form of β. Despite this, there are good reasons for suspecting that such an effect occurs near the maximum in $G(T)$ for poly(phenylene sulfide), PPS[157] as implied by the $\log G$ vs. T_x data. It has been contended[158] that regime III has neither a theoretical, a computational, nor an experimentally sound basis. This cannot be accepted as a generally correct statement. Having herein presented a detailed case for regime III and the II → III transition in PE on all of the above bases, and noted solid experimental evidence for this regime in PE as well as in other polymers by a number of investigators, it would appear that no convincing general case can be made against its existence.

A check on the consistency of the theory given for regime III for PE is to note that the ratio of the pre-exponential factors for regime I and regime III is, according to equations (27b) and (33b), given by $C_I/C_{III} \cong n_L/n_{III}$ where a relatively minor temperature correction factor is omitted. With n_{III} taken as 2.0, we earlier found that C_{III} was $2.326 \times 10^{11}\,\mathrm{cm\,s^{-1}}$. Then, with $\bar{C}_I = 2.10 \times 10^{13}\,\mathrm{cm\,s^{-1}}$ one has $C_I/C_{III} = 90.3$ whereas n_L/n_{III} is $190/2 = 95$. An interesting point here is that if we had not known n_L, but had experimental values of C_I and C_{III}, we could have estimated n_L by assuming a reasonable value for n_{III}.

It is worth recording a practical point related to the engineering properties of PE that has to do with regime III crystallization. When slabs of PE are cooled from the melt after moulding, it is of interest to know how to model the development of crystallinity at various positions in the slab, which is related to the temperature profile. Keith and Loomis[159] found that knowledge of regime III was important to such modelling, since on entering this regime rapid crystallization with considerable evolution of heat took place—this tended to maintain the interior of the slab at a temperature just somewhat below $T_{II \to III}$. The modelling was successful but would not have been so had the existence of regime III been unknown[160]. This work shows how crystal growth rate studies can assist the modelling of practical systems containing crystallizable polymers. It is to be expected that an extension of this approach will in the future see application in the fabrication of polymer composite structures involving such polymers.

We consider now the question of the onset of reptation by 'slack'. As mentioned previously, at some point in regime III, it must be expected that, because of the rapidly increasing nucleation rate, the transport of segments to the growth front will occur mostly through reptation of this type. When this occurs, the transport process and hence the crystal growth rate will, at fixed ΔT, tend to become less dependent on molecular weight in contrast to the behaviour defined here as steady-state forced reptation of the near-ideal or perturbed type characteristic of regimes I and II where $G \propto 1/n$ (*Figure 11*).

In the near-ideal steady-state case, the 'reeling in' rate in both regimes I and II as given by $\bar{r} = g(l_g^*/a_0)$ changes but little with T_x—recall the earlier calculation for $\bar{n}_{nw} = 2000$ showing a variation of $\bar{r}$ of only $5.5\text{–}7.1 \times 10^{-3}\,\mathrm{cm\,s^{-1}}$ from the lowest T_x in regime II to the highest T_x employed in regime I. Such low reeling rates are easily sufficient to permit fairly long substrate runs in these regimes, and are consistent with the ability of the system to attain relatively high p_{tf} and p_{ar} values.

The situation is radically transformed when the system is crystallized in the body of regime III—the reeling rate is then given by $\bar{r}_{III} \simeq a_0 i l_g^*$, which as shown previously must begin to have an effect at $\Delta T = 24.4°$, $T_x = 119.2°C$ for $\bar{n}_{nw} = 2000$, and extremely high reeling rates then obtain deep in this regime. For example, at $T_x = 100°C$, $\Delta T = 43.6°$, i is $\sim 1.46 \times 10^{14}$ stems $\mathrm{s^{-1}\,cm^{-1}}$ as estimated by $i = G_{III}/a_0 b_0 n_{III}$ from equation (32) using $n_{III} = 2.0$ and the experimental G_{III} of $0.55\,\mathrm{cm\,s^{-1}}$ from *Table 3*; this leads directly to a reeling rate of $\bar{r}_{III} \simeq 6.9\,\mathrm{cm\,s^{-1}}$! (The foregoing method of obtaining i deep in regime III does not involve a long extrapolation as does equation (41b), the latter giving a slightly higher result.) Clearly, such a high reeling rate is unrealistic in terms of steady-state reptation where the entire pendant chain resists the force of crystallization. Since lamellar crystallization occurs at 100°C in regime III, albeit with but a minimal degree of 'tight' folding, it is evident that only a short section of chain (slack) toward the end of the tube can be drawn onto the substrate at the high rate cited. The n_{III} of 2.0 employed above (which corresponds to a very limited 'substrate run') is consistent with a roughly equal mixture of singlet and doublet stems with intervening non-adjacent events corresponding to $p_{tf} \simeq 1/2$; also implied is a mean cluster size of $\bar{\nu}_c = 1.5$, which means with equation (53b) to be given later that p_{ar} can be $\sim 1/3$. The p_{tf} just noted is already known to be close to correct (*Table 3*) and the p_{ar} of $\sim 1/3$ is within the bounds suggested by neutron scattering data for PEH–PED crystallized in regime III (Section V.I). A singlet stem corresponds to $n_s = 82$ and a doublet to $n_s = 164$ $-CH_2-$ units at 100°C ($\Delta T = 43.6°$) as calculated with equation (48b) for l_g^* to follow shortly. These n_s values represent the number of $-CH_2-$ units that must be supplied by reptation of slack to form the crystalline stems.

How to explain the extraordinary reeling rate of $\sim 6.9\,\mathrm{cm\,s^{-1}}$ at 100°C? The answer lies in recognizing that *lateral* as well as longitudinal motions are allowed at or just outside the end of the reptation tube on a length scale comparable to the distance (*ca.* 340 Å corresponding to $n_e \simeq 267$) between entanglements. In simplified terms, one can envisage the tube as being flared like a

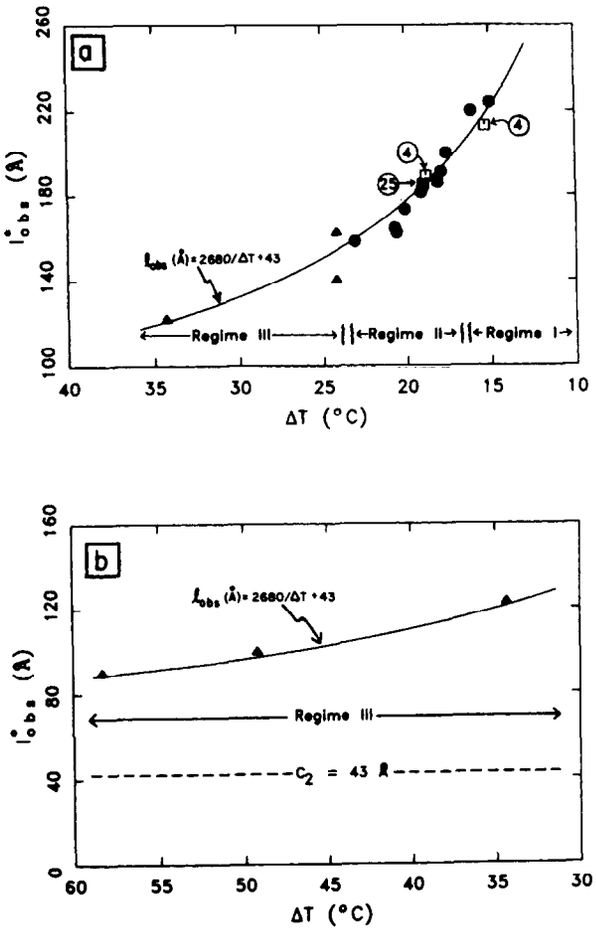

Figure 14 *Observed initial lamellar thickness vs. undercooling for melt-crystallized PE in regimes I, II, and III.* Data of Barham[79]: (●) real-time SAXS and (▲) Raman LAM, both for NBS $M_w = 32.1$K standard fraction. Data of HFRL[77]: fraction 4, $M_w = 30.6$K and fraction 25, $M_w = 11.7$K (open squares). Circles with numerals give fraction number. MW range is B–B′ except for fraction 25 which is at upper part of range A–A′. Note that a single expression for l_{obs} fits all three regimes as predicted by nucleation theory

funnel at either end thus permitting lateral as well as longitudinal motion on a considerable scale within this limited region. Then, following a treatment relevant to this situation of enhanced motion at the end of a chain by DiMarzio *et al.*[65], the reeling rate may be calculated as

$$\bar{r}_{slack} = {}_1\bar{f}_c/0.46\xi_0 n_s^{1/2} \qquad (47)$$

With the ξ_0 of equation (21) and ${}_1\bar{f}_c$, both fully corrected to 100°C, one finds $\bar{r}_{slack} \simeq 6.0\,cm\,s^{-1}$ for $n_s = 82$ and $4.4\,cm\,s^{-1}$ for $n_s = 164$. Being well within an order of magnitude of the estimated actual reeling rate of $\sim 6.9\,cm\,s^{-1}$, these results indicate how reptation of slack can be rapid enough in PE to allow lamellar structures with the minimal degree of 'tight' folding of ~0.51 and a p_{ar} of ~1/3 to form deep in regime III. This approach has the advantage of making it easier to understand how a molecule can shuttle back and forth across the substrate during stem deposition. Disturbances are to be expected beginning somewhat below 90–100°C, but at higher T_x in regime III reptation of slack will be fully active and readily allow small chain folded clusters consistent with the Gambler's Ruin lower bound to form. There is evidence from droplet experiments that unexpectedly low growth rates occur at ~60°C and below[120]. This may be the result of homogeneous nucleation which has an enormous rate[3] at this temperature; such massive spontaneous nucleation in the subcooled melt could tend to at least partially block normal crystal growth.

Though a similar process allowing a rapid uptake of a short section of slack may occur initially in regimes I and II, this will not significantly alter the main features of the forced steady-state reptation effect. In these regimes, the force of crystallization has time to propagate through the much longer main part of the chain in the reptation tube, which leads to the observed $G_{I,II} \propto 1/n$ behaviour at constant ΔT illustrated in *Figure 11*.

The theory is clear on the points that for an appropriate set of moderate molecular weights, steady-state reptation with its $G \propto 1/M$ at constant ΔT law should hold in the body of regime II and that slack should begin to be employed after the onset of regime III. With further decrease in T_x, G at constant ΔT would then at one point in regime III pass through a $1/M^{1/2}$ stage as the effect of slack strengthened—at least a few polymers are known to behave in close to this manner near the maximum in the growth rate—and at even lower T_x, reptation of slack should predominate and G at constant ΔT become independent of M or nearly so. The above predictions hold for polymers with a sufficiently low friction coefficient which exhibit the I → II and II → III regime transitions. The subject of reptation of slack will appear again in Section IV where it will be shown that, for sufficiently high molecular weights, it tends to become the dominant mechanism for transport of chain segments to the surface nucleus over a wide T_x range.

I. Initial lamellar thickness

It remains to examine the behaviour of the initial lamellar thickness as a function of undercooling for lamellae formed in melt-crystallized PE fractions. The emphasis will be on two very similar fractions of moderate molecular weight (range B–B′) and, for comparison, one of lower molecular weight (range A–A′). All three regimes will be covered. Because of the occurrence of chain folding, crystalline polymers are evidently unique in allowing what is essentially one dimension of a surface nucleus, namely l_g^*, to be directly observed over a wide range of undercoolings. An outstanding example of this behaviour follows.

The interlamellar spacings measured by SAXS techniques are generally analysed in terms of the expression

$$l_{obs} = C_1/(\Delta T) + C_2 \qquad (48a)$$

which is based on nucleation theory through equations (9). From equations (9), the theory has C_1 as $2\sigma_e T_m/\Delta h_f$ and gives one of the major components of C_2, namely, $\delta \cong kT/b_0\sigma$. As mentioned earlier, the other components of C_2 consist of a 'rough fold surface' term which is part of the more exact form of l_g^*, and a term accounting for the thin amorphous or quasi-amorphous layer of cilia and non-adjacent structures of thickness d_a that reside on either 'fold' surface and contribute to the overall interlamellar spacing l_{obs}. The components of C_2 will be discussed shortly in some detail. Meanwhile we shall show that equation (48a) describes the variation of l_{obs} with ΔT, which is that predicted by equations (9). The fit of the experimental data provides an independent confirmation of the value of σ_e.

Figure 14 shows a plot (solid line) of l_{obs} vs. ΔT as

calculated with

$$l_{obs}(\text{Å}) = 2680/(\Delta T) + 43 \qquad (48b)$$

where C_1 was based on a σ_e of 90 erg cm^{-2}, Δh_f of 2.8×10^9 erg cm^{-3} (orthorhombic form) as listed in *Table 1*, and $T_m = 144.2$°C, the latter being the melting point of the NBS standard fraction $M_w = 32.1$K determined from T'_m vs. T_x and T'_m vs. $1/l$ plots by Barham[120,121]. The molecular weight corresponds to range B–B′.

The l_{obs} data in *Figure 14* were obtained by Barham[121] for the aforementioned standard fraction, which is very similar to our fraction 4. The points designated by solid circles (●) were determined during melt crystallization in regimes I and II using synchrotron radiation in real-time SAXS studies (sweep time 1 s). Because of the long induction period, these SAXS data are believed to be essentially free of the effects of isothermal thickening[161] and, accordingly, the SAXS data are taken to reflect rather closely the actual stem length. The stems are slightly tilted (typically ~19°) (VMFM[78]) which in effect lengthens them, but this is largely compensated by the thin amorphous layers of net thickness $2d_a$. Additional though less precise l_{obs} values on the $M_w = 32.1$K fraction designated as solid triangles (▲) were obtained by Barham *via* Raman LAM studies on micron-sized droplets which were all in regime III (*Figure 14*). Not shown is an LAM data point at 20°C ($\Delta T \simeq 124$°) that also conforms to equation (48b). All the LAM data are free of lamellar thickening effects. The Raman LAM method gives the actual stem length irrespective of the angle of tilt. The LAM data do not register the amorphous component, but may reflect some contribution from those colinear parts of the stems that reside in the rough folds. These low temperature data evidently fit quite well on the line described by equation (48b) with no evidence of a discontinuity.

Based on Barham's LAM data, there is no indication of a 'δ catastrophe' in melt-crystallized PE even at the very large ΔT of 124°. The lamellae formed in the droplets in this experiment were likely mostly homogeneously nucleated at a somewhat higher temperature where such initiation is already very rapid[3], and no claim is made that the l_{obs} value associated with this run involves isothermal conditions. Nevertheless, the result is still generally consistent with the 'low ψ' feature of the deposition of the first ($\nu = 1$) stem associated with the theory for l_g^* and σ outlined in Sections II.B and II.C. The rate of homogeneous nucleation is negligible at undercoolings $\Delta T \sim 55$° and lower for PE[3].

Observe that the fit of the l_{obs} data, including both the SAXS and LAM results, gives a C_1 corresponding closely to a σ_e of 90 erg cm^{-2}, which is well in line with the σ_e of 89.3 erg cm^{-2} estimated by Barham from a T'_m vs. $1/l$ plot *via* use of equation (7a). The good agreement between the fold surface free energy σ_e as determined from a kinetically-based formula through equation (48a), on the one hand, and a thermodynamic one *via* equation (7a), on the other, justifies the σ_e listed in *Table 1* and stands as an important point of consistency in the overall treatment. As noted earlier, recent molecular energy calculations[55] based on traverses between adjacent stems in the orthorhombic lattice lead to a σ_e in the vicinity of 90 erg cm^{-2} for {1 1 0} folds.

In accord with the nucleation approach, there are no breaks in the l_{obs} vs. ΔT data as the regimes are traversed despite the changes in slope of the growth rate that occur on either side of each regime transition. It is evident that this aspect of the theory also corresponds closely to experiment.

In addition to Barham's l_{obs} data, two data points for fraction 4, also of range B–B′, that were derived from the SAXS investigations of HFRL are shown in *Figure 14*. The higher l_{obs} point is for $T_x = 128.3$°C, $\Delta T = 15.3$°, $l_{obs} \cong 213 \pm 14$ Å and the lower one is for $T_x = 124.8$°C, $\Delta T = 18.8$°, $l_{obs} = 189 \pm 5$ Å. The l_{obs} values just quoted were estimated as $(L_1/2 + L_2)/2$ where L_1 is the strongest SAXS Bragg reflection representing an almost doubling of the lamellar thickness of the mass of the older lamellae in the sample that had thickened—and L_2 is the weaker and broader reflection resulting from the less prevalent new lamellae that had not undergone isothermal thickening. Note that the ratio L_1/L_2 is close to two, which confirms the origin of the thickening factor $\gamma \cong 2$ observed from the slope of T'_m vs. T_x plots for PE.

We note further an l_{obs} data point obtained by HFRL for a fraction whose molecular weight is at the upper end of the low molecular weight region A–A′ where the 'quantization' effect in Regime I is still apparent but beginning to die out (see later). This is fraction 25 of range A–A′ to be treated in Section V, $M_n = 11.0$ K, $M_w = 11.74$ K. For the SAXS work, the fraction was crystallized in regime II at $T_x = 122.0$°C, $\Delta T = 18.9_5$°. The experimental value of l_{obs} estimated as above from L_1 and L_2 is 185 ± 1 Å; the value calculated from equation (48b) is 184.4 Å (*Figure 14*). This provides some confidence in applying equation (48b), including the use of a C_2 of ~43 Å, at the upper end of range A–A′. This will assume some importance in the treatment to be given subsequently of the quantized chain folding effect in range A–A′.

The foregoing results for σ_e and C_2 for melt-crystallized PE coincide quite closely with those found for PE single crystals, also with an orthorhombic unit cell, formed in dilute solution. Based on the l_{obs} vs. ΔT data of Lieser and Fischer[162] for PE single crystals formed in three different solvents (tetrachloroethylene, xylene, and *n*-octane), a value of σ_e of 91 erg cm^{-2} is readily calculated which is similar to that given above for the melt, and C_2 was 43 Å (ref. 3, p. 585). The studies of Korenaga *et al.*[163] show that σ_e for PE single crystals formed from dilute solution over a ΔT range in toluene, xylene, tetralin, *n*-octane, and *n*-hexadecane averages to 90.4 ± 5.0 erg cm^{-2}. Thus, for single crystals formed in dilute solution as well as in melt-crystallized PE lamellae, the undercooling ΔT, acting according to the term $C_1/(\Delta T)$ with $\sigma_e \cong 90$ erg cm^{-2}, controls the variation of the initial thickness of the chain-folded entities present. (This is unaffected by the fact that σ is different in the two cases.) It is also worth noting that the degree of crystallinity of PE crystals from dilute solution is typically 0.85 ± 0.05[164,165], which is similar to that for melt-crystallized fractions in the upper part of range A–A′ and range B–B′ (*Figure 7b*).

J. Origin of C_2 and nature of fold surface

We now take up the question of the make-up of the constant length C_2 in the practical expression for l_{obs} as given in equation (48b), which has just been shown to apply quite well in the upper part of molecular weight range A–A′ and in the body of range B–B′. A

consideration of the components that comprise C_2 will provide insights concerning the nature of the 'fold' surface and the amorphous or quasi-amorphous interfacial zone associated therewith. We shall consider below the nature of the contributions to C_2 for regime I and the upper part of regime II, which emphasizes the more precise real-time SAXS results, and where there is a theoretical background deriving from the nucleation-based treatment of Lauritzen and Passaglia (LP)[10] that takes into account fluctuations of fold period during substrate completion. The fluctuations lead to roughness of the fold surface, which contributes to C_2.

The LP theory has its mathematical complexities that beckon us to a semiempirical form of discussion, but the physical ideas are clear enough and it is these that we wish to convey together with some approximate numerical estimates of the contributions to C_2. A highly significant result of the LP theory is that for regime I and the upper part of regime II, it justifies the existence of a constant mean value of l_g^* for long substrate runs.

The LP model assumes sharp adjacent re-entry folds that are associated with stems of varying length $l_i, l_j, \ldots$ that are put down on the substrate in sequence. The resistance to a fold protruding too far above the mean fold period of the previously-formed 'averaged' substrate is caused by the exposed lateral surface of such a fold. Thus, the lateral surface free energy σ plays a major role in determining the roughness of the fold surface, the larger σs giving the smoother surfaces. Such a system has an *equilibrium roughness* dependent on the absolute temperature; this component of C_2, which we denote $2d_{eq}$, is relatively small and falls only slowly and monotonically as T_x is lowered. For a value of σ similar to that cited in *Table 1*, $2d_{eq}$ comes to *ca.* 6 Å, i.e. a d_{eq} of *ca.* 3 Å for one face at T_m[166].

The LP theory recognizes that in a subcooled system an important additional cause of fluctuations is the degree of departure from equilibrium as measured by ΔT. Thus, as ΔT is increased, the roughness of the fold surface becomes progressively larger than the equilibrium roughness and this added effect is denoted *kinetic roughness*. This increasing kinetic roughness, in turn, causes σ_e to become somewhat larger with increasing ΔT because the lateral 'σ' surfaces of the randomly staggered folds become progressively more exposed[10]. As shown below, the dependence of σ_e on undercooling permits an estimate of the kinetic roughness contribution to C_2. A related point is that at any T_x below T_m, the kinetic roughness on storage will naturally tend to relax toward the lesser equilibrium roughness. This means that insofar as the initially-formed interfacial zone consists of kinetically-induced rough folds, annealing at T_x should cause this zone to become thinner. Such a thinning of the quasi-amorphous interfacial region has been observed by real-time SAXS measurements in once-folded lamellae for ultra-pure *n*-paraffins crystallized from the melt, where the effect is readily separable from subsequent isothermal thickening to the extended chain state[167]. This is significant because it provides direct experimental support for the LP thesis that the initially-formed interfacial layer is thicker than the annealed one[10,166]. It is of interest that an AFM study implies the presence of a somewhat rough fold {1 1 0} surface in a PE single crystal[110].

A fold surface free energy $\sigma_{e(k)}$ is associated with the initially-formed, kinetically rough fold period, and a slightly smaller surface free energy $\sigma_{e(eq)}$ applies to the smoother equilibrium surface (ref. 166, *Figure 4*). These surface free energies will appear in the analysis of C_2 to follow, as will a term $2d_a$ to account for the amorphous component on each face of the lamella caused by the presence of short-range nonadjacent events that re-enter the lamella of origin in the interfacial zone in range B B′.

The range of applicability of the LP theory is now considered. One of the assumptions employed by LP was that the substrate run was rather long, which did not contemplate the then undisclosed existence of regime III where primary stems injected at the rate i at very closely spaced intervals dominate the 'substrate completion' process (see plot of separation of primary nuclei S_k/a_0 in *Figure 10b*). Accordingly, the LP approach can only be applied in regime I and the upper part of regime II, i.e. at $\Delta T \leq 22°C$. The heretofore troublesome 'blow-up' at $\Delta T = \sigma T_m/(\Delta h_f)a_0 \cong 38°$, which no value of ψ will eliminate, is actually far outside the true range of applicability of the original LP theory because of the long substrate run assumption. A different fluctuation model must apply in regime III (see later). We shall employ the LP approach only for $\Delta T \leq 22°$.

In consideration of the above, and introducing the term $2d_a$ to account for short-range nonadjacent events associated with the interface, one has

$$C_2 = 43\,\text{Å} = \delta + 2d_{eq} + 2\sigma_{e(eq)}yT_m/(\Delta h_f) + 2d_a \quad (49)$$

Here δ is the previously-calculated contribution of $\sim kT/b_0\sigma$ to C_2 for the case of no fluctuations of fold-period, $2d_{eq}$ the LP 'equilibrium roughness' component, and $2\sigma_{e(eq)}yT_m/(\Delta h_f)$ the LP 'kinetic roughness' component resulting from the dependence of σ_e on ΔT to be evaluated shortly. The kinetic roughness term as well as δ in equation (49) are obtained by inserting equation (50a) below into equation (9a)[3,166]. The quantities δ, $2d_{eq}$, and a portion of $2\sigma_{e(eq)}yT_m/(\Delta h_f)$ may be regarded as part of the core crystal as first formed. The ingredients of an 'interfacial zone' are clearly present in equation (49) but its exact makeup depends on how this term is defined. In practical terms, one might choose to think of this zone as consisting of the rougher folds plus the (semi-oriented, but amorphous) chains in the term d_a that undergo relatively nearby but still greater than second-nearest neighbour nonadjacent re-entries back into the lamella of origin. The portion of the interfacial zone on one of the lamellar surfaces that may be regarded as amorphous includes the nonadjacent events involved in d_a. If some of the more extended rough folds had looplike character, they could contribute to the amorphous content of the interfacial zone.

The 'kinetic roughness' component is based here on the temperature dependence of σ_e, which we approximate as[3,166]

$$\sigma_e = \sigma_{e(k)} \cong \sigma_{e(eq)}[1 + y(\Delta t)] \quad (50a)$$

where $\sigma_{e(eq)}$ is the equilibrium fold surface free energy at T_m and y is a temperature coefficient of roughly $0.0025\,\text{deg}^{-1}$. Calculations by LP theory of the kinetic value of σ_e for the nominal value $\sigma = 10\,\text{erg cm}^{-2}$ imply that y is fairly close to the value just cited though as an approximate upper bound it could be twice as large (ref. 3, p. 595). Taking $\sigma_{e(eq)}$ to be $86.5\,\text{erg cm}^{-2}$, one finds, as required, that σ_e is $90\,\text{erg cm}^{-2}$ at the I → II regime transition as listed in *Table 1*. With the input data for

$\sigma_{e(eq)}$ and y, the kinetic rough surface component in equation (49) comes to ~6 Å counting both lamellar faces or ~3 Å for one face. LP give the rough surface term (both faces) as ~10–15 Å in the main crystallization region.

Based on $\delta \cong 10$ Å, $2d_{eq} \cong 6$ Å, and a $2\sigma_{e(eq)} yT_m/(\Delta h_f)$ of ~6 Å, this leaves 43 Å less 22 Å or about 21 Å for $2d_a$. While there is clearly some latitude in its value caused by the uncertainty in y, the estimate that d_a is ~10–11 Å seems reasonable. It yields crystallinities calculated as $1 - 2d_a/l_{obs}$ ranging from 0.87 to 0.91. The experimental degree of crystallinity from the high χ_c plateau region characteristic of the upper part of range A–A′ and the body of range B–B′ is 0.8–0.9 (*Figure 7b*). As noted, some of the more exposed rough folds could have some loop-like character and contribute to the amorphous component, as might a few short cilia. In any case, a significant portion of d_a is reasonably attributed to nonadjacent events corresponding to third- and higher nearest neighbour (but still relatively short range) re-entries into the lamella of origin. There is nothing that suggests anything more than a small concentration of tie chains or long loops between the lamellae in regimes I and II in ranges A–A′ and B–B′. Thus, in major respects the lamellae resemble well-formed single crystals as obtained from dilute solution. The development of numerous tie chains and long loops and cilia, with their increasing contribution to the amorphous component resulting from large scale flights prior to re-entry, is reserved for the upper part of C–C′ and higher ranges where l_a as calculated by means of equation (43b) becomes much greater than d_a.

The outcome of the above is that nucleation theory, with the help of the LP extension with rough folds as modified to admit of some nonadjacent re-entry, leads to a reasonable, if approximate, account of the magnitude of the C_2 component of l_{obs} for the molecular weight ranges and regimes specified.

A treatment of the above type cannot be employed to explain the observed C_2 term of ~43 Å implied by the LAM measurements in regime III, since the LP approach is inapplicable in this regime. As noted, the fluctuation problem is rather different in this regime. Development of a theory of kinetic fold period roughness valid in regime III, where the primary stems that are put down at a rate i are so numerous as to re-establish the value of l_g^* virtually every second stem, presents an interesting challenge to theorists. It is evident from the LAM results in *Figure 14* that fluctuations of fold period do not lead to abnormal behaviour in regime III. The model pictured in *Figure 2c*, which has the proto-fold forming by a generally proximate but nevertheless distributed attachment to the niche, might permit an alternative calculation of the initial roughness of the chain-folded surface along the lines of the 'first passage' calculation of Sanchez and DiMarzio[51].

Both earlier[3] and recent[8,9] studies indicate that σ has a small dependence on temperature opposite to that of σ_e. Thus, one has the approximation

$$\sigma = \sigma_1[1 - x(\Delta T)] \qquad (50b)$$

where x may be estimated from equation (1) to be ~0.0024 deg^{-1}. With $\sigma_1 = 12.3$ erg cm^{-2}, this expression yields a σ of 11.8 erg cm^{-2} at $\Delta T_{I \to II} = 16.37°$ in accord with that cited in *Table 1*. The importance of this is that the product $\sigma\sigma_e$ in K_g, which comes to $\sigma_1\sigma_{e(eq)}[1 - x(\Delta T)][1 + y(\Delta T)]$, has only a trivial dependence on undercooling and $\sigma\sigma_e$ is virtually identical to $\sigma_1\sigma_{e(eq)}$. On this basis, neither $K_{g(I)}$ nor $K_{g(II)}$ will depart noticeably from a constant value with changing undercooling because of the individual variations of σ and σ_e. The estimates of x and y given here are both smaller (and likely more accurate) than those given in ref. 3.

K. Summary: intermediate molecular weight ranges B–B′ and C–C′, $\bar{M}_{nw}$ = 15.3K to $\bar{M}_{nw}$ = 90.6K

Beginning with the rate constants A_0, B_1, A, and B, which are given a direct physical meaning, flux-based nucleation theory from a common central framework leads to expressions for the surface nucleation rate, substrate completion rate, and the initial lamellar thickness. When these are combined with regime concepts and calibrated and unified with reptation theory, a considerable variety of data for the molecular weight range considered here can be organized and understood in molecular terms. The phenomena so accommodated include: (i) crystal growth rates in regimes I, II, and III and their dependence on undercooling and molecular weight as correlated with the presence of nonadjacent events and the corresponding degree of crystallinity; (ii) the variation of the initial lamellar thickness with undercooling; and, with the help of the LP extension of the elementary theory, (iii) certain properties of the thin interfacial region, including the presence of an initially rough fold surface with mainly 'tight' folds combined with some nonadjacent events. In molecular weight range B–B′ most of the nonadjacent events in regimes I and II are in the form of a modest number of rather early 'amorphous' returns to the lamella of origin; in the higher molecular weight range C–C′ a contribution from longer range nonadjacent events initiates what subsequently becomes a rapid descent of the degree of crystallinity and a perturbation of the reptation mechanism. Topological constraints based on the Gambler's Ruin calculation require a marked preponderance of 'tight' folds at the lamellar surfaces in molecular weight range B–B′ in regime I and a lesser degree of 'tight' folding in regime III. Steady-state forced reptation occurs in regimes I and II, but reptation of slack is involved in regime III as justified by a special calculation of the reeling rate. The rate constants A_0 and B_1 based on the 'low ψ' approximation for the first stem, which derive from the physically adsorbed 'segmentalized–aligned' model of the rate-determining activated complex for that stem, are consistent with the new entropic theory for σ as well as the absence of a 'δ catastrophe'. A detailed account of the adjacent re-entry question emphasizing the role of the 'proximity' effect in augmenting such re-entry will be found in subsequent sections for range B–B′ as well as those of higher and lower molecular weight.

IV. GROWTH KINETICS AND MORPHOLOGY IN HIGH MOLECULAR WEIGHT RANGE D–D′; ALSO ULTRA-HIGH MOLECULAR WEIGHT, RANGE E–E′. REGIME III-A AND REPTATION OF SLACK

A. $\bar{M}_{nw}$ 103K to 640K, range D–D′

HFRL[77] give spherulite growth rate data for seven fractions beginning at $M_n = 78.8$K, $M_w = 134$K,

$\bar{M}_{nw} = 103$K and ending at $M_n = 507.5$K, $M_w = 807$K, $\bar{M}_{nw} = 640$K, which constitute range D–D′. (Sample preparation was identical to that described for the fractions in *Table 2*.) All the fractions exhibited irregular spherulites of the type shown in *Figure 6d* in the isothermal T_x range, and none exhibited the regime I → II rate transition. This major departure in spherulite type and regime behaviour occurred over a rather short range of molecular weight. Fraction 10 of range C–C′ in *Table 2*, $M_n = 71.4$K, $M_w = 115$K, $\bar{M}_{nw} = 90.6$K, exhibited axialites at high growth temperatures (regime I) and non-banded spherulites in the main body of regime II, while the first specimen showing only irregular spherulites and no regime I → II transition was $\bar{M}_{nw} = 103$K, which signalled the onset of range D–D′. The next higher fraction in range D–D′, again with irregular spherulites and no I → II transition, was $M_n = 94.4$K, $M_w = 119$K, $\bar{M}_{nw} = 105.6$K. No spherulites could be observed much above $\bar{M}_{nw} = 640$K, $M_w = 807$K, thus terminating range D–D′.

The $\log G$ vs. T_x data for fractions in range D–D′ showed no break of the type illustrated in *Figure 5a*, and the $\ln G + Q_D^*/RT$ vs. $1/T(\Delta T)$ plots were strictly linear over the entire wide ΔT range studied, which included the ΔT of $16.37 \pm 0.50°$ where the I → II transition would have been seen had it been present. These plots led to 'mixed' K_g values that were near 1.5×10^5 deg^2, i.e. roughly midway between $K_{g(II)}$ and $K_{g(III)}$, at the lower molecular weights in range D–D′; at the higher molecular weights in this range sporadic values of $1.5–1.8 \times 10^5$ deg^2 were observed. (All K_g values corrected to $T_m^0 = 145.5$°C.) *Figure 7* illustrates how range D–D′ fits into the kinetic, morphological, and degree of crystallinity classification scheme. The growth rate of irregular spherulites was considerably less than that of the spherulites or axialites in ranges B–B′ and C–C′ at a comparable ΔT.

While some of the background for the absence of the I → II regime transition in range D–D′ has already been given, it is of interest to examine the origin of the 'mixed' K_g values observed in D–D′ and what this implies in terms of molecular mechanisms. After doing this we discuss the nature of the increasingly prominent amorphous zone and the generation of tie chains.

It is believed that the 'mixed' K_g values in range D–D′ are a combination of regime II and a manifestation of a form of regime III behaviour (designated here as III-A) caused by the circumstance that the transport mechanism for substrate completion is being forced to begin to employ reptation of slack. This occurs because many of the now very long molecules form copious multiple attachments with some large pinned loops on the growth front (*Figure 12a*). In this situation, the perturbed steady-state reptation of range C–C′ begins to give way to reptation of slack, which will in the extreme of very high molecular weight drive the system toward even lower crystallinity and a practically pure form of a regime III-type of behaviour (i.e. III-A) with its characteristic K_g of $\sim 1.9 \times 10^5$ deg^2 (*Figure 7*).

There is independent support for the concept that even limited retardation of forced steady-state reptation will lead to a form of regime III behaviour in melt-crystallized PE. In a highly interesting paper, Phillips and Lambert[168] have shown that a modest degree of chemical crosslinking forces the PE system into a regime III-like mode whereas the uncrosslinked system exhibited the I → II transition (see their Figure 6). This effect occurs where the crosslinks are far enough apart so that they do not determine the lamellar thickness. The conversion to the regime III type of behaviour was attributed by these authors to the fact that there were no free chains in the crosslinked samples, which interrupted the (steady state) reptation process and thus forced the system to employ only local motions in the surface nucleation process. In the terms of the present work, the local motions correspond to reptation of slack—this allows surface nucleation at a relatively high rate i but strongly inhibits long substrate completion runs. As noted in Sections II.H and III.H, these are precisely the conditions that foster a tendency toward a regime III form of behaviour. Here we denote this as regime III-A and emphasize that it occurs over a wide ΔT range and *replaces* the I → II transition. That a significant degree of kinetically characterizable lamellar crystallization occurs in crosslinked PE testifies compellingly to the reality of the concept of reptation of slack.

By analogy with the above, in the melt crystallization case an increase of molecular weight with its concomitant larger population of pinned looplike structures on the growth front should cause a tendency toward regime III-A behaviour over a large range of ΔT owing to the necessity of employing slack as a transport mechanism. One would expect this to begin as 'mixed' regime II and III-A behaviour, as in the first part of range D D′ because of only partial use of slack, and to culminate in the ultrahigh molecular weight range E–E′ with a close approach to ideal regime III-A with its K_g of $\sim 1.9 \times 10^5$ deg^2. In accord with this, the HFRL results for range D–D′ begin with three specimens giving the 'mixed' II and III-A regime result of $\sim 1.5 \times 10^5$ deg^2 and values of $1.5–1.8 \times 10^5$ deg^2 for specimens of higher molecular weight in this range. Additional evidence that the overall trend with increasing molecular weight is toward full regime III-A behaviour is afforded by the K_g values that can be deduced from the early dilatometric rate studies of Ergoz, Fatou, and Mandelkern[125] at ultrahigh molecular weights in range E–E′. Our analysis of their $\ln(1/\tau_{0.04})$ vs. $T_m/T(\Delta T)$ data for three specimens $M = 3–8 \times 10^6$ in this range yielded a value of K_g of $\sim 1.86 \times 10^5$ deg^2, which is indicative of a close approach to pure regime III-A over the entire practical set of isothermal T_x (*Figure 7*).

The foregoing indicates that there are *two* manifestations of a regime III form of behaviour in PE, both of which result from the substrate completion process being interrupted by some agency so that reptation of slack has to be invoked as a transport mechanism. The *first*, denoted simply as 'regime III', appears in the intermediate molecular weight ranges B–B′ and C–C′ where the operative agency is the low T_x. Such a low T_x causes rapid surface nucleation that outpaces the ability of the steady-state reptation process to supply chain segments to the growth front, thus requiring reptation of slack. This is the type of regime III depicted in *Figures 3b* and *13*, wherein regimes I, II, and III appear in succession with lowering T_x as in ranges B–B′ and C–C′. The *second* manifestation, denoted III-A, results from the necessity of invoking reptation of slack because of retardation of the transport mechanism by chemical crosslinking or, alternatively, by multiple attachment of chains on the growth front at high molecular weights as in ranges D–D′ and E–E′. In these cases, the clear-cut

regime I and regime II effects are replaced by 'mixed' regime II and III-A or by virtually pure regime III-A behaviour at the highest molecular weights over the entire practicable range of isothermal T_x (*Figure 7*). Both regime III and regime III-A (when in pure form) are associated with a K_g close to 1.9×10^5 deg^2.

The 'mixed' regime effect in range D–D′ was originally assumed by HFRL to be a combination of regimes I and II, the existence of regime III or III-like effects being unknown at the time. The present treatment is, of course, to be preferred. Fatou *et al.*[148] recognized in qualitative terms that disturbances of the transport process could affect regime behaviour and suggested a regime classification scheme for PE with this as part of their interpretive background. Our scheme differs at points from theirs, among other reasons because we related aspects of regime behaviour to highly specific molecular transport mechanisms, as in the role assigned above to reptation of slack in regimes III and III-A, and because we employed the clearly defined and measurable quantity K_g as an indicator of regimes. The theoretical framework employed by Fatou *et al.* does not give an explicit expression for the substrate completion rate since its nucleation component is based on a 'saddle point' approach and, in application, leaves σ_e as a parameter that is numerically highly uncertain.

Consider now the nature of the amorphous zone and the formation of tie chains in range D–D′. A striking feature of range D–D′ is the marked drop in the limiting degree of crystallinity χ_c at T_x with increasing molecular weight (*Figure 7b*). This fall of χ_c is reasonably attributed to the build-up (actually beginning in the upper part of range C–C′) of a layer nominally of thickness l_a of relatively normal amorphous material consisting of long random coil loops and long cilia of varying lengths on either face of each lamella. The postulated origin of these amorphous structures for an *isolated* lamella is shown in *Figure 12a*, where it is seen that widely separated nonadjacent events at the growth front at these high molecular weights leave behind them a trail of trapped large loops and long cilia of varying size on each lamellar surface. These are interspersed with some short-range nonadjacent re-entries and a fraction of 'tight' folds which likely is beginning to approach the Gambler's Ruin lower bound, as is consistent with reptation of slack. In parallel with this minimal degree of tight folding, one expects only a limited degree of adjacency that is approaching on the order of, say, ~0.37 as in the 'equilibrium' calculations of Mansfield[19]; the p_{ar} would approach ~0.30 if the chains were tilted, say, 35°. The foregoing picture is consistent with the additional amorphous material (represented here as a total of $2l_a \cong l_{amorph}$ for each lamella) increasing with rising molecular weight. That this is qualitatively correct is readily inferred from the increase in the amorphous component $1 - \chi_c$ in *Figure 7b* for range D–D′.

The model shown in *Figure 12b* illustrates the origin of the bulk of the tie chains and loops that make up l_{amorph} and shows in schematic terms why $2l_a \cong l_{amorph}$ tends to maintain itself during growth—if a 'following' lamella came too close to a 'leading' lamella, it would encounter too many non-reptatable pinned loops and cilia belonging to the latter that would cause the growth rate of the 'following' lamella to be unduly retarded. Thus, for a 'following' lamella to exhibit a relatively normal if slightly slower growth rate, it must maintain a distance not less than $\sim 2l_a$ from the 'leading' lamella. The work of Bank and Krimm[169] suggests that there may be another mechanism for tie molecule formation. These authors noticed in their studies of pure PEH and PED single crystals that at surprisingly low temperatures interpenetration of chains from one type of crystal to the other occurred when they were in contact. This implies that the unattached end of a long cilium might, on occasion, penetrate a vacancy in a neighbouring lamella forming a tie chain or re-enter a vacancy in the lamella of origin forming a large loop. None of the mechanisms discussed here excludes the occasional formation of a tight knot in a tie chain[170] or intertwined loops between lamellae[171].

It is instructive to give estimates of the scale of the dimensions of the amorphous component and of the molecules in range D–D′. The thickness l_a belonging to one face of a lamella and the total thickness $l_{amorph} \simeq 2l_a$ between the contiguous lamellae are readily estimated using equation (43b) with the nominal value $l_{core} = 180$ Å together with the estimated values of χ_c at $T_x = 128$°C given in *Figure 7b*. The values of l_{amorph} as a function of M estimated in this way are compared below with the corresponding root-mean-square radius of gyration r_g calculated as $(C_\infty/6)^{1/2} l_b n^{1/2}$.

$$\begin{aligned} M &= 150\text{K}, \quad r_g = 169\,\text{Å}, \quad l_{amorph} \simeq 128\,\text{Å} \\ M &= 250\text{K}, \quad r_g = 218\,\text{Å}, \quad l_{amorph} \simeq 270\,\text{Å} \\ M &= 400\text{K}, \quad r_g = 275\,\text{Å}, \quad l_{amorph} \simeq 460\,\text{Å} \end{aligned} \tag{51}$$

It is seen in these illustrative examples that with increasing M, the value of $l_{amorph} \simeq 2l_a$ begins to outrun the r.m.s. value of r_g. Of course, the actual 'reach' of a molecule is considerably larger than r_g so that formation of tie chains is still possible at the higher M. Another point is that l_{amorph} is large enough, particularly for $M = 250$K and $M = 400$K, to permit chain-folded microlamellae 75–150 Å thick to form by kinetic processes in the amorphous phase between the crystalline cores on cooling to room temperature, thus increasing the degree of crystallinity to a level well in excess of χ_c, i.e. that present at $T_x = 128$°C.

The content at $T_x = 128$°C of the large l_{amorph} at high M may to an approximation be thought of as consisting of two regions: (i) an interfacial zone of modest thickness consisting of some of the rougher folds plus chains with relatively short-range re-entries greater than those involved in p_{tf} that exhibit definite net orientation and (ii) a substantially thicker region composed of long tie chains, large loops, and long cilia, all with considerable random coil character with little net orientation that exhibit relatively close to normal thermodynamic and relaxational properties. Of course the thermodynamic properties of type (ii) chains will be modified somewhat relative to those of free chains because the partition functions for long once- and twice-pinned chains differ from that of a free chain[172]. Though the tie chains and loops may be able to participate only marginally because they are doubly or multiply tethered, it is reasonable to assume that it is the type (ii) entities just mentioned that partially crystallize on cooling to room temperature forming thin lamellae. These new lamellae are thin because of the lower crystallization temperature.

B. Ultra-high molecular weights, $M_{nw} \sim 640$K to $M \sim 8 \times 10^6$, range E–E′

Molecular weight range E–E′ begins somewhat above $M_n \sim 508$K, $M_w \sim 807$K, $\bar{M}_{nw} = 640$K where even irregular spherulites visible in an optical microscope fail to appear and where much of the crystallinity is of an ill-informed microlamellar type (VMFM[78]). There is clear evidence that fibrillar structures[173,174] are also present. Though the dividing point is somewhat uncertain, the cessation of range D–D′, where irregular spherulites grow, and the beginning of range E–E′, where they do not, appears to coincide approximately with the onset of the low crystallinity plateau at point *J* in *Figure 7b*. Thus, in range E–E′, it is evident that some agency is preventing formation of large objects such as spherulites and is at the same time strongly limiting the fraction of the polymer that can crystallize at T_x.

Because melt-crystallized PE of ultrahigh molecular weight is of considerable scientific and technical interest, it is thought useful to highlight here certain observations on fractions $M \geq 10^6$ noted by HFRL. The sample preparation technique for these fractions was identical to that employed for those in *Table 2*.

On heating one of the fractions $M > 10^6$ on the hot stage to the initial melt temperature $T_l = 155$°C, the birefringence refused to disappear in the 'melt' even after prolonged storage. The same result obtained for brief storage at $T_l = 190$°C. Both T_l values just mentioned are well above $T_m^0 \cong 145.5$°C. The retention of birefringence far above T_m^0 for a fraction $M \sim 6 \times 10^6$, which is well in range E–E′, was subsequently verified by Zachariades and Logan[174]. On cooling from T_l to any of a set of normal T_x values, no objects such as even ill-formed spherulites could be detected with a polarizing microscope though DTA measurements showed that significant crystallization had occurred. After crystallization, the field of view had a granular appearance at high magnification. Nothing of this kind occurred for specimens $M_n = 508$K, $M_w = 807$K, $\bar{M}_{nw} = 640$K and below—heating to $T_l = 155$°C for even a short period completely removed the birefringence in the melt and spherulites were readily detected on cooling to T_x.

The birefringence observed above T_m^0 by HFRL was evidently caused, at least in part, by fibrillar structures formed when the molten specimens were pressed between the cover slips. Even minimal mechanical forces can induce formation of such structures at a foreign surface. When in concentrated subcooled solution, PE containing a high molecular weight component readily forms shish-kebab structures on a foreign surface even under conditions of very low shear rates, e.g. 1 cm s^{-1}. The fibrillar 'shish' originates on the foreign surface, e.g. carbon grid, and forms a typical shish-kebab structure downstream; as observed by electron microscopy, the attachment site appeared to be a small chain folded aggregate on the surface[175] (see also Figure 7 in ref. 176). Similar fibrillar structures likely formed on the cover slips in the HFRL specimen preparation process. Retained orientation in the melt also likely contributed to the birefringence in the HFRL ultrahigh *M* fractions.

There is evidence for melt-crystallized PE of $M \sim 6 \times 10^6$ that can be interpreted in terms of the fibrillar structures leading to birefringence being present up to about 220°C, where they transform into a semi-ordered liquid crystalline or pseudohexagonal phase, also with birefringence, which persists up to even higher temperatures[174]. One might surmise from this that the fibrils exhibit an unusual degree of superheating leading to strikingly slow melting behaviour. A rather similar interpretation can be advanced for melt-crystallized PE of $M \cong 900$K[177]. Rastogi and Odell[178] confirm for gel-spun PE fibres, which were constrained by being embedded between cover slips with cured cyanoacrylate, the presence of the orthorhombic form well above T_m^0, and its conversion at higher temperatures into the hexagonal form, even though the externally applied stresses were very low.

The general type of morphology involved in melt crystallization of PE in range E–E′ can be deduced from the work of Keith, Padden, and Vadimsky[173]. By crystallizing PE of $M = 726$K from a 50% solution in n-$C_{32}H_{66}$ and extracting the n-$C_{32}H_{66}$ at room temperature with xylene, these authors found aggregates of chain-folded lamellae connected to other such aggregates by occasional essentially linear fibrillar strands that were more or less parallel to each other and which were typically $\rightarrow 1.5\,\mu$m long and 50–100 Å in diameter. Since the mean length of the molecules was $\sim 6.6\,\mu$m, their size was more than sufficient to form the fibrillar strands. The remarkable electron micrograph showing these structures may be found in the original work[173]; it has also been reproduced (ref. 3, p. 505). Probably the structures formed by crystallization from the melt are less perfect than those formed from concentrated solution. Nevertheless, the two types of structure (i.e. fibrillar and chain-folded) inferred to be present in the melt case[174] are clearly delineated in the concentrated solution studies.

As seen in *Figure 7b*, the degree of crystallinity in range E–E′ for melt-crystallized PE is 0.2–0.3 at $T_x = 128$°C, but on cooling to room temperature it rises to 0.52–0.56[174]. This increase is attributable to crystallization in the form of thin, new lamellae of part of the amorphous material (type ii) between the pre-existing lamellar crystallites in the aggregates.

That there are formidable obstacles to crystallization in this molecular weight range is shown by the low χ_c at $T_x = 128$°C (*Figure 7b*). The molecules are long enough for many to become involved in a nearby lamella, or fairly distant points in the same lamella, thereby creating a situation where steady-state reptation is vestigial leaving reptation of slack as the principal transport mechanism. Even this mechanism is likely rendered inactive in many instances after a relatively short section of a specified chain has been reeled onto a lamella because another part of the long chain is firmly tethered on a nearby lamella or elsewhere on the same lamella, the molecule involved then being in a state of tension. This may be viewed as a reasonable explanation of the low crystallinity plateau in χ_c in the ultra-high molecular weight range. With this background, it is hardly surprising that the chain folded lamellae are ill-formed and sometimes only several hundred Å in their lateral dimensions; VMFM aptly refer to them as 'degenerate lamellae'. The degree of adjacency and 'tight' folding in range E–E′ is unknown, but is conceivably even less than that present in hard-quenched regime III specimens of lower molecular weight.

Despite the impediments to crystallization in range E–E′ that are basically the result of the enormous length of the molecules, there is nevertheless good reason to believe that the rate of bulk crystallization is still nucleation controlled. Dilatometric studies on ultrahigh

Table 4 Characterization data and values of $\sigma\bar{\sigma}_e$ and $\bar{\sigma}_e$ for PE fractions of low MW exhibiting quantized chain folding: MW range A–A′

Fraction	M_n[a] (in K)	M_w[a]	M_w/M_n	$\bar{M}_{nw}$[a]	T_m[b] (°C)	Observed $\sigma\bar{\sigma}_e$ (erg^2 cm^{-4})	$\bar{\sigma}_e$[c] (erg cm^{-2})	Length of molecule, l_m[d] (Å)	Remarks
11	3.19K	3.60K	1.13	3.39K	132.40	526	**44.6**	**307.5**	$f = 1$, $\overline{\Delta T} = 12.65$°C
12	3.33K	4.20K	1.26	3.74K	134.06	575	48.7	—	
13	4.64K	5.10K	1.10	4.87K	135.87	740	62.7		
14	5.35K	5.62K	1.05	5.48K	136.7	698	59.2		
15	5.38K	6.29K	1.17	5.82K	137.5	839	71.1		
16	5.64K	6.15K	1.09	5.89K	137.35	1022	**86.6**	**534**	$f = 1^+$ and $f = 2$ $\overline{\Delta T} = 13.85$°C
16′[e]	5.64K	6.15K	1.09	5.89K	137.35	1011	**85.7**		
17	5.99K	6.35K	1.06	6.17K	137.6	764	65.0		
18	7.20K	8.06K	1.12	7.62K	139.1	887	75.2		
19	7.61K	7.84K	1.03	7.72K	138.9	831	70.5		
20	7.74K	8.59K	1.11	8.15K	139.5	882	74.7		
21	7.85K	8.56K	1.04	8.20K	139.44	1029	**87.2**	**744**	$f = 2^+$ and $f = 3$ $\overline{\Delta T} = 14.49$°C
21′[e]	7.85K	8.56K	1.04	8.20K	139.44	1016	**86.1**		
22	9.15K	9.70K	1.06	9.42K	140.1	935	79.2		
23[f]	10.43K	11.4K	1.09	10.90K	140.83	1003	**85.0**	**1000**	$f = 3^+$ and $f = 4$ $\overline{\Delta T} = 14.75$°C
24[f]	10.71K	11.7K	1.09	11.19K	140.9	1011	**85.6**		
25	11.0K	11.74K	1.07	11.36K	140.95	982	83.2		End of range A–A′
2[g]	18.5K	19.8K	1.07	19.14K	142.68	1071	90.8		MW range B–B′

[a] Symbol K stands for ×1000 in numbers referring to molecular weight
[b] Calculated with Flory–Vrij equation given numerically in footnote of *Table 2*. T_m^0 for $M_w \rightarrow \infty = 145.5$°C
[c] $\bar{\sigma}_e$ calculated as $\sigma\bar{\sigma}_e/11.8$. All $\sigma\bar{\sigma}_e$ given here are 0.86 of those given in HFRL because of change of T_m^0 from 146.5° to 145.5°C
[d] l_m calculated as $\bar{M}_{nw} \times 1.273/14.03$ in Å
[e] Total rerun, same as described in *Table 2*
[f] These fractions treated as one fraction of $\bar{M}_{nw} = 11.05$K as regards l_m; $\overline{\Delta T}$ was very similar for the fractions, and that quoted is the average
[g] From *Table 2* for comparison. Values of $\sigma\bar{\sigma}_e$ and $\bar{\sigma}_e$ new

molecular weight PE by Ergoz *et al.*[125] have shown that the stage 1 part of the bulk crystallization process has a rate with a negative temperature coefficient at normal undercoolings. On this basis these authors suggested that the crystallization process was nucleation controlled. As noted earlier, our analysis of their data for range E–E′ gave a K_g of $\sim 1.86 \times 10^5$ deg^2. This shows directly that a surface nucleus of the slack-induced regime III-A type with its characteristic $\sigma\sigma_e$ of ~ 1060 erg^2 cm^{-4} is the rate-determining step in the bulk crystallization process in the ultra-high molecular weight range. With σ taken to have its established value of 11.8 erg cm^{-2}, the $\sigma\sigma_e$ just quoted implies that the scale of σ_e therein is set at ~ 90 erg cm^{-2} by the presence of a certain fraction of 'tight' chain folds with a normal work of folding in the regime III-A surface nucleus.

We now turn to the opposite end of the molecular weight spectrum, range A–A′ in *Figure 7a*, where 'quantized' chain folding occurs in regime I, indicative of a remarkably high degree of 'tight' folding and adjacent re-entry in crystallization from the melt.

V. QUANTIZED CHAIN FOLDING IN MELT-CRYSTALLIZED PE FRACTIONS OF LOW MOLECULAR WEIGHT, RANGE A–A′: EVIDENCE FOR HIGH DEGREE OF ADJACENCY IN REGIME I

A. Background and data base, $\bar{M}_{nw} = 3.39$K *to* 11.36K

Having established a number of features of the basic molecular picture of crystal growth with chain folding in the intermediate molecular weight range and to some extent that in the higher ranges, it is now feasible to address the nature of the 'quantized' chain folding effects at lower molecular weights. The 'quantization' effect, which leads to large variations in $K_{g(I)}$ in range A–A′, has already been noted in *Figure 7a*. From what has previously been shown, one can be sure that forced reptation from the subcooled melt is near-ideal in this lower molecular weight range and that multiple attachment effects at widely distant points will not seriously lower the degree of crystallinity or otherwise interfere with the chain folding process. By appropriate treatment of the growth rate data in the lower range, we shall be able to obtain new evidence for chain folding with a p_{ar} of close to 0.7 in regime I that has consequences that extend to melt-crystallized specimens of intermediate molecular weight crystallized in that regime. The outcome will be that there is good evidence for the proposition that crystallization in regime I leads to considerably higher adjacency than that in regime III—the p_{ar} in the latter regime is typically 0.3–0.4 (see Section VI). The treatment includes a discussion of the reference states employed in dealing with chains of low molecular weight.

Prior to giving details, it is helpful to indicate the type of experiment that led to the conclusion that quantized chain folding had occurred and to mention the general nature of the explanation of the effects observed. The axialite growth rates as a function of isothermal crystallization temperature were determined by HFRL[77] for each of a number of fractions in the range $\bar{M}_{nw} = 3.39$K to 11.36K. [Here we employ $\bar{M}_{nw}$ since this is the correct moment of the molecular weight for application to systems involving near-ideal reptation—see equations

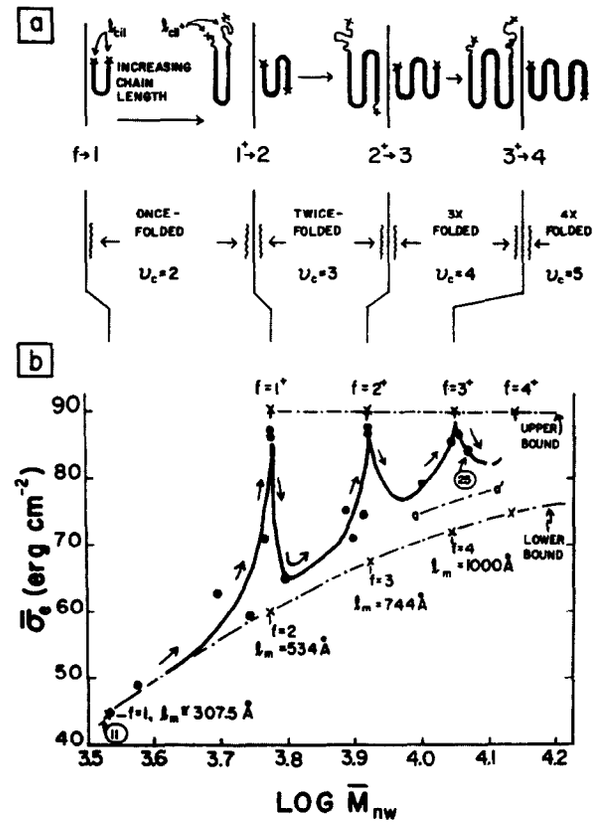

Figure 15 *Quantized chain folding in melt-crystallized PE fractions, regime I, MW range A A′.* (a) Chain folded structures formed in regime I with increasing molecular weight at approximately constant undercooling. The symbol f represents the number of folds per molecule. Plus sign (+) refers to a ciliated species, no (+) sign means very short localized chain ends. (b) Experimental effective fold surface free energy $\bar{\sigma}_e$ as function of $\bar{M}_{nw}$ at approximately constant undercooling showing abrupt changes in number of folds per molecule with increasing MW. Circles with numerals give fraction number. Data base from HFRL in *Table 4*, detailed analysis in *Table 5*. Results show that mean cluster size $\bar{\nu}_c$ of ~ 3.5 adjacent stems can be attained at the higher molecular weights in range A–A′ in regime I giving $p_{ar} \cong 0.71$

(25) and (27).] These fractions together with their melting points and other characterization data are listed in *Table 4*. The growth rates of each of these fractions were then analysed to obtain $K_{g(I)}$ according to equations (27). The growth temperature was well within regime I for all of the fractions. The mean undercooling $\overline{\Delta T}$ for the various fractions was approximately the same. The actual mean undercoolings relevant to the determination of $K_{g(I)}$ at important critical molecular weights are listed in *Table 4*. These $\overline{\Delta T}$ values were calculated from the temperature ranges of typically 3–4° over which $G_I(T_x)$ was measured for each fraction as given in HFRL. The K_g values were analysed to obtain the product $\sigma\bar{\sigma}_e$ for each fraction as listed in *Table 4*, following which $\bar{\sigma}_e$ was calculated as $\sigma\bar{\sigma}_e/\sigma$ where σ was set at 11.8 erg cm^{-2}.

The values of $\bar{\sigma}_e$ for each fraction are plotted as a function of $\log \bar{M}_{nw}$ as shown in *Figure 15b*. Thus, this figure is essentially a plot of the mean fold surface free energy $\bar{\sigma}_e$ at an approximately constant undercooling as a function of increasing molecular length l_m where l_m is calculated as $\bar{M}_{nw} l_u / 14.03$. It is emphasized that the $\bar{\sigma}_e$ vs. $\log \bar{M}_{nw}$ data given in *Table 4* and plotted in *Figure 15b represent a statistical (time) average of what was actually happening at the kinetically dominant 1 1 0 growth front during the nucleation and substrate completion processes in regime I.* There is no doubt about the reality of the peak value points in *Figure 15b*. Because of their

unusual character, which was noted by HFRL during the original work, those at $f = 1^+$ and $f = 2^+$ were fully confirmed by total reruns (*Table 4*). *Figure 15* as shown here is based on an earlier brief report[179].

Figure 15b exhibits the 'quantized' chain folding effect, i.e. an abrupt change in $\bar{\sigma}_e$ with increasing chain length, first from the once-folded state to the twice-folded state ($1^+ \rightarrow 2$), then from the twice-folded state to the three-times folded state ($2^+ \rightarrow 3$), and so on, as shown in *Figure 15a*. The quantity f refers to the number of folds per molecule. The symbol '+' refers to a chain-folded cluster that has long terminal cilia while the absence of the plus sign denotes a cluster with short terminal cilia; thus, the symbolism $1^+ \rightarrow 2$ means a relatively abrupt transition with increasing molecular weight from a once-folded cluster with long terminal cilia to a twice-folded cluster with very short terminal cilia (see *Figures 15a* and *b*).

This brings us directly to the physical picture of what is occurring. The short cilia contribute little if anything to the mean surface free energy. (This point is subsequently discussed in greater depth.) Thus, for $f = 1$ one expects in accord with the mean field approximation[11,13]

$$\bar{\sigma}_e = \sigma_{e(\infty)}\left(\frac{f}{f+1}\right) \quad \text{(lower bound, short localized cilia)} \tag{52a}$$

where $\sigma_{e(\infty)} = 90\,\text{erg cm}^{-2}$, as for an ideal fully folded surface, that $\bar{\sigma}_e$ should be close to $45\,\text{erg cm}^{-2}$. (The observed value is $44.6\,\text{erg cm}^{-2}$, showing the mean field approximation to be quite accurate in this application.) Then, as the molecular length (at an approximately fixed undercooling) is increased the system reacts at first by increasing the length of the cilia, which tends to increase the initial lamellar thickness l_g^* somewhat because the longer confined cilia involve an additional surface free energy termed generally σ_{cil}. It is for this reason the fold period for $f = 1^+$ is depicted as being larger than that for $f = 1$ in *Figure 15a*. Now, when the terminal cilia within the interfacial zone become sufficiently long and spatially confined with increasing chain length, σ_{cil} will become equal and then tend to exceed the fold surface free energy $\sigma_{e(\infty)} = 90\,\text{erg cm}^{-2}$. The condition

$$\sigma_{cil}^{+} = \sigma_{e(\infty)} = 90\,\text{erg cm}^{-2}$$

(upper bound, long spatially confined cilia) (52b)

where σ_{cil}^{+} is the surface free energy associated with the long confined cilia, defines the point where any further increase in molecular length l_m would have the ciliation effect incurring more surface energy that a chain fold. (The reason that the longer spatially confined cilia within the interfacial zone lead to the σ_{cil}^{+} just cited will be given shortly.) At this juncture the system finds that the rate-determining parameter $\bar{\sigma}_e$ in $K_{g(I)}$ can afford to fall to the lower bound value characteristic of the doubly-folded, only weakly ciliated $f = 2$ structure, which leads to the $1^+ \rightarrow 2$ quantized chain-folding transition. Thus, the system chooses the lower $\bar{\sigma}_e$ at the $1^+ \rightarrow 2$ transition to attain a lower $K_{g(I)}$ and, thence, a faster growth rate. The same type of processes account for the $2^+ \rightarrow 3$ and the $3^+ \rightarrow 4$ transitions, though the latter is less prominent than the others. The detailed analysis to follow will reveal the presence of some effects attributable to a recognizable amount of nonadjacent re-entry in the vicinity of the $3^+ \rightarrow 4$ transition. The general expression for $\bar{\sigma}_e$ is

$$\bar{\sigma}_e = \sigma_{e(\infty)}[(f + w)/(f + 1)] \tag{52c}$$

where $w = (\sigma_{cil}$ or $\sigma_{cil}^{+})/\sigma_{e(\infty)}$; this gives $w = 0$ for $\sigma_{cil} = 0$ (lower bound) as in equation (52a) and $w = 1$ for $\sigma_{cil}^{+} = \sigma_{e(\infty)}$ (upper bound) as is consistent with equation (52b).

Even before giving a more detailed analysis, it is evident from *Figure 15* that the quantized chain-folding effect is both striking and real. It will emerge from the quantitative treatment to follow that it is only possible to understand the clear-cut $1^+ \rightarrow 2$ and $2^+ \rightarrow 3$ transitions by invoking the concept of virtually complete adjacent re-entry. While the $3^+ \rightarrow 4$ transition is obviously less pronounced, it is certain that even in this case some adjacent re-entry is present. Because of the convergence of the upper and lower bounds with increasing chain length, which is a natural result of the lower bound being controlled by $\bar{\sigma}_e$ as in equation (52a), this kinetic method of identifying quantized chain folding loses its sensitivity at the larger f values at the higher molecular weights (*Figure 15*).

It is relevant to note here that other investigators have shown that 'quantized' chain folding occurs in the $-(CH_2)_n-$ system for specimens crystallized from the melt. In an important paper, Ungar, Stejny, Keller, Bidd, and Whiting[180] gave firm evidence based on LAM and SAXS data for once- and twice-folded lamellae structures of high degree of adjacency and fold surface perfection in ultrapure melt-crystallized n-$C_{390}H_{782}$. This study, taken together with parallel work on solution-formed single crystals of such n-paraffins[180] began the process of convincing a number of scientists, previously sceptics, that chain folding of some considerable quality *could* actually occur in crystallization from the solution and melt states. The structures observed in melt crystallization by Ungar *et al.* corresponded to what we have termed here the $f = 1$ and $f = 2$ states in ideal form for a monodisperse specimen $M = 5.464$K and molecular length $l_m = 479.9$ Å. The fold surface was initially rather rough in such specimens, this situation being termed by Ungar and Keller[167] as representing 'non-integral folding', but soon settled down to a smoother fold surface while retaining the very high adjacency. The results for n-$C_{390}H_{782}$ cited above bear the implication that clear-cut evidence for 'quantized' folding, whatever the source of such evidence, is highly suggestive of the presence of a high degree of adjacent re-entry. In other terms, we find the results for n-$C_{390}H_{782}$ fully supportive of our theme that there is a strong relationship between quantization and adjacent re-entry in this general molecular weight range (*Figure 15b*).

The quantization effect is not the exclusive behaviour of the $(-CH_2-)_n$ system. For example, the oligomers of poly(ethylene oxide) exhibit clearly evident 'quantized' chain folding behaviour from $f = 1$ up to and including $f = 4$. Details, including references to the original experimental data of Kovacs and coworkers are given in ref. 11.

In dealing with molecular trajectories in chain-folded lamellar systems, there are two useful indices for defining the degree of adjacency. Referring to the trajectory of a given molecule, the first of these is[181]

$$p_{ar} = \frac{\text{number of successful tries for adjacency}}{\text{total number of tries}} \tag{53a}$$

Thus, if a molecule on adding to the substrate forms a cluster of three adjacent stems in two tries, forming two folds, and then executes a non-adjacent re-entry on the third try, and then repeats this process a number of times, p_{ar} comes to 2/3. This expression is applicable to both long polymer chains and quantized systems. In the latter case, a terminal cilium is not counted as a nonadjacent event unless it is long enough to have formed a fold with full stem length but has not done so.

Another index for finding the degree of adjacency is

$$p_{ar} = 1 - 1/\bar{\nu}_c \tag{53b}$$

where $\bar{\nu}_c$ is the mean cluster size, i.e. the mean number of adjacent stems averaged over all clusters. This expression applies well to a long molecule that forms a number of adjacent-stem clusters with nonadjacent events intervening between them. In the example above, where the mean cluster size was $\bar{\nu}_c = 3$, p_{ar} again comes to 2/3. If applied to a quantized system, equation (53b) gives only a lower bound for p_{ar}. Equations (53a) and (53b) give convergent results for a long molecule possessing many clusters.

The degree of 'tight' folding is defined as

$$p_{tf} = p_{ar} + p_{aar} = \frac{\begin{pmatrix}\text{number of successful}\\ \text{tries for adjacency}\end{pmatrix} + \begin{pmatrix}\text{number of successful}\\ \text{tries for next-nearest}\\ \text{neighbour re-entry}\end{pmatrix}}{\text{total number of tries}} \tag{53c}$$

All other events, such as a third or higher-nearest neighbour re-entry in the same lamella or a transit to another lamella (interlamellar link = 'tie molecule') are taken to be endowed with amorphous character and are denoted p_{nar}. The above definitions will subsequently be found useful in dealing with molecular trajectories in higher molecular weight systems.

Note from *Figure 15* that there is firm evidence for chain folded clusters with three adjacent stems as for $f = 2$, $\bar{\nu}_c = 3$, which already gives a lower bound for p_{ar} of 2/3 with equation (53b). Meanwhile, it is evident from *Figure 15* that there are some clusters with four adjacent stems present, as for $f = 3$, $\bar{\nu}_c = 4$.

B. Cilium free energy; also reference states

Because the interpretation suggested above holds that a very short localized cilium has a negligible local surface free energy and that a long and topologically confined cilium in the interfacial zone is associated with a large local surface free energy, it is useful to examine these points in the light of current treatments of the subject.

Lauritzen and DiMarzio[182] derived the partition function for a cilium confined to a wedge angle ϕ_0, the origin of the cilium being at the inner vertex of the wedge. The angle of sweep ϕ_0 of the cilium within the confines of the wedge is taken to represent in general terms the crystal surfaces present and the crowding effect of other cilia in the immediate vicinity of the cilium under consideration. The partition function leads to the expression[77]

$$\sigma_{cil}\,(\text{erg cm}^{-2}) \cong \Lambda\left(\frac{kT}{a_0 b_0}\right) \ln N_s \tag{54a}$$

in which the numerical constant Λ is given by

$$\Lambda = \pi/2\phi_0 \tag{54b}$$

where ϕ_0 is in radians and N_s the number of statistical chain segments in the cilium. As a sufficient approximation, we take N_s to be given by

$$N_s = \frac{n_b l_b}{C_n l_b} = \frac{n_b}{C_n} = \frac{(l_{cil}/l_u) - 1}{C_n} \tag{54c}$$

where $n_b l_b$ is the length of the cilium in l_b units, $C_n l_b$ the length of a statistical segment, and C_n the characteristic ratio relevant to the number n_b of C–C bonds in l_{cil}. From the above, it is readily deduced that for a cilium with a specified angle of sweep, σ_{cil} is minimized if a chain initially attaches to a niche with one end quite short and the other long. Then, through the interplay of the forward and backward reactions A and B, new chains will initially tend to attach in this manner during substrate completion.

For the purpose of estimating σ_{cil}^{+}, the above formulation is valid for $l_{cil} \geq \sim 15$, $n \geq \sim 12$, $n_b \geq \sim 11$ where the mutual crowding effect of the cilia can be expected to be present; the n_b range corresponds to a C_n of ~4.0 or higher. (Values of C_n for $n_b > 3$ are readily calculated with a simple empirical formula give by Mansfield and Syi[35]; see also ref. 36, p. 327.) Note that when $l_{cil}/l_u = 2$, $n_b = 1$, $C_n = 1$, so σ_{cil} is zero.

That high values of σ_{cil} approaching 90 erg cm^{-2} can arise when the angle of sweep of a cilium in the interfacial zone is topologically confined can be developed by an illustrative calculation. Shortly it will be shown that the excess cilium length in the 1^+ and 2^+ states is ~55 Å. For this length, $n \cong 43$, n_b is ~42, and the latter leads to a C_n of 6.03. Then, with equations (54), one finds with $kT/a_0 b_0 \simeq 30$ erg cm^{-2} that σ_{cil} is $53.4(\pi/2\phi_0)$ erg cm^{-2}. Taking $\pi/2\phi_0$ to be 1.69, which corresponds to a ϕ_0 of 53.4°, one then has

$$\sigma_{cil}^{+} \cong 90\,\text{erg cm}^{-2} \tag{54d}$$

as in equation (52b). The angle of sweep of 53.4° employed above is arbitrary, but it does reflect what we deem to be a correct physical concept. The restricted angle of sweep implies a high degree of mutual exclusion of the densely spaced cilia as they compete for configuration space in the interfacial zone at the growth front. This general idea would appear to be reasonable in terms of the $f = 1^+$ and $f = 2^+$ ciliated structures depicted in *Figure 15a*, especially if portrayed to actual scale. Note that the confined but still coiled cilia of the length considered here are taken to be part of the interfacial zone and, therefore, contributors to the surface free energy associated with the stems of origin. That part of a very long cilium that projected into the bulk melt phase from the dividing surface between the interfacial zone and the bulk melt would be assumed to modify slightly the entropy of that melt but not contribute to the surface free energy.

Though not given here, a large σ_{cil}^{+} can be obtained with expressions derived by Guttman *et al.*[183] for a polymer cilium restricted to a cone with generating angle Θ_0. (This Θ_0 is not to be confused with the θ employed earlier to represent the angle of tilt.) Rather large values of $2\Theta_0$ suffice to give estimates of σ_{cil}^{+} comparable to a fold surface free energy of 90 erg cm^{-2}, but some mutual exclusion of the cilia must still be assumed.

Consider now the very short cilia characteristic of the lower bound $f = 1$, $f = 2$, and $f = 3$ states (*Figure 15a*). Data to be brought forth shortly will show that in these

states the cilium lengths are indeed quite short. In this context it needs to be shown why very short localized cilia (chain ends at or very near the lamellar surface) are taken to have a nil surface free energy (leaving only the chain folds to be considered as in equation (52a) for the non-ciliated lower bound states) when the undercooling is measured from T_m, i.e. the melting point of an extended-chain crystal of large lateral extent with an equilibrium degree of perfection consisting of chains of the molecular weight under consideration. The treatment to follow clarifies this point as well as certain questions[146] relating to the reference states based on T_m that we have employed both here and in earlier work.

We begin with a simplified version of the Flory–Vrij[76] equation based on a straightforward expansion of the free energy about T_m^0 noted by Broadhurst[184] who showed that for extended-chain *n*-alkane crystals with moderate to large n the depression of the melting point below the equilibrium melting temperature T_m^0 for $n \rightarrow \infty$ is given in molar units by

$$T_m^0 - T_m = T_m^0 \left\{ \frac{-\Delta G_{e.g.}^* + RT_m^0 \ln n}{(\Delta H_f) n} \right\} \qquad (55a)$$

where n is the number of $-CH_2-$ units, $\Delta G_{e.g.}^*$ a free energy traceable to the repulsion of $-CH_3$ end groups relative to the interior $-CH_2-$ units, ΔH_f the heat of fusion, and $RT_m^0 \ln n$ a term associated with the entropy of localization of the end groups. This expression can readily be converted directly to the form involving surface free energies

$$T_m^0 - T_m = T_m^0 \left\{ \frac{2\sigma_{e.g.}^* + (kT_m^0/a_0 b_0) \ln n}{(\Delta h_f) l_m} \right\} \qquad (55b)$$

Here l_m is the length of the molecule and both the quantities in the brackets in the numerator are, in effect, surface free energies in erg cm^{-2} associated with the localized $-CH_3$ end groups that cause the actual melting point T_m of the equilibrium extended-chain crystal to fall below T_m^0. With $\sigma_{e.g.}^* = 58.15$ erg cm^{-2} (corresponding to $\Delta G_{e.g.}^* = -3161$ cal mol^{-1}, which is fairly close to Broadhurst's estimate based on *n*-alkane data), $kT_m^0/a_0 b_0 = 30.62$ erg cm^{-2}, $\Delta h_f = 2.80 \times 10^9$ erg cm^{-3}, and $T_m^0 = 418.7$ K, one can calculate any T_m value in *Tables 2* or *4* with an accuracy of better than 0.1° from the lowest n_w, which is 256.6, to the highest n_w of 8197. Following earlier practice, we base T_m estimates on M_w, so n here is $n_w = M_w/14.03$ and l_m above is $n_w l_u$. In numerical terms equation (55b) comes to

$$T_m^0 - T_m = [1366 + 359.7 \ln n_w]/n_w \qquad (55c)$$

which is valid for the orthorhombic form for $n_w \geq \sim 250$. The basic physics required to discuss the reference temperature from which the undercooling ΔT is to be measured for orthorhombic $(-CH_2-)_n$ systems $n_w \geq \sim 250$ involving substantially localized chain ends and chain folds is embodied in equations (55a) and (55b). There will be a certain degree of natural unpairing near T_m in the equilibrium extended-chain crystal, and our use of the term 'localized chain ends' is assumed to include this effect.

It is evident from the above that when T_m is chosen as the melting point from which to measure the undercooling as $\Delta T = T_m - T_x$, a short localized end group (or set of such end groups) contributes nothing further to the depression of the melting point or to the surface energetics generally. All the surface energy effects associated with short localized end groups that cause T_m to fall below T_m^0 are in equation (55b). Thus, if T_m is chosen as the reference temperature, only the effects of the chain folds (and in appropriate instances any topologically confined longer cilia in the interfacial layer) will further lower the melting point as, for example, in a T_m' vs. $1/l$ plot based on equation (7a) for lamellae containing chain folds. The depression of T_m' below T_m in such a plot is a result of the chain folds that are present plus any contribution of confined cilia in the interfacial zone; any short localized chain ends that are present make no contribution to the depression of T_m' below T_m. Moreover, the T_m obtained from an experimentally solid T_m' vs. $1/l$ plot based on equation (7a) is, in principle, consistent with the Flory–Vrij equation—for an example of an experimental verification, compare melting point results in Section III.B for $M_w = 32.1$ K fraction. It follows on the same basis that in the mean field approximation, equation (52a), which will shortly be successfully applied in a kinetic context, any short localized chain ends make no contribution to $\bar{\sigma}_e$. Thus, through the use of the T_m from the Flory–Vrij development or from a T_m' vs. $1/l$ plot to find the undercooling $\Delta T = T_m - T_x$, one can without undue complication clearly bring out the direct effects of chain folds, yet at the same time have their treatment ultimately related to the properties of the infinite equilibrium extended-chain crystal *via* equations (55) should that be considered desirable.

Attainment of the true equilibrium T_m of the *n*-alkanes for n of ~150–200 upward simply by direct measurement is not practical, as is evident from the work of Stack *et al.*[185] who showed that the estimation of T_m must be approached through extrapolation. For *n*-$C_{192}H_{386}$ (C-192), these authors found that a specimen rapidly crystallized at low T_x in the extended-chain form melted *ca.* 1.3° lower than the T_m obtained by extrapolation with a T_m' vs. T_x plot using a set of higher T_x; as noted elsewhere[13] the extrapolated T_m of ~127.5°C came to within 0.5° of the T_m calculated with Broadhurst's[184] detailed version of the Flory–Vrij equation that led to a T_m^0 of 144.7 ± 0.5°C. It has been suggested[13] that as initially formed at low T_x in the extended-chain domain, some of the chain ends in a higher *n*-alkane are, for kinetic reasons, unpaired to the point that the surface is actually somewhat ciliated creating a small σ' (or σ_{cil}^+ in the current notation) that lowers the melting point. (It would be asking a lot to require that virtually all of the chain ends in a long *n*-alkane initially line up in equilibrium localized array even in a relatively slow crystallization.) It was noted further that this highly persistent effect would be lessened at higher T_x because of the much longer crystallization/annealing time, thus explaining the increase of T_m' with T_x in the T_m' vs. T_x plot. This model is also consistent with a somewhat low heat of fusion and the presence of 'premelting' effects of the type seen in C-192[186]. For those *n*-alkanes that exhibit a maximum in $G(T_x)$ in the extended-chain domain, the data for the T_m' vs. T_x extrapolation should be confined to T_x values *above* the maximum. Failure to note the above points could lead to serious underestimation of the true equilibrium melting points of the higher *n*-alkanes, thereby apparently casting doubt on the basis of the Flory–Vrij approach. The authors

Table 5 Analysis of quantized chain folding in regime I for low MW polyethylene fractions[a] (range A–A′, M_n 3.19K to 11.0K)

A. Clusters with short localized cilia (lower bound, $\bar{\sigma}_e = \sigma_{e(\infty)}[f/(f+1)]$ with $\sigma_{e(\infty)} = 90\,erg\,cm^{-2}$)

T_m (K)	Folds per molecule, f	Length of molecule, $l_m = \bar{M}_{nw} \times 1.273/14.03$ (Å)	l_g^* calc. as $(l_m - 7.6f)/(f+1)$ (Å)	Mean undercooling, $\overline{\Delta T}$ (°C)	$\bar{\sigma}_e$ at quantized transition from equation (52a) ($erg\,cm^{-2}$)	$l^*_{g(\text{lower bound})}$ with $\bar{\sigma}_e$ by equation (56b) (Å)	l_{cil} from equation (56a), $l_m - 7.6f - (f+1)l^*_{g(\text{lower bound})}$ (Å)
405.60	1	307.5	**150.0**	12.65	45	**146.1**	7.7
410.55	2	534	**172.9**	13.85	60	**170.0**	8.8
412.64	3	744	**180.3**	14.49	67.5	**180.3**	0.0
							$\langle \bar{l}_{cil} \rangle$ is 5.5 ± 3.7 Å
414.03	4	1000	**193.9**	14.75	72	**187.4**	32.6†

† At $f = 4$, $l_{nar} \cong 32.6 - 5.5 \cong 27.1$ Å

B. Clusters with long spatially confined cilia (upper bound, $\sigma^+_{cil} = \sigma_{e(\infty)} - 90\,erg\,cm^{-2}$)

T_m (K)	Folds per molecule, f	Length of molecule, l_m (Å)	Mean undercooling, $\overline{\Delta T}$ (°C)	$l^*_{g(\text{upper bound})}$ with $\sigma^+_{cil} = \sigma_{e(\infty)} = 90\,erg^{-2}$ by equation (57b) (Å)	l^+_{cil}, total length (both cilia) calc. as $l_m - 7.6f - (f+1)l^*_{g(\text{upper bound})}$ (Å)
410.55	1^+	534	13.85	233.6	59.2
412.64	2^+	744	14.49	226.1	50.5
					$\langle \bar{l}^+_{cil} \rangle \cong 54.9 \pm 4.4$ Å
414.03	3^+	1000	14.75	223.45	83.2††

†† At $f = 3^+$, $l_{nar} = 83.2 - 54.9 \cong 28.3$ Å

[a] Structures for short-cilium lower bound species ($f = 1$, 2, 3, etc.) and long-cilium upper bound species ($f = 1^+$, 2^+, 3^+, etc.) are depicted in *Figure 15a*

believe that the Flory–Vrij development with its $R\ln n$ entropic term is basically valid from a theoretical point of view and further that the detailed numerical versions of their equation (though they differ somewhat and may be subject to further refinement) give estimates of the melting points of the true equilibrium extended-chain state that, within the stated error limits, are far more reasonable for both finite and infinite n than those from early developments that omitted the $R\ln n$ term and gave a T_m^0 of *ca.* 141°C.

C. Estimate of cilium lengths and degree of adjacency: also onset of non-adjacent events at highest chain length

The low molecular weight quantized chain-folded systems in range A–A′ are well enough defined experimentally to extract further information from them. In particular, it will prove possible to obtain estimates of the mean length l_{cil} of the short cilia at $f = 1, 2, 3$, and 4 at the lower bound and, in addition, the mean length l^+_{cil} of the much longer cilia at $f = 1^+$, 2^+, and 3^+ at the upper bound (see *Figure 15a*). In this process we shall find clear evidence of the beginnings of some adjacent re-entry in the higher molecular weight cases $f = 3^+$ and $f = 4$.

To estimate the mean length of the cilia for a system with a given number of folds per molecule f, we subtract from the length of the molecule l_m the total length of the $(f+1)$ stems as well as the length of the chain folds $f(l_f)$. Here we use $l_f = 7.6$ Å as for the case of six bonds per fold. The length l_m of the molecule is calculated according to $l_u \bar{M}_{nw}/14.03$. In the case of short localized cilia (chain ends) such as occur when the number of folds per molecule corresponds to $f = 1$, 2, etc., at the lower bound we thus employ

$$l_{cil} = l_m - 7.6f - (f+1)l^*_{g(\text{lower bound})} \quad \text{(short localized cilia)} \tag{56a}$$

to calculate the sum of the two short cilium lengths, where we set

$$l^*_{g(\text{lower bound})} = \frac{2\bar{\sigma}_e T_m}{\Delta h_f(\overline{\Delta T})} + C_2 = \frac{2\sigma_{e(\infty)}[f/(f+1)]T_m}{\Delta h_f(\overline{\Delta T})} + C_2 \tag{56b}$$

with $\bar{\sigma}_e$ being given by the mean field approximation according to equation (52a).

For the situation involving the long spatially confined cilia occurring within the interfacial zone at the upper bound in *Figure 15b*, such as obtains at $f = 1^+$, 2^+, etc., the mean value of the sum of the two cilium lengths, which is l^+_{cil}, is given by

$$l^+_{cil} = l_m - 7.6f - (f+1)l^*_{g(\text{upper bound})} \quad \text{(long spatially confined cilia)} \tag{57a}$$

in which

$$l^*_{g(\text{upper bound})} = \frac{2\sigma^+_{cil} T_m}{\Delta h_f(\overline{\Delta T})} + C_2 = \frac{2\sigma_{e(\infty)} T_m}{\Delta h_f(\overline{\Delta T})} + C_2 \tag{57b}$$

where σ^+_{cil} at the 1^+, 2^+, and 3^+ states is set at $\sigma_{e(\infty)} = \sigma_{e(\text{fold})} = 90\,erg\,cm^{-2}$ in conformity with equation (52b). In equations (56b) and (57b), C_2 is 43 Å.

The calculations for l_{cil} and l_{cil}^{+} are detailed in *Table 5*. The first point to notice is that for the lower bound in *Table 5A*, l_g^* calculated directly from the length of the molecule as corrected for the length of the fold(s) according to $(l_m - 7.6f)/(f+1)$ coincides closely with $l_{g(\text{lower bound})}^*$ as determined by equations (56) using the mean field approximation, equation (52a); compare the two columns of **bold face** numbers for $f = 1$, 2, and 3. Note further in *Table 5A* that the $\bar{l}_{cil}$ value for $f = 1, 2$, or 3, though involving some scatter, indicates that the cilia are certainly very short for these f numbers as is consistent with one of the precepts of the quantization effect as illustrated in *Figure 15a*. No mutual exclusion effect is expected for such short cilia, so at most only a vestigial σ_{cil}^{+} would be present. With the full length of the molecules being accounted for within a few Å units in the 'lower bound' chain folded structures with short localized cilia for $f = 1$, 2, and 3, a very high degree of adjacency in these structures is directly indicated. In these cases, there is simply no additional molecular length available to provide for a random coil excursion to even a nearby non-adjacent site. Importantly, the case $f = 4$ shows a notable departure; the apparent l_{cil} value has suddenly risen to ~27 Å. Our interpretation of this number is that it actually represents a non-adjacent re-entry effect, rather than a long cilium, and we have therefore labelled it as l_{nar} in *Table 5A*. The value of l_{nar} suggests that a certain fraction of the attempts to form the fourth fold actually execute a random flight to a relatively nearby, but nonadjacent, site. The intervention of these nonadjacent events is doubtless the cause of the somewhat muted character of the quantization effect and the augmentation of the lower bound in the $f = 4$ region (see line a–a′ in *Figure 15b*).

Consider now the case of the longer cilia treated in *Table 5B*. The $l_{g(\text{upper bound})}^*$ values as calculated with $\sigma_{cil}^{+} = \sigma_{e(\infty)} = 90\,\text{erg cm}^{-2}$ as for spatially confined cilia involving mutual exclusion with equations (54) when employed in equations (57) at the various mean undercoolings $\overline{\Delta T}$ noted conform closely to the l_{obs}^* vs. ΔT curve exhibited in *Figure 14*, so with the reliable values of l_m, a reasonable estimate of $\bar{l}_{cil}^{+}$ is expected. The $\bar{l}_{cil}^{+}$ value for $f = 1^+$ or 2^+ centres around *ca.* 55 Å and is clearly much longer than $\bar{l}_{cil}$ for $f = 1$ and $f = 2$. These longer confined cilia are the cause of $\bar{\sigma}_e$ reaching upper bound 'peak' values at $f = 1^+$ and $f = 2^+$ and are not associated with a nonadjacent re-entry effect; in each case a small increase of chain length leads $\bar{\sigma}_e$ rather abruptly to fall toward the lower bound because of the now short terminal cilia. Thus, it is firmly established that, in accord with the proposed origin of the quantization effect, there is a sharp fall in the overall cilium length at the $f = 1^+ \rightarrow 2$ and $f = 2^+ \rightarrow 3$ transitions as depicted schematically by the molecular trajectories in *Figure 15*, which then leads to the notable changes in $\bar{\sigma}_e$.

The case $f = 3^+$ exhibits an excess apparent cilium length of about 28 Å (*Table 5B*) which is comparable to the l_{nar} of ~27 Å found for $f = 4$. Accordingly, we have labelled this excess length as being also l_{nar}, i.e. the result of some nonadjacent events occurring as attempts are made to form the third fold in the sequence. This in turn leads to the augmentation of the lower bound base line as shown by the line a–a′ in *Figure 15b* in the vicinity of the $f = 3^+ \rightarrow 4$ transition.

The results given in *Table 5* and the related discussion provide quantitative support for the quantization effect. In particular, the results in *Table 5A* for $f = 1$, $f = 2$, and $f = 3$ cannot be explained by other than mostly adjacent re-entry, and it is reasonable that the same holds for the ciliated $f = 1^+$ and 2^+ states treated in *Table 5B*. The $f = 3^+$ and $f = 4$ states evidently occur with adjacent re-entry to a definite extent as depicted in *Figure 15a*, but perhaps one-half of the 'tries' for adjacent re-entry clearly failed. The l_{nar} values of ~27–28 Å associated with the $f = 3^+$ and $f = 4$ states listed as l_{nar} in *Table 5* are typical of what would be expected for a short random flight transit within the thin interfacial zone to a nearby but nonadjacent site.

Based on the relative depth of the minimum in $\bar{\sigma}_e$ between $f = 2^+$ and $f = 3^+$ in relation to the more ideal approach to the theoretical lower bound between $f = 1^+$ and $f = 2^+$ in *Figure 15b*, we estimate that the mean cluster size $\bar{\nu}_c$ the system can attain if the molecules are long enough is close to 3.5. Also, one can readily deduce from the data in *Table 5* that a mean cluster size of $\nu_c \cong 3.5$ is reasonable. In *Table 5A* the $f = 3$ case with $\nu_c = 4$ gives a close match of the l_g^* data by two methods (**bold face** numbers) and in *Table 5B* the $f = 2^+$ case with $\nu_c = 3$ gives consistent results for l_{cil}^{+}; the divergences resulting from l_{nar} appear only at $f = 4$, $\nu_c = 5$ and $f = 3^+$, $\nu_c = 4$, respectively.

With equation (53b) the cluster size of $\bar{\nu}_c \cong 3.5$ gives a probability of adjacent re-entry directly relevant for PE in the range 9–11 K melt-crystallized in regime 1 of

$$p_{ar} \cong 0.71 \tag{58}$$

This is an interesting result in that it is close to the value of p_{ar} of ~0.75 estimated from neutron scattering and i.r. studies by Spells[98] for PEH–PED single crystals of moderate molecular weight formed in dilute solution. (An early and frequently overlooked indication of a high degree of surface regularity implying good adjacency in solution-grown chain-folded single crystals was given by Holland and coworkers[187–189] who found dislocation networks in bilayered single crystal mats for a fraction of $M_\eta = 10$K.) The estimate of p_{ar} in equation (58) supports our theme that crystallization from the melt in regime I can lead to a high degree of adjacency. Here the ρ_{tf} or the Gambler's Ruin lower bound is ~0.64 as for $\theta = 19°$. With p_{ar} at 0.71, the true p_{tf} must be even higher. Thus it is readily apparent that kinetic effects can, for crystallization in the melt in regime I, give a degree of 'tight' folding p_{tf} much in excess of that required by strictly topological considerations.

The high adjacency seen here for the {1 1 0} sector for PE crystallized from the melt in regime I is all the more striking in view of the fact that according to theoretical modelling the chain stiffness (work of chain folding) opposes adjacent re-entry[19]—these calculations would seemingly have p_{ar} for PE in the vicinity of ~0.37, or slightly lower if there is a small angle of tilt. However, this is not a contradiction in this case since this type of 'equilibrium' calculation actually represents a *lower bound* for p_{ar} and is therefore more representative of regime III than regime I. While we certainly believe that chain stiffness in principle lessens the 'equilibrium' lower bound of p_{ar}, it is evident that for PE fractions crystallized in regime I this obstacle is readily overcome by kinetic effects associated with the high probability of an emergent chain entering an adjacent 'niche'.

It is emphasized that the results quoted here for p_{ar}

refer to the {1 1 0} sector, which has the kinetically dominant growth front exhibiting the quantized effects shown in *Figure 15*. As pointed out earlier, PE crystals formed in regime I tend to possess large but kinetically subordinate {2 0 0} growth sectors with curved edges. The present treatment does not give estimates of p_{ar} for these sectors. Because of the strain known to occur in the {2 0 0} sectors resulting from repulsion of the chain folds, it has been suggested[32] that the degree of adjacency is less in these sectors than in the {1 1 0}.

D. Summary

Clear evidence for quantized chain folding in PE fractions crystallized in regime I has been presented. At what amounts to an approximately fixed undercooling, once-folded systems appear at the lowest chain lengths, but with increasing chain length twice-folded entities with two folds per molecule and three adjacent stems appear rather abruptly at the $f = 1^+ \rightarrow 2$ transition. With further increase in chain length a well-defined $f = 2^+ \rightarrow 3$ transition appears, signifying the presence of chain-folded clusters with four adjacent stems with three chain folds connecting them. These 'quantized' transitions are a direct result of the increase of the mean length of the spatially confined terminal cilia within the interfacial zone to a point that the surface energy σ_{cil}^{+} associated with them begins to exceed that of a chain fold—at this point the molecule elects to add a new stem with an intervening chain fold and an accompanying chain end that has a short cilium which induces a lowered $\bar{\sigma}_e$; this then leads to a faster growing (observable) crystal because $\sigma\bar{\sigma}_e$ in K_g is now lower. A definite though less pronounced $f = 3^+ \rightarrow 4$ quantized transition is seen (*Figure 15*), signifying the presence of some four times folded entities with five stems, but at the same time definite evidence of some non-adjacent re-entry was also found. This took the form of a length l_{nar} of ~27–28 Å that is required to be ascribed to an 'amorphous' excursion of a chain from some of the clusters to a relatively nearby but non-adjacent site. This may well be regarded as the preliminary onset of what many investigators think of as typical polymeric behaviour.

Provided that the forced reptation effect is fully active, a mean cluster size of 3.5 or slightly below may be expected to hold in regime I for the {1 1 0} sector for molecular weights greater than 9–11K, as in molecular weight range B–B′. In such a system, this leads to the 'variable cluster' model for the chain trajectory in a lamella. This concept will be followed up in the next section where the trajectories for regimes I and III are compared. The present analysis holds that the initially-formed fold surface in the quantized species is rough and contributes to C_2.

Lastly, we emphasize that the $f = 2$ and $f = 2^+$ structures with $\bar{\nu}_c = 3$ shown in *Figure 15* are particularly strongly supported by the data and have an assured adjacency of $p_{ar} \cong 2/3$ with equation (53b). It is clearly evident from this that the adjacent 'niche', through its energetically favourable character combined with the 'proximity' effect associated with the emergent chain, proves in regime I to be a highly advantageous site for adjacent re-entry during the substrate completion process. Also, in the substrate completion process in regime I, any excursion of an emergent chain to a higher energy nonadjacent site with no 'niche' is apt to be removed by the backward reaction B_1 of equation (3d) before it is pinned in place by addition of another stem. It is these effects, together with the ease of reptation and the virtual absence of multiple attachment at distant sites, that deter the chaos of the melt state from imposing itself in anything remotely approaching full measure on the surface structure of the lamellar crystal in regime I in range A–A′.

VI. MOLECULAR TRAJECTORIES AS A FUNCTION OF MOLECULAR WEIGHT AND UNDERCOOLING IN MELT-CRYSTALLIZED PE: NEUTRON SCATTERING AND INFRARED STUDIES

A. Objective

Here we bring together a body of experimental results and theoretical insights concerning the degree of perfection of the fold surface in melt-crystallized PE fractions as a function of molecular weight and crystallization conditions. It is convenient to do this by first selecting the regime of crystallization and then indicating the trends with molecular weight if they are known or subject to reasonable inference. The indices employed to describe the regularity of the chain folding are p_{ar} and p_{tf}, the estimated probability of adjacent re-entry and the probability of 'tight' folding, respectively. Some emphasis is given to comparisons at a molecular weight of ~40K since it is in this vicinity that the most valid comparisons of the chain trajectories characteristic of regimes I and III can be made. Schematic diagrams are given to illustrate the general nature of the molecular trajectories and to highlight certain details not readily apparent simply from the values of p_{ar} and p_{tf}. Despite the presence of considerable gaps and uncertainties in our knowledge, a reasonably clear overall picture can be developed.

B. Regime III

A considerable amount of work has been carried out on melt-crystallized PEH–PED systems by neutron scattering and infrared spectroscopic techniques. The reader will recall that from the necessity of subduing segregation effects, the PEH–PED mixtures were crystallized at low temperatures corresponding to regime III. One does not anticipate particularly regular folding in such specimens. In fact, it is expected that p_{tf} will be close to the Gambler's Ruin lower bound and p_{ar} to be rather smaller. We discuss the neutron scattering results first.

B.1. Neutron scattering. The small and intermediate angle neutron scattering (hereafter denoted generally NS) results for melt-crystallized PEH–PED systems are often reported and interpreted according to $F_N(\mu)$ vs. μ Kratky plots where $F_N(\mu)$ is a function dependent on intensity and molecular weight and μ is $(4\pi/\lambda)\sin(\psi/2)$ in which λ is the neutron wavelength and ψ as used in this context is the scattering angle. The experimental NS results of Schelten *et al.*[190], Stamm *et al.*[191], Bai[192] (see also ref. 193), and Sadler and Keller[194,195] for crystallized PEH–PED have been gathered together by Guttman, DiMarzio, and Hoffman[104] (GDH) and plotted as $F_N(\mu)$ vs. μ in *Figure 3* of the last-mentioned paper. The molecular weight range was roughly 40K to 150K, depending on the particular investigation. This corresponds to the upper

part of range B–B′, the main part of C–C′, and the first part of D–D′ (*Figure 7b*). The study[190] covering the largest range of μ involved a molecular weight of either ~47K or ~60K (see below), which is in the vicinity of the borderline between ranges B–B′ and C–C′. The actual temperature of crystallization of the PEH–PED specimens is in most cases not known accurately, since one is faced with such statements as 'slow cooled' or 'rapidly cooled'. However, in one case a thin 'air-cooled' specimen of the type commonly employed in NS experiments that was associated with data showing minimal segregation was formed with a thermocouple embedded in it and found[196] to crystallize mainly at $T_x \cong 117 \pm 3°$ or $\Delta T \sim 27 \pm 3°$. From *Figure 13*, this is seen to correspond to the upper part of regime III; on entering this regime the crystallization rate increases markedly so that the resultant release of the heat of fusion tends to hold the specimen at a T_x somewhat below the II → III transition.

While we do not reproduce here the plot of $F_N(\mu)$ vs. μ obtained by various investigators gathered together by GDH, it is sufficient to note that $F_N(\mu)$ rises at first with increasing μ, showing only a minimal degree of structure, and then tends to level off. Superficially at least, the plot is quite like that of the parent molten PEH–PED mixture; if it were not known that the specimen had a moderately high degree of crystallinity (typically $\chi \simeq 0.60$–0.65) and a decidedly lamellar structure, one might be tempted from the $F_N(\mu)$ vs. μ data alone to say that nothing important happened on crystallization. The theoretical $F_N(\mu)$ vs. μ curve for high or essentially perfect adjacency in the {1 1 0} plane has been computed, e.g. refs 197 and 198, and exhibits distinct maxima each with relatively high $F_N(\mu)$. At best, the experimental results show only vestiges of maxima and the general magnitude of $F_N(\mu)$ is too low. Standing alone, the NS data can be well fit[104,198] with a model featuring a p_{ar} near or at zero, apparently indicative of a 'random switchboard'—however, it is just such models that, on further examination employing only parameters inherent in them, exhibit serious density anomalies in the interfacial region which invalidate them[104]. For the most extensive set of data[190], which has been widely used, the absolute value of $F_N(\mu)$ is uncertain because of a discrepancy in the molecular weight—g.p.c. gave $M \simeq 60$K whereas NS gave ~47K, the latter giving the lower $F_N(\mu)$. Both sets of $F_N(\mu)$ were considered by GDH.

Whatever the uncertainties in the $F_N(\mu)$ vs. μ results, it is evident that a high degree of adjacency in the {1 1 0} plane is not present in the regime III specimens. As noted, the NS data standing alone are not clearly indicative of the value of p_{ar}, and to obtain approximate estimates of this quantity it is necessary to bring in additional information and invoke certain provisos. These are outlined below.

In developing molecular trajectories for the regime III case, GDH, in addition to requiring a reasonable fit of the $F_N(\mu)$ vs. μ data, applied the following restrictions and considerations:

(1) *The proposed model must be consistent with the p_{tf} of equation (36)*, i.e. a density anomaly at the interfacial boundary is not permitted. (This already eliminated two irregular re-entry 'switchboard' models that had been suggested—see *Figure 2* of GDH.) Values of p_{tf} of 0.51–0.58 are applicable, corresponding to $\theta = 45°$ and 35°, respectively[25,103]. This revises downward the estimate of 0.6–0.7 originally given by GDH, which was based on $\theta \cong 0°$.

(2) *The model shall reproduce the observed characteristic ratio C_∞ of the semicrystalline PEH–PED system.* The observed characteristic ratios for the crystallized PEH–PED systems are similar to but somewhat higher than those of the parent melt.

(3) *The degree of crystallinity shall be reproduced by the proposed model.* For modelling purposes, various workers have standardized on $\chi \cong 0.64$, corresponding to an amorphous spacing l_{amorph} of 90 Å and a lamellar crystal thickness l_{core} of 160 Å[104,190]. For trial purposes, these assumptions are adequate for specimens crystallized in the upper part of regime III. The degree of crystallinity is such as to require that some of the nonadjacent re-entries form tie chains with relatively normal amorphous character between the crystalline lamellae.

(4) *The radius of gyration determined for the model shall vary as $M^{1/2}$.* From NS studies[190] this $M^{1/2}$ law is known to hold for regime III semicrystalline PEH–PED specimens in the intermediate molecular weight range of interest here, which corresponds approximately to the upper part of range B–B′ and most of range C–C′ (see *Figure 7b*). This $M^{1/2}$ law applies to the melt state of PE as well.

In connection with the GDH analysis of the NS results, it is well to recall here the work of Guttman and DiMarzio who modelled regime III crystallization with the 'bricklayer' scheme[95]. It was found that space-filling in regime III could only be attained if stems were put down on more than one lattice plane. This is illustrated schematically in the lower part of *Figure 16a*. (Observe the extended definitions of p_{ar} and p_{aar} in this case.) This provides a theoretical basis for the use in the analysis of the NS results of a larger mean separation of the stems involving p_{ar} and p_{aar}, which is essential to matching the rather low $F_N(\mu)$ that is observed at various μ. The $F_N(\mu)$ vs. μ results simply cannot be fitted without invoking a 'stem dilution' effect such as arises from short-range excursions to different lattice planes or 'leapfrogging' within a specified lattice plane, the latter being suggested by Sadler[105] and also employed as part of the GDH analysis.

Figure 16a shows a sample molecular trajectory of PE that exhibits in a schematic way a number of features associated with regime III crystallization. A large angle of tilt θ is shown to illustrate this feature, which is known to be required by experiment. The chain typifies a 'variable cluster' model, which leads to a radius of gyration for the semicrystalline polymer that varies[199,200] as $M^{1/2}$ as required by the NS data in this general molecular weight range. The chain is allowed to show a change of lattice plane, as predicted by Guttman and DiMarzio. In *Figure 16a*, dotted lines ··· denote stems laid down on lattice plane (ii) and solid lines — denote stems put down in plane (i). The mean cluster size for the molecule shown in *Figure 16a* is 1.67, giving a p_{ar} of 0.40 with equation (53b) or 0.42 with equation (53a). For the variation of this model with a rough growth front, GDH have shown that the NS data (g.p.c. molecular weight assumed) are consistent with p_{ar} of 0.34–0.40. Some of these adjacencies were in the same lattice plane, while others represented traverses to a nearest neighbour in

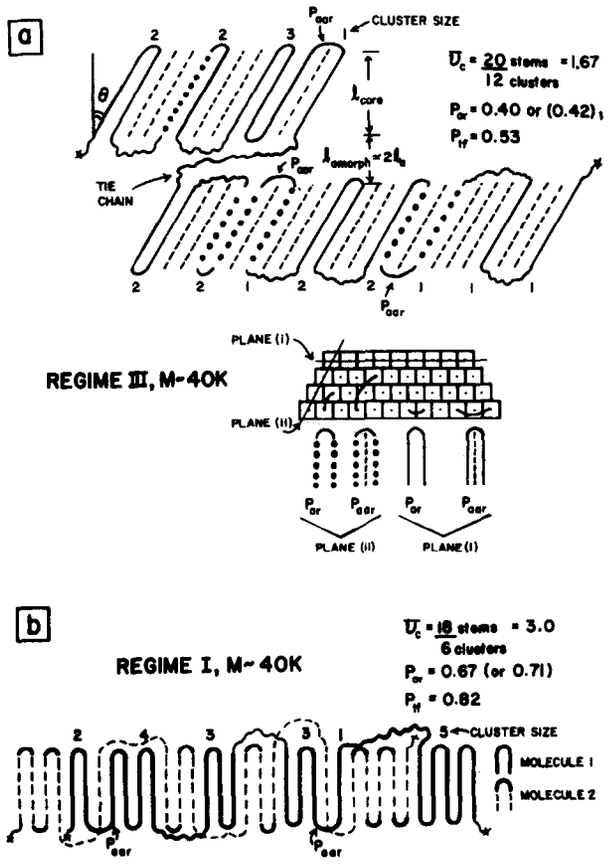

Figure 16 *Molecular trajectories for melt-crystallized PE in regimes I and III for* $M \sim 40$K, *upper part of MW range B–B′.* (a) Typical trajectory showing low p_{ar} and p_{tf} and large angle of tilt characteristic of regime III crystallization. Inset shows types of adjacency p_{ar} and next-nearest re-entry p_{aar} for two lattice planes for 'bricklayer' model—see text. (b) Estimated regime I trajectories for two molecules each with high p_{ar} and p_{tf}. Small angle of tilt not shown. Mean cluster size (average for both molecules) is $\bar{\nu}_c \cong 2.92$ giving $\bar{p}_{ar} \cong 0.66$. The mean degree of 'tight' folding is $\bar{p}_{tf} \cong 0.82$. Chain folding in regime I is much more regular than in regime III

another lattice plane, as is possible in a 'bricklayer' model. The particular molecule shown in *Figure 16a* has two 'tight' folds of the p_{aar} type which with the adjacent folds gives a p_{tf} of 0.526. Appropriately, this is essentially the Gambler's Ruin lower bound.

Observe in *Figure 16a* that the most common type of adjacent re-entry is taken to be a doublet; restriction of most of the adjacent re-entries to this conformation is consistent with the concept that reptation of slack is involved in regime III crystallization. The various subclasses of the 'variable cluster' model employed by GDH to fit the neutron scattering data, which in general resemble that of *Figure 16a*, gave an acceptable match to the observed C_∞ for the semicrystalline polymer and had the proper degree of crystallinity. On balance, we consider the sample trajectory depicted in *Figure 16a* a reasonable one for regime III-crystallized PE for $M \simeq 40$K, especially in view of the fact that it can match the $F_N(\mu)$ vs. μ data and obeys the provisos stated earlier. The question of the number of tie chains will be dealt with later.

As matters now stand, the available $F_N(\mu)$ vs. μ data are not able to distinguish which lattice plane (or planes) are involved, nor do they permit identification of other factors that might cause the stem dilution. Probably, stem dilution has multiple causes, such as isolated singlets, 'leapfrogging', and varying fold plane; all of these mechanisms are consistent with the small niche separations inherent in regime III crystallization[15].

Based on the analysis outlined above, the probability of adjacent re-entry for PE crystallized in regime III is reasonably placed in the range $p_{ar} \simeq 0.3$–0.4 for molecular weights in the vicinity of 40K (*Table 3*). Significantly, this range is in line with the careful Metropolis Monte Carlo study[19] mentioned previously that was carried out by Mansfield for a chain of stiffness comparable to that of PE wherein p_{ar} was estimated to be ~ 0.37; as noted earlier this result would fall to ~ 0.30 if the chains were tilted 35° or so. The lower bound of $p_{ar} \simeq 0.3$ just cited is the same as that given by Sadler[105].

The behaviour of the radius of gyration and its relationship to proposed molecular trajectories is of interest. Earlier, much had been made of the fact that the r.m.s. radius of gyration r_g of quench-crystallized PEH–PED varied as $M^{1/2}$ and was only a little larger than that of the parent melt in what we have termed the intermediate molecular weight range. This was interpreted in some instances as meaning that a random or near-random 'switchboard' model was almost certainly correct. As we have indicated, this oversimplistic deduction missed the fact that a density anomaly at the lamellar surface could not be permitted. Subsequently it was shown that a 'variable cluster' model with a modest degree of strict adjacency and a higher degree of 'tight' folding easily reproduced the observed behaviour of r_g for the semicrystalline lamellar system[199,200] without at the same time predicting a density anomaly. Thus, the observation of an r_g that varies as $M^{1/2}$ and that is only a little larger than that of the parent melt clearly cannot be construed as uniquely supporting a random re-entry switchboard model. For a case where segregation is absent and r_g does not vary as $M^{1/2}$, see subsequent remarks concerning *it*-PS.

Mansfeld has provided important theoretical insights into the behaviour of the r.m.s. radius of gyration r_g as a function of angle of tilt θ and degree of crystallinity χ to the accuracy that p_{tf} conforms to the Gambler's Ruin lower bound in the simplified form $1 - 1/3\cos\theta$ [cf. equation (36)]. The explicit formula is[201]

$$\frac{C_{\infty(\text{semicryst})}}{C_{\infty(\text{melt})}} = [2(1-\chi) + (1+\chi^2\tan^2\theta)/(1-\chi)]/3 \tag{59}$$

where one recalls that the mean square radius of gyration varies as C_∞. Here, $C_{\infty(\text{semicryst})}$ is the characteristic ratio of the regime III-crystallized PE sample and $C_{\infty(\text{melt})}$ that of the parent melt. With $C_{\infty(\text{melt})} = 6.7$, $\chi = 0.64$, and $\theta = 35°$, one finds $C_{\infty(\text{semicryst})} \simeq 9.1$; the experimental value is ~ 8.7[190]. This article explains in depth why $C_{\infty(\text{semicryst})}$, and thence r_g, does not differ greatly from that of the parent melt at the relatively modest χ attainable when PE is crystallized in regime III, the latter being required to minimize segregation effects. See also the detailed NS study by Crist and Nicholson[97] which supports the Gambler's Ruin model with its 'near-adjacent re-entry' property as embodied in equation (59). Readers interested in the segregation problem will find this work highly illuminating.

Unlike PE, segregation of the protonated and deuterated species does not occur to a detrimental extent in the *it*-PS system, so preparation of samples suitable for NS

experiments is feasible at high T_x where good single crystals can be formed from the melt. For this polymer r_g varies as M^{α} where $\alpha \cong 0.78$ for the semicrystalline state. On this basis Guenet *et al.*[202] could justify a model with chain-folded clusters of moderate size and tie chains to adjacent lamellae.

Consideration is now directed to the question of the number of tie chains between the lamellae and the relationship of this number to the 'Gambler's Ruin' problem. *Figure 16a* features a tie chain which contributes to the amorphous phase between the lamellae. The amorphous zone between the lamellae has a thickness l_{amorph} and consists of tie chains plus contributions from the nonadjacent events of the type where an emergent chain re-enters the lamella of origin at a more distant point that corresponds to a third-nearest neighbour or beyond. Thus, there are two sources for the interlamellar amorphous phase in melt-crystallized PE.

At the lower bound of p_{tf}, which corresponds to regime III, the Gambler's Ruin calculation has the fraction of surface sites occupied by tie chains, f_{link}, as the reciprocal[14] of the number of statistical steps N_p connecting the two lamellae by a straight-line perpendicular. Assuming that the length of a statistical step is $C_\infty l_b$ one then has in parallel with equation (54e)

$$f_{link} = \frac{1}{N_p} = \frac{C_\infty}{[(l_{amorph}/l_u) - 1]} \simeq \frac{C_\infty l_u}{l_{amorph}} \qquad (60)$$

From the standpoint of the Gambler's Ruin model, which is a limiting case based on random flights with space filling and topological constraints, this expression makes sense: for lamellae that are very close together a random flight quickly reaches the opposite lamella so f_{link} is large, but if far apart the probability of a random flight excursion reaching from one lamella to the other is low. To obtain a rough estimate of f_{link} for regime III for PE, we may employ the standard regime III model with an l_{amorph} of 90 Å corresponding, with an l_{core} of 160 Å, to a crystallinity of close to 0.64. (The degree of crystallinity χ for $M \sim 40$K in *Figure 7b* for PE crystallized in regime I is 0.8 to 0.9, but χ_c is generally lower for regime III crystallization.) The result with an l_{amorph} of 90 Å and a C_∞ of 6.7 is that f_{link} is about 0.095. It is on this basis that we have ventured to show a tie chain between the two lamellae in *Figure 16a* for regime III crystallization. It is worth noting that the Gambler's Ruin calculation indicates that the interlamellar amorphous phase consists of one-third long random flight tie chains to the opposite lamella and two-thirds of the amorphous traverses greater than p_{aar} that re-enter the lamella of origin[14,15]. Because of the higher degree of tight folding and adjacency, a lower number of links per unit area is to be expected in regime II and especially regime I. In these cases, more of the emergent chains return to the lamella of origin rather than execute a random flight to another lamella. Hence, f_{link} will be well below that given by equation (60) in regime I and the upper part of regime II.

The subject of the number of interlamellar links formed under various crystallization conditions is an important one, but has been left largely untouched in the experimental sense. However, one highly interesting approach to the problem was carried out by Backman and Devries[203] who employed electron spin resonance (e.s.r.) techniques to determine the number of free radicals formed in chain scission of links at fracture surfaces in PE. Their results can be interpreted to mean there was about one tie molecule for every 20 stems, i.e. $f_{link} \cong 0.05$[104]. In the present work the regimes and molecular weight ranges where the tie chains are expected to be prevalent have been outlined in broad terms. The concentration of tie chains must surely bear a connection to mechanical properties such as toughness and brittle → ductile effects. The authors believe that this connection could profitably be explored through combination mechanical, morphological, and e.s.r. studies on fractions crystallized under various controlled conditions.

B.2. Infrared studies. Jing and Krimm[204] investigated the infrared (i.r.) spectra of a number of 80 PEH/1 PED specimens that were cooled from the melt ($T_l = 165$°C) at a rate of ~1° min^{-1} to room temperature and the spectra subsequently measured at liquid nitrogen temperature. The PED molecular weights included 39.5K, 91.6K, and 150K and the results mentioned in what follows involve these specimens. The degree of crystallinity was taken to be in the range 0.64–0.77. The mode of preparation and the degree of crystallinity point to crystallization near the upper end of regime III.

The analysis of the i.r. spectra concentrated on the CD_2 bending mode line shape which was resolved into four components. In this resolved group, a doublet with a splitting of ~3.1 cm^{-1} was stated to be associated with adjacent re-entry in the {1 1 0} plane. This is of interest since it implies that at least some of the limited adjacencies are in the {1 1 0} growth plane. The actual contribution to p_{ar} from adjacencies in this plane has not been quantified, but one can certainly accept the statement[204] that adjacency in the {1 1 0} plane is not the predominant mode of re-entry. This is in general accord with the findings from neutron scattering for crystallization in regime III.

B.3. Summary and comment: regime III, intermediate molecular weights. The neutron scattering results, when considered in the light of additional experimental information and theoretical insights, indicate that a degree of adjacency of 0.3–0.4 is achieved in PEH–PED specimens of intermediate molecular weight crystallized from the melt in regime III. In particular, this result is expected to hold at 40K. The degree of tight folding p_{tf} is 0.51–0.58 depending on the prevailing angle of tilt (*Table 3*). The relatively low degree of adjacency and tight folding, the latter closely approaching the Gambler's Ruin lower bound at low T_x, can be traced to the high frequency of surface nucleation acts predicted by nucleation theory, which causes very closely spaced stems to be put down rapidly on the substrate at the large undercoolings characteristic of regime III. This high surface nucleation rate forces the system to begin to require 'slack' to provide segments for stem formation, which tends to limit the mean cluster size to a mixture of singlets, adjacent re-entrant doublets, and possibly an occasional triplet (*Figure 16a*). Also, the excursion of an emergent chain to a nonadjacent site is often quickly rendered permanent by the rapid deposition of other stems; in this situation the backward reaction cannot remove it.

The crowding of the emergent chains at the lamellar surface resulting from the rapid nucleation promotes a large angle of tilt with its reduced degree of tight folding.

It is appropriate to mention here the type of molecular trajectory that may hold at very high molecular weights, particularly in the limit of ultrahigh range E–E′ that conforms to essentially pure regime III-A growth behaviour. Here the limiting crystallinity at T_x is very low for PE ($\chi_c \cong 0.2$–0.3 as in *Figure 7*) and the lamellae have been stated to be ill-formed (VMFM[78]). (There are many unknowns, including the angle of tilt, but in any case we would hesitate to apply the Gambler's Ruin criteria to such degenerate lamellae.) The low crystallinity alone is enough to suggest the possibility of a relatively close approach to the random re-entry 'switchboard' model, but this conjecture remains to be supported by other means. It is worth recalling that $\sigma\sigma_e$ is close to 1060 erg cm^{-2} in range E–E′, which implies that the rate-determining nucleus involves some chain folding. The detailed nature of the actual molecular trajectory at T_x for the lamellae in range E–E′ is surely worthy of further study.

C. Regime I

The proposed molecular trajectory for PE $M \simeq 40$K (upper part of range B–B′) melt-crystallized in regime I is based largely on a reasonable extrapolation of the results obtained on the lower molecular weight quantized systems of range A–A′ crystallized in this regime. The key points involved in the extrapolation will be the mean cluster size, the relatively unperturbed character of the reptation process, and the high degree of crystallinity. The estimate of p_{ar} for $M \simeq 40$K for PE crystallized in regime I given in what follows applies to the {1 1 0} sector only. Neutron scattering of PEH–PED mixtures crystallized in regime I exhibit strong segregation effects that prevent analysis to determine molecular trajectories, but the method discussed below does not suffer this difficulty.

C.1. Details of extrapolation and results. *Figure 16b* delineates in schematic form typical molecular trajectories for two PE molecules $M \simeq 40$K as we envisage them to occur after crystallization from the melt in regime I. As demonstrated by VMFM, the mean angle of tilt is small (~19°) for a fraction of this molecular weight crystallized in regime I, so this feature is not emphasized in the figure. Reference to *Figure 7a* and *Table 2* serves to remind one that at 40K the regime I → II transition effect is distinct in this range so the occurrence of regime I crystallization is definite. Inspection of *Figure 7b* shows the degree of crystallinity at 40K to be still quite close to that extant in the upper part of the 'quantized' range A–A′, i.e. at $M \cong 8$–10K. In addition, the near-ideal steady-state forced reptation process characteristic of range B–B′ may be taken to be fully active at $M \cong 40$K as discussed earlier (see *Figure 11*).

Given the above background, the mean cluster size relevant to $M \simeq 40$K was deduced by the following line of reasoning. First, it was noted from the lower molecular weight quantized systems illustrated in *Figure 15* that a mean cluster size $\bar{\nu}_c$ of about 3.5 could be developed in regime I in the absence of excessive retardations to the near-ideal reptation process if the molecules were long enough. A notable decrease in adjacency is expected only when one sees a decided fall in the degree of crystallinity and a perturbation of the reptation process. From *Figures 7b* and *11*, it is evident that neither effect has occurred to a significant extent between 8–10K and ~40K. Then, with the degree of crystallinity for 40K being nearly as high as that at 8–10K where the cluster size was known to be ~3.5, we deemed it reasonable to require a similar though slightly smaller mean cluster size in regime I for the $M = 40$K case. In the event, we chose to be conservative and selected a mean cluster size $\bar{\nu}_c$ centring around 2.9. This leads to a probability of adjacent re-entry with equation (53b) of

$$p_{ar} \simeq 0.66 \tag{61}$$

for a PE fraction $M \simeq 40$K melt-crystallized in regime I, {1 1 0} growth face.

The molecular trajectories for the two molecules shown in *Figure 16b* were constructed on the basis that $\bar{\nu}_c$ was 2.9 giving a p_{ar} of 0.66. The degree of 'tight' folding p_{tf} was adjusted upward from its lower bound since p_{tf} must exceed p_{ar}. The number of adjacent stems in each cluster is noted in the figure for molecule *1*. This molecule has a $\bar{\nu}_c$ of 3.0: molecule *2* has a $\bar{\nu}_c$ of 2.83. The p_{ar} for molecule *1* is 0.67 as calculated with equation (53b) and 0.71 as determined with equation (53a). The corresponding p_{ar} values for molecule *2* are 0.65 and 0.69. Each molecule has some next-nearest neighbour re-entries. (The additional trajectories p_{aar} were chosen on the basis that p_{tf} should be about midway between p_{ar} and unity.) The two such for molecule *1* are marked p_{aar} in the figure. Calculations with equation (53c) yield a probability of tight folding p_{tf} of 0.82 for molecule *1* and 0.81 for molecule *2*. This is well in excess of the Gambler's Ruin lower bound, which is 0.637 (*Table 3*). Both molecules occupy only one lattice plane as required for substrate completion in regime I crystallization.

Table 3, item 4, summarizes the results for p_{ar} and p_{tf} for a fraction $M \sim 40$K crystallized in regime I and regime III. Even allowing for some latitude in these results, it is evident that adjacent re-entry and tight folding are much more prominent in regime I than in regime III.

Observe in *Figure 16b* that the clusters have not been shown as having uniform size—for example, molecule *1* has one singlet cluster and one with five stems, the other clusters having an intermediate number of stems. We have thus chosen a 'variable cluster' type of representation, which we see as that most consistent with the surface nucleation model. The largest clusters likely form towards the end of the reptation process where the overall friction coefficient is lower.

No interlamellar link is shown in *Figure 16b*. While these undoubtedly occur to some extent in regime I for $M = 40$K, f_{link} is likely considerably smaller than in regime III by reason of the fact that more excursions of emergent stems return soon to the lamella of origin in regime I than in regime III.

That the estimated p_{ar} of ~0.66 given above for PE melt-crystallized in regime I for $M \simeq 40$K is reasonable is afforded by a comparison with single crystals of similar molecular weight and crystallinity formed in dilute solution. As noted previously, single crystals formed from solution typically have a degree of crystallinity from density measurements of 0.85 ± 0.05 and a mean fold surface free energy close to 90 erg cm^{-2}. Also, we

recall here that Spells[98] showed that p_{ar} was ~0.75 for solution-formed single crystals as based on both i.r. and NS data. As shown in *Figure 7b*, the degree of crystallinity of $M \simeq 40$K regime I melt-crystallized PE is similar to that cited above for single crystals from solution and the fold surface free energy is essentially identical. These similarities lend general support to our estimate of a p_{ar} of ~0.66 for regime I melt-crystallized PE $M \simeq 40$K which is only slightly below that of single crystals of similar molecular weight formed from solution.

We consider now the expectations for regime I behaviour for molecular weights exceeding 40K, such as in the body of molecular weight range C–C′. Here the degree of crystallinity has begun its marked downward trend and the forced reptation process is perturbed (*Figures 7b* and *11*), both of these effects being ascribable to increasing interference from widely separated non-adjacent events as described earlier (*Figure 12*). Even though regime I still appears in range C–C′, one must expect that a lower degree of adjacency and tight folding will obtain than that shown in *Figure 16b*. As one progresses upward in molecular weight, the regime I → II effect disappears as irregular spherulites are formed in range D–D′, so regime I and regime II as distinct entities become abstractions (*Figure 7a*). At these higher molecular weights reptation of slack becomes an increasingly important transport mechanism, so one can expect a trend toward the regime III-like trajectories of the general type illustrated in *Figure 16a*. This trend may possibly even culminate in a relatively close approach to a random 'switchboard' in range E–E′ as noted earlier, but this is unproved and far removed from any considerations based on regime I.

C.2. Summary: regime I, intermediate molecular weights. At a molecular weight in the vicinity of 40K, the degree of adjacency in the {1 1 0} sector is approximately 0.66 and the degree of tight folding about 0.8 for PE crystallized from the melt in regime I. This is far in excess of the corresponding estimates for a fraction of the same molecular weight crystallized in regime III (see *Table 3*, item 4, and *Figure 16*). The high p_{ar} values in ranges A–A′ and B–B′ are mainly a result of the unperturbed nature of the forced reptation processes in regime I coupled with the 'proximity' effect illustrated in *Figure 2c* leading to early fold formation by the emergent stem followed by preferential deposition of the stem into the adjoining niche during substrate completion. The occurrence of multiply-nucleated chains such as those depicted in *Figure 12*, which reduce adjacency, are minimized because of the limited molecular length in ranges A–A′ and B–B′. Meanwhile in regime I, unlike regime III, the backward reaction B_1 can readily remove 'wrong' nonadjacent high energy structures; because of the low surface nucleation rate in regime I, such 'wrong' entities are not promptly pinned in place by rapid addition of new stems. The value of p_{ar} in regime I is predicted to begin to fall in the higher molecular weight range C–C′ where the reptation process is perturbed and the degree of crystallinity begins its steep decline, both these effects being indicative of the presence of a decreasing degree of adjacency.

D. Conclusions

The foregoing quantifies the theme that adjacency in melt-crystallized PE is substantially better in regime I than regime III. The results are given in *Table 3* and apply in the vicinity of 40K. The degree of adjacent re-entry in regime I will be somewhat higher at lower molecular weights, but will begin to decline at higher ones. Molecular trajectories in PE are in the main understandable in terms of nucleation theory as modified to include the impact of regime, the 'proximity' effect, steady-state reptation, and reptation of slack, as well as topological and chain energetic effects.

VII. DISCUSSION AND PERSPECTIVE

A. General

The strategy employed here in developing the theory for the low and intermediate molecular weight ranges was to assume an ideal or near-perfect chain-folded model and then to introduce 'imperfections', such as chain ends and cilia, fold surface roughness, and non-adjacent events, as befitted the particular situation at hand. While this often involved approximations, some doubtless capable of improvement, the authors make no excuses for taking this approach. It led to numerous mathematical expressions based on stated physical concepts that were amenable to experimental test, a number of which, subject to the judgement of the reader, appeared to be successful. Had we initially viewed the fold-bearing surface as a structureless entity, we should have evaded important molecular issues of high interest. Alternatively, had we begun with a random switchboard, it would soon have become necessary to reconsider in the light of the quantization effect as well as the Gambler's Ruin topological calculation, the latter placing a lower bound on the degree of 'tight' folding that is at least one-half and normally higher. The treatment of chain folding finally settled upon deals with the 'imperfections' noted above and takes into account thermodynamic, statistical mechanical, transport, topological, and regime effects as they impact flux-based nucleation theory as applied to flexible-chain polymeric systems crystallizing isothermally in a bladelike mode.

The treatment brings out in readily understandable terms the factors that cause chain folding in melt-crystallized PE of low and intermediate molecular weight. One of these is the 'proximity' effect wherein during substrate completion in regimes I and II the greater presence of an emergent chain near the energetically favourable adjacent niche fosters a high probability of adjacent re-entry when forced steady-state reptation is active. This leads to lamellae with a relatively high overall degree of chain folding with adjacent re-entry of the 'variable cluster' type shown in *Figure 16b*. Another effect that requires chain folding is operative in regime III where forced steady-state reptation is replaced by reptation of slack and the 'proximity' effect thereby partly muted. Here the system confronts the lower bound on the degree of 'tight' folding of topological origin that rejects pathological models with a density anomaly at the lamellar interface ('Gambler's Ruin' topological effect). In this instance the adjacency is rather lower and the mean cluster size smaller as in *Figure 16a*, but the degree of 'tight' folding is still sufficient to justify referring to the lamellae formed as being basically chain folded. Another point is that each new surface nucleation act that occurs during substrate completion re-establishes the thickness of a growing

chain-folded lamella very close to the value $l_g^* = 2\sigma_e/(\Delta G) + \delta$ as noted in the 'kinetic snare' argument given at the end of Section II.D and followed up at the end of Section II.H. Given relatively slow or no thickening, the above arguments go a long way toward explaining the presence of a massive array of thin chain-folded lamellae in the final melt-crystallized system whether it be spherulitic or axialitic.

The present form of the LH nucleation approach has a considerably closer connection with the properties of polymer chains than did the original version. In addition to the role of chain folds noted in the earliest treatment, the chain properties considered now include: (i) forced steady-state reptation and reptation of slack; (ii) the Gambler's Ruin topological constraints on non-adjacent events and also the effect of chain stiffness in reducing adjacency; (iii) the segmental nature of the sections of a polymer chain in the activated state that controls the rate of putting down the first stem where the Kuhn length makes itself felt (theory of σ); (iv) the importance of molecular length in the generation of nonadjacent events and their effect on growth rate, degree of crystallinity, and regime behaviour; and (v) the contribution of short localized chain ends on the one hand and spatially-restricted long cilia on the other, in determining the mean fold surface free energy in systems exhibiting quantized chain folding. We would add that the bulk polymer melt prior to any surface effects was taken to be an interpenetrated random coil system and, further, that the form of the Gambler's Ruin topological limitation on tight folding given as equation (36) is explicitly based on the RIS model. Thus, major aspects of flexible chain polymer behaviour have been brought to bear on surface nucleation theory as applied to melt-crystallized PE in this work. The authors believe that these developments, which cover a lot of ground—growth rates, regimes, lamellar thickness, quantized chain folding, tie chain formation, etc.—when summed up, provide a more detailed and meaningful outlook on the chain folding phenomenon.

The surface nucleation treatment featured here embodies concepts that supplement and extend the original LH version and which have significant consequences. An example is provided by the theory for σ and the concomitant elimination of the 'δ catastrophe'. An examination of the formulation of A_0 for the rate-determining step for putting down the first ($\nu = 1$) stem on the niche-free substrate will reveal that the same physical rationale (high free energy barrier $\Delta\phi_1^*$ of entropic origin resulting from 'segmentalization-alignment' of a physically adsorbed section of chain prior to crystallographic attachment) that leads to the useful 'low ψ' form of surface nucleation theory with no 'δ catastrophe', also allows development of the theory for σ in terms of C_∞^{-1}. Here we remind the reader that the elimination of the 'δ catastrophe' and the theory for σ are both fundamentally based on the generally accepted fact that flexible polymer chains lose entropy on close approach to a 'flat' niche-free substrate and the solid proposition that physical adsorption can occur on such a surface. Recognition and application of these effects both here and earlier has strongly reinforced surface nucleation theory in its 'low ψ' form as a legitimate vehicle for treating and understanding the crystallization of flexible-chain polymers with chain folding. In our view, the fact that a 'δ catastrophe' can be predicted with a ψ_1 for the first stem near unity cannot be used as a strategem for setting aside the 'low ψ' formulation featured here, which was explicitly constructed to apply to simple flexible chain polymers whose molecules exhibit normal weak physical adsorption behaviour and are thus devoid of special strong interactions with the substrate. We deliberately hold in reserve the general formulation with ψ_1 and ψ differing (with one or both substantially greater than zero) and cases where $B \neq B_1$ to deal with atypical situations involving special interactions or unusual chain structures that may arise in the future. With the treatment of σ, together with molecular energy calculations for estimating σ_e, one has a theoretical basis for calculating and understanding the physical origin of these centrally important parameters for melt-crystallized PE. A key feature of early LH developments has been retained, namely the barrier system for a bladelike crystal depicted in *Figure 1*. This construction, which mathematically has no saddle point, allows both surface nucleation rates and substrate completion rates to be calculated and leads, through the generation of δ, to a lamella that is thermodynamically stable at its formation temperature. The formerly conventional 'saddle point' calculation, which was commonly employed in early times, does not provide a platform for calculating the substrate completion rate nor does it lead to a δ that directly answers the initial lamellar stability question at the outset.

The present work deals with the growth regime problem in more detail than heretofore. The treatment of the regime I $\rightarrow$ II rate transition rests on the proposition that a substrate of length L exists on the exposed {1 1 0} growth surface that is an inherent property of the underlying crystal. An estimate of L was obtained here that was based in part on the growth rate data for melt-crystallized PE, and this was found to be of the same order as the range of lattice coherence as estimated from X-ray broadening data. The concept that such a finite substrate naturally exists on the {1 1 0} growth face of a lamellar PE crystal has been difficult for some to accept, but it is well to remember that the relatively small range of lattice coherence values from X-ray line width studies provides undeniable evidence that the underlying orthorhombic crystal begins to exhibit significant imperfection on a length scale not far removed from the value of L consistent with crystallization kinetics. Given a substrate of length L, a quantitative theory for all three regimes follows directly from the surface nucleation model as has been shown herein. The authors are aware of no other treatment that with molecular detail straightaway predicts all three regimes, the slope changes between them, the molecular weight dependence of the growth rate in each regime, the initial lamellar thickness, and has the lamellae in all three regimes being thermodynamically stable as first formed—all in a context that elucidates the nature and origin of the chain folding phenomenon itself. It has not been shown that models based solely on the 'roughening' concept can accurately reproduce either the I $\rightarrow$ II or II $\rightarrow$ III regime transition effect, or more to the point, accurately reproduce both transitions in sequence.

Probably the most significant developments related to the regime of crystallization concern regimes III and III-A. In each case, reptation of 'slack' at the end of the reptation tube is the agency of transport of chain segments to the growth front at a rate sufficient to sustain

the formation of small chain folded clusters. The model presented here explains in quantitative terms the origin of the high reeling rates associated with slack that facilitate the formation of lamellae deep in regime III in PE and also provides a basis for understanding how an incoming molecule can shuttle back and forth across the crystal surface during stem deposition in the substrate completion process. For reasons to be outlined below, the authors expect regime III-A, or 'mixed' II and III-A, to be dominant in certain polymers over a considerable range of crystallization temperature and molecular weight.

B. Application to other polymers

The treatment outlined in the body of this work should prove useful as a starting point in dealing with highly crystallizable, flexible-chain polymers which, like PE, exhibit regimes I, II, and III in succession with increasing ΔT, and which, at least approximately, obey a $G \propto 1/n$ growth rate law at constant ΔT in regimes I and II. As in PE, such behaviour is to be expected over only a certain range of moderate molecular weights, and even then the I $\rightarrow$ II regime transition may not appear in some cases[156]. (A list of polymers that exhibit all three regimes has already been given.) Even when all three regimes are detected within a limited range of moderate molecular weights, the appearance of 'mixed' II and III-A, and eventually pure III-A regime behaviour, is to be anticipated with further increase of molecular weight.

The developments in this work do not uniquely demand that all three regimes be observable or that a $G \propto 1/n$ at constant ΔT law be present in all polymers. In fact, the basis for a quite different class of crystallization behaviour is inherent in the basic theory. An extreme form of this class could arise if some intrinsic aspect of chemical chain structure caused the friction coefficient for reptational translation to be very large. Then, reptation of slack would become the major or possibly the only available mode of transport of chain segments to the growth front even for moderate molecular weights. A polymer fully in this class would show only III-A regime behaviour over a wide range of molecular weight and undercooling (no II $\rightarrow$ III transition and no I $\rightarrow$ II effect except perhaps at quite low molecular weights), and at a specified ΔT exhibit little or no variation of G with widely changing molecular weight. A polymer that bordered on this extreme type could show 'mixed' II and III-A regime behaviour at moderate molecular weights and pure III-A behaviour at high molecular weights, but again with no I $\rightarrow$ II or II $\rightarrow$ III regime transitions (except possibly at low molecular weights) and but little variation of G at constant ΔT over a wide range of molecular weight. A polymer of this less extreme type would exhibit a K_g structure extending from high MW down to intermediate or even low MW that resembled that shown by PE in high MW ranges D–D′ and E–E′ (*Figure 7*). The authors opine that polymers which behave in the general manner described above because of the dominance of reptation of slack will in due course be identified. Poly(TMPS) and *it*-PS are potential candidates for III-A behaviour for a considerable range of molecular weights[205]. Causes of a high overall friction coefficient might include: (i) large side groups; (ii) a very large group grafted to one end of the chain; (iii) hydrogen bonding; (iv) branching; and (v) large diameter main segments of high polarizability. A recognition of the wide variety of regime behaviour implicit in the treatment given here may well expand the scope of nucleation theory to include crystallization of polymers whose behaviour had heretofore been puzzling and unexplained.

A note of caution and some recommendations: it is essential to remember that there is an upper limit to the chain stiffness (and, in parallel, an upper limit to the work of chain folding) at and above which the theory outlined in the main text is not valid. As remarked in the beginning, application of the type of theory presented here is properly limited to polymers where the molecules are in principle flexible enough at points within the chain to bend back upon themselves and re-enter the lattice of origin with adjacent re-entry and the formation of a more or less sharp fold. Of course, more distant re-entry is also allowed, but some adjacent re-entry must be possible. The LH theory is known to be applicable to a high melting polyester[149] (PPVL, $T_m = 269°C$) that exhibits a clear-cut II $\rightarrow$ III regime transition and has a work of chain folding of $\sim 7.5\,\text{kcal mol}^{-1}$, which is well above that of PE, but the actual upper bound of applicability is unknown. However, it is not surprising that difficulties were encountered in attempted application of the LH approach to very high melting semirigid chain polymers including poly(aryl ether ether ketone), PEEK[208]. (Could it be in polymers of this type that one might find a relatively close approach to the heretofore elusive random-re-entry switchboard mode of crystallization?) From a practical standpoint, it would be prudent in dealing with melt-crystallization studies on polymers suspected of having stiff chains to limit attempted application of the LH formulation to those for which it is known that high quality single crystal platelets exhibiting evidence of chain folding can be formed from dilute solution. This would imply that the polymer in question was potentially capable of some adjacent re-entry and tight folding, which might then be present under appropriate conditions of crystallization from the melt. Again from a practical standpoint, it would be most helpful—we would even say essential—to have available a proper T_m' vs. $1/l$ plot. Carefully conducted, this plot establishes a value of $\sigma_e/\Delta h_f$ and gives a close estimate of T_m from which a credible ΔT scale then follows. As shown here for the case of PE, such information is fundamental to carrying out a quantitative analysis of growth rate and other data, including a supportable treatment of regime transitions. We emphasize again that the authenticity of regime transitions is more firmly corroborated if $\log G$ vs. T_x data are given in addition to the customary plots involving $1/T(\Delta T)$ or $1/T(\Delta T)f$. The experimental situation is all the more complete if $\log \tau^{-1}$ vs. T_x data based on bulk crystallization rates are available.

ACKNOWLEDGEMENTS

During the preparation of this work the authors received previously unpublished data, criticisms, special calculations, suggested references, or general comments on a wide range of relevant topics from a number of persons. It is highly fitting that those who rendered such valuable assistance be noted and thanked. Some have already been acknowledged in specific citations but repetition of thanks is surely justifiable. All had an effect on the final manuscript. These individuals include: J. P. Armistead,

F. J. Baltá-Calleja, P. J. Barham, D. C. Bassett, S. Z. D. Cheng, E. A. DiMarzio, C. M. Guttman, H. D. Keith, A. Keller, F. Khoury, S. Krimm, A. J. Lovinger, M. L. Mansfield, H. Marand, G. B. McKenna, R. S. Parnas, P. J. Phillips, D. H. Reneker, C. R. Snyder, S. J. Spells, S. J. Sutton, A. Toda, I. G. Voigt-Martin, and B. H. Zimm. While greatly appreciating the input of the above individuals, the authors condemn none of them to agreeing with all that has been said in the text.

REFERENCES

1. Lauritzen, J. I. Jr. and Hoffman, J. D., *J. Res. Natl. Bur. Stand., Sect. A*, 1961, **64,** 73.
2. Hoffman, J. D. and Lauritzen, J. I. Jr., *J. Res. Natl. Bur. Stand., Sect. A*, 1961, **65,** 297.
3. Hoffman, J. D., Davis, G. T. and Lauritzen, J. I. Jr., in *Treatise on Solid State Chemistry*, Vol. 3, ed. N. B. Hannay. Plenum Press, New York, 1976, pp. 497.
4. Hoffman, J. D., *Polymer*, 1983, **24,** 3.
5. Klein, J. and Ball, R. C., *Faraday Discuss. Chem. Soc.*, 1979, **68,** 198.
6. Hoffman, J. D., *Polymer*, 1982, **23,** 656.
7. Hoffman, J. D. and Miller, R. L., *Macromolecules*, 1988, **21,** 3038.
8. Hoffman, J. D., *Polymer*, 1992, **33,** 2643.
9. Hoffman, J. D., Miller, R. L., Marand, H. and Roitman, D. B., *Macromolecules*, 1992, **25,** 2221.
10. Lauritzen, J. I. Jr. and Passaglia, E., *J. Res. Natl. Bur. Stand., Sect. A*, 1967, **71,** 261.
11. Hoffman, J. D., *Macromolecules*, 1986, **19,** 1124.
12. Hoffman, J. D., *Polym. Commun.*, 1986, **27,** 39.
13. Hoffman, J. D., *Polymer*, 1991, **32,** 2828.
14. Guttman, C. M., DiMarzio, E. A. and Hoffman, J. D., *Polymer*, 1981, **22,** 1466.
15. Guttman, C. M. and DiMarzio, E. A., *Macromolecules*, 1982, **15,** 525.
16. Mansfield, M. L., *Macromolecules*, 1988, **21,** 126.
17. Mansfield, M. L., *J. Phys. Chem.*, 1989, **93,** 6926.
18. Mansfield, M. L., *J. Phys. Chem.*, 1990, **94,** 6144.
19. Mansfield, M. L., *Macromolecules*, 1983, **16,** 914.
20. Kumar, S. K. and Yoon, D. Y., *Macromolecules*, 1989, **22,** 3458.
21. Keller, A., *Philos. Mag.*, 1957, **2,** 1171.
22. Eppe, R., Fischer, E. W. and Stuart, H. A., *J. Polym. Sci.*, 1959, **34,** 721.
23. Flory, P. J., *J. Am. Chem. Soc.*, 1962, **84,** 2857.
24. Hikosaka, M., Rastogi, S., Keller, A. and Kawabata, H., *J. Macromol. Sci., Phys.*, 1992, **B31,** 87.
25. Bassett, D. C., Olley, R. H. and Al Raheil, I. A. M., *Polymer*, 1988, **29,** 1539.
26. Toda, A. and Keller, A., *Coll. Polym. Sci.*, 1993, **271,** 328.
27. Toda, A., *Faraday Discuss. Chem. Soc.*, 1993, **95,** 129.
28. Passaglia, E. and Khoury, F., *Polymer*, 1984, **25,** 631.
29. Organ, S. J. and Keller, A., *J. Mater. Sci.*, 1985, **20,** 1571.
30. Mansfield, M. L., *Polymer*, 1988, **29,** 1755.
31. Hoffman, J. D. and Miller, R. L., *Macromolecules*, 1989, **22,** 3038.
32. Miller, R. L. and Hoffman, J. D., *Polymer*, 1991, **32,** 963.
33. Chan, H. S., Wattenbarger, M. R., Evans, D. F., Bloomfield, V. A. and Dill, K. A., *J. Chem. Phys.*, 1991, **94,** 8542.
34. Marand, H., Personal communication.
35. Mansfield, M. L. and Syi, J.-L., *Macromolecules*, 1987, **20,** 894.
36. Flory, P. J., *Statistical Mechanics of Chain Molecules*, Repr. ed. Hanser, New York, 1988.
37. Turnbull, D. and Spaepen, F., *J. Polym. Sci., Polym. Symp.*, 1978, **63,** 237.
38. Turnbull and Spaepen[37] reported the results of their homogeneous nucleation studies on extended-chain *n*-alkanes in terms of the parameter $\bar{\alpha}_1$ which we later denoted α_{TS}[9]. The experimentally determined quantity α_{TS}, which is close to 0.15 for $n \geq 40$, is related[37,39] to σ by $\sigma = \alpha_{TS}(a_0 b_0 l_u)^{1/3}\Delta h_f$. With $\alpha_{TS} = 0.15$, $\sigma = 12.1\,\mathrm{erg\,cm^{-2}}$. This is reassuringly close to the σ listed in *Table 1* as calculated from $\sigma\sigma_e/\sigma_e = 1063/90 = 11.8\,\mathrm{erg\,cm^{-2}}$ where $\sigma\sigma_e$ is from growth rate studies on chain-folded PE fractions and σ_e from T_m' vs. $1/l$ plots. For $n < 40$, α_{TS} progressively increases with diminishing n and attains a value corresponding to a σ notably larger for *n*-pentane than for PE.
39. Hoffman, J. D., *Faraday Discuss. Chem. Soc.*, 1979, **68,** 371.
40. Equating the σ of equation (1) of this work for the case $T = T_m$, with C_n replacing C_∞, and the $\sigma = \alpha_{TS}(a_0 b_0 l_u)^{1/3}\Delta h_f$ of Turnbull and Spaepen[37], one finds $C_n = (a_0/2)(l_b/l_u)/\alpha_{TS}(a_0 b_0 l_u)^{1/3}$ or $C_n = 0.954/\alpha_{TS}$. The C_n obtained with this expression using the expeirmental $\bar{\alpha}_1 = \alpha_{TS}$ given by Turnbull and Spaepen that were deduced from homogeneous nucleation studies on 18 *n*-alkanes n-C_5H_{12} (C-5) to n-$C_{32}H_{66}$ (C-32) (no chain folds) compare favourably with the theoretical C_n from the RIS model[35] (see also ref. 36, p. 147). This holds from C-5, *n*-pentane ($\alpha_{TS} = 0.38$–0.44, $C_n = 2.17$–2.51; $C_n(\mathrm{RIS}) = 2.15$) to C-32 ($\alpha_{TS} \cong 0.16$, $C_n = 5.96$; $C_n(\mathrm{RIS}) = 5.73$). Meanwhile, equation (1) with $\sigma = 11.8\,\mathrm{erg\,cm^{-2}}$ from growth rate studies on chain folded PE (*Table 1*) yields $C_n = C_\infty = 6.53$, the experimental RIS value being 6.7 ± 0.1. The implications are that: (i) the active segment length in the nucleation process in the subcooled melt (whether it be homogeneous for short extended chains or surface nucleation in chain folded PE lamellae) is $l_{seg} - l_b$ where l_{seg} is the generalied Kuhn length $C_n l_b$ as assumed in the derivation[9] of equation (1) and (ii) the theory for σ given as equation (1) with C_n replacing C_∞ holds with fair accuracy from pentane to polyethylene.
41. Spaepen, F., *Acta Metallurgica*, 1975, **23,** 729.
42. Sadler, D. M. and Gilmer, G. H., *Polymer*, 1984, **25,** 1446.
43. Sadler, D. M. and Gilmer, G. H., *Phys. Rev.*, 1988, **38B,** 5684.
44. Goldbeck-Wood, G., *Macromol. Symp.*, 1994, **81,** 221.
45. Spinner, M. A., Watkins, R. W. and Goldbeck-Wood, G., *J. Chem. Soc., Faraday Trans.*, 1995, **91,** 2587.
46. Tonelli, A. E., *Macromolecules*, 1992, **25,** 7199.
47. Fletcher, D. P. and Klein, J., *Polym. Commun.*, 1985, **26,** 2.
48. Hoffman, J. D. and Weeks, J. J., *J. Chem. Phys.*, 1962, **37,** 1723.
49. Turnbull, D. and Fisher, J. C., *J. Chem. Phys.*, 1949, **17,** 71.
50. Lauritzen, J. I. Jr. and Hoffman, J. D., *J. Appl. Phys.*, 1973, **44,** 4340.
51. Sanchez, I. C. and DiMarzio, E. A., *J. Chem. Phys.*, 1971, **55,** 893.
52. McMahon, P. E., McCullough, R. L. and Schlegel, A. A., *J. Appl. Phys.*, 1967, **38,** 4123.
53. Davé, R. S. and Farmer, B. L., *Polymer*, 1988, **29,** 1544.
54. Petraccone, V., Allegra, G. and Corradini, P., *J. Polym. Sci., Part C*, 1972, **38,** 419.
55. Chum, S. P., Knight, G. W., Ruiz, J. M. and Phillips, P. J., *Macromolecules*, 1994, **27,** 656.
56. Ungar, G. and Organ, S. J., *Polym. Commun.*, 1987, **28,** 232.
57. Frank, F. C. and Tosi, M., *Proc. R. Soc. London, Ser. A*, 1961, **263,** 323.
58. Weeks, J. J., *J. Res. Natl. Bur. Stand., Sect. A*, 1963, **67,** 441.
59. Hoffman, J. D. and Weeks, J. J., *J. Res. Natl. Bur. Stand., Sect. A*, 1962, **66,** 13.
60. Because of the long residence time required to attain a specific χ at high T_x, the thickening process (which begins only after an induction period and then goes as $l \propto K \log t$) can cause deviant high T_m' points at sufficiently high T_x. For Marlex 50 PE, a T_m' vs. T_x plot for $\chi = 0.1$ data points confined to $T_x \leq 129.5$°C gave a straight line with $\gamma \simeq 2$ and the satisfactory result for high MW of $T_m^0 \cong 145.5$°C (ref. 3, p. 533 and ref. 58). The induction period for both bulk crystallization[58] and thickening (Section III.I) increase dramatically with increasing T_x. These effects tend to offset partially the larger K at high T_x and, together with the low initial χ, thereby promote 'straight line' behaviour with a nearly constant γ at and below 129.5°C.
61. Keller, A. and O'Connor, A., *Discuss. Faraday Soc.*, 1958, **25,** 114.
62. Frank, F. C., *Faraday Discuss. Chem. Soc.*, 1979, **68,** 7.
63. Flory, P. J., *J. Chem. Phys.*, 1949, **17,** 303.
64. Flory, P. J. and Yoon, D. Y., *Nature*, 1978, **272,** 226.
65. DiMarzio, E. A., Guttman, C. M. and Hoffman, J. D., *Faraday Discuss. Chem. Soc.*, 1979, **68,** 210.
66. Hoffman, J. D., Guttman, C. M. and DiMarzio, E. A., *Faraday Discuss. Chem. Soc.*, 1979, **68,** 177.
67. McKenna, G. B., Ngai, K. L. and Plazek, D. J., *Polymer*, 1985, **26,** 1651.
68. Flory, P. J. and Yoon, D. Y., *Faraday Discuss. Chem. Soc.*, 1979, **68,** 389.
69. de Gennes, P. G., *J. Chem. Phys.*, 1971, **55,** 572.

70. Bartels, C. R., Crist, B. and Graessley, W. W., *Macromolecules*, 1984, **17,** 2702.
71. Klein, J. and Briscoe, B. J., *Proc. R. Soc. London, Ser. A*, 1979, **365,** 53.
72. Graessley, W. W., *J. Polym. Sci., Polym. Phys. Ed.*, 1980, **18,** 27.
73. Doi, M. and Edwards, S. F., *J. Chem. Soc. Faraday Trans. 2*, 1978, 1802.
74. Perkins, T. T., Smith, D. E. and Chu, S., *Science*, 1994, **264,** 819.
75. Hoffman, J. D. and Miller, R. L., *Macromolecules*, 1990, **23,** 3544.
76. Flory, P. J. and Vrij, A., *J. Am. Chem. Soc.*, 1963, **85,** 3548.
77. Hoffman, J. D., Frolen, L. J., Ross, G. S. and Lauritzen, J. I. Jr., *J. Res. Natl. Bur. Stand., Sect. A*, 1975, **79,** 671.
78. Voigt-Martin, I. G., Fischer, E. W. and Mandelkern, L., *J. Polym. Sci., Polym. Phys. Ed.*, 1980, **18,** 2347.
79. Martinez-Salazar, J., Barham, P. J. and Keller, A., *J. Polym. Sci., Polym. Phys. Ed.*, 1984, **22,** 1085.
80. Phillips, P. J., *Rep. Progr. Phys.*, 1990, **53,** 549.
81. Hoffman, J. D., Guttman, C. M. and DiMarzio, E. A., *Faraday Discuss. Chem. Soc.*, 1979, **68,** 394.
82. The authors are indebted to Dr M. L. Mansfield of MMI and Dr E. A. DiMarzio of NIST for independently pointing out this relationship to them. Result obtained by quadrature.
83. Organ, S. J. and Keller, A., *J. Polym. Sci., Part B: Polym. Phys.*, 1986, **24,** 2319.
84. Frank, F. C., *J. Cryst. Growth.*, 1974, **22,** 233.
85. Mansfield, M. L. and Klushin, L. I., *Polymer*, 1994, **35,** 2937.
86. Lauritzen, J. I. Jr., *J. Appl. Phys.*, 1973, **44,** 4353.
87. Seto, T., *Rept. Progr. Polym. Phys. Jpn.*, 1964, **7,** 67.
88. Mansfield, M. L., *Polymer*, 1993, **34,** 4904.
89. Point, J. J. and Dosière, M., *Macromolecules*, 1989, **22,** 3501.
90. Point, J. J. and Dosière, M., *Polymer*, 1989, **30,** 2292.
91. Hoffman, J. D. and Miller, R. L., *Macromolecules*, 1989, **22,** 3502.
92. Phillips, P. J., *Polym. Prepr. (Am. Chem. Soc., Div. Polym. Chem.)*, 1979, **22**(2), 483.
93. Hoffman, J. D., *Faraday Discuss. Chem. Soc.*, 1979, **68,** 378.
94. Sanchez, I. C., *J. Macromol. Sci., Rev. Macromol. Chem.*, 1974, **C10,** 113.
95. Guttman, C. M. and DiMarzio, E. A., *J. Appl. Phys.*, 1983, **54,** 5541.
96. Bates, F. S., Keith, H. D. and McWhan, D. B., *Macromolecules*, 1987, **20,** 3065.
97. Crist, B. and Nicholson, J. C., *Polymer*, 1994, **35,** 1846.
98. Spells, S. J., in *Characterization of Solid Polymers: New Techniques and Developments*, ed. S. J. Spells. Chapman and Hall, New York, 1994, p. 166.
99. DiMarzio, E. A., Personal communication.
100. If a highly curved interface is assumed, small bundlelike crystallites can form without a density excess at the rounded end surface. Such microcrystalline objects can form cross-links in a high molecular weight system, leading to gel formation.
101. Mansfield, M. L., Personal communication.
102. Bassett, D. C. and Hodge, A. M., *Proc. R. Soc. London, Ser. A*, 1978, **359,** 121.
103. Bassett, D. C. and Hodge, A. M., *Proc. R. Soc. London, Ser. A*, 1981, **377,** 25.
104. Guttman, C. M., DiMarzio, E. A. and Hoffman, J. D., *Polymer*, 1981, **22,** 597.
105. Sadler, D. M., in *Structure of Crystalline Polymers*, ed. I. H. Hall. Elsevier, London, 1984, p. 125.
106. Krimm, S. and Cheam, T. C., *Faraday Discuss. Chem. Soc.*, 1979, **68,** 244.
107. Cheam, T. C. and Krimm, S., *J. Polym. Sci., Polym. Phys. Ed.*, 1981, **19,** 423.
108. Jing, X. and Krimm, S., *J. Polym. Sci., Polym. Phys. Ed.*, 1982, **20,** 1155.
109. The authors thank Dr S. J. Spells, Sheffield Hallam University, for providing them with a copy of the text of his book chapter which they found most helpful. The authors further thank Prof. A. Keller, University of Bristol, for bringing this work to their attention.
110. Patil, R. and Reneker, D. H., *Polymer*, 1994, **35,** 1909.
111. Adsorbed polymer molecules on the lamellar surface may hinder the ability of AFM to detect details of the fold surface, especially at higher molecular weights where adsorbed molecules are tenaciously held. There is sound evidence in one case that such a layer exists on the fold surface of a single crystal, and that it can be removed by mechanical forces[112,113]. AFM might be more effective in detecting the true nature of the fold surface itself if the technique noted in the works just cited (or other methods) were employed first to clear the lamellar surface of adsorbed molecules. An adsorbed layer could simulate a random switchboard when in fact a chain-folded surface of some quality existed beneath the layer. The fold surface profile found in one case by Patil and Reneker[110] was evidently free of such an adsorbed layer. Regarding removal of the adsorbed molecules, we speculate that prolonged storage of single crystals at an appropriate temperature in the presence of excess solvent may permit migration of most of the molecules adsorbed on the fold surface to the growth front at the crystal edge where they could crystallize.
112. Jones, J. B. and Geil, P. H., *J. Res. Natl. But. Stand., Sect. A*, 1975, **79,** 609.
113. Hoffman, J. D. and Davis, G. T., *J. Res. Natl. Bur. Stand., Sect. A*, 1975, **79,** 613.
114. Sonntag, P., Care, C. M., Spells, S. J. and Halliday, I., *J. Chem. Soc. Faraday Trans.*, 1995, **91,** 2593.
115. Gedde, U. W., Eklund, S. and Jansson, J.-F., *Polymer*, 1983, **24,** 1532.
116. Winram, M. M., Grubb, D. T. and Keller, A., *J. Mater. Sci.*, 1978, **13,** 791.
117. Toda, A., *Coll. Polym. Sci.*, 1992, **270,** 667.
118. Toda, A., *Polymer*, 1991, **32,** 771.
119. Toda, A., in *Crystallization of Polymers*, ed. M. Dosière. Kluwer Academic Publishers, The Netherlands, 1993, p. 141.
120. Barham, P. J., Personal communication.
121. The authors are much indebted to Dr P. J. Barham of the University of Bristol for providing them with the l_{obs} data and for making known to them the values of C_1, C_2, T_m, and σ_e derived therefrom. The authors are also indebted to Dr Barham for providing them at an early date with growth rate data on the same fraction (NBS $M_w = 32.1$K) at 90°C and 100°C.
122. Allen, R. C. and Mandelkern, L., *Polym. Bull. (Berlin)*, 1987, **17,** 473.
123. Point, J. J. and Villers, D., *Polymer*, 1992, **33,** 2263.
124. Mandelkern, L., McLaughlin, K. W. and Alamo, R. G., *Macromolecules*, 1992, **25,** 1440.
125. Ergoz, E., Fatou, J. G. and Mandelkern, L., *Macromolecules*, 1972, **5,** 147.
126. The authors thank Prof S. Z. D. Cheng, University of Akron, for providing independent confirmation of the existence of irregular spherulites in range D–D′. The measurements were made by Mr Fang-Chyou Chiu.
127. Bassett, D. C., Hodge, A. M. and Olley, R. H., *Proc. R. Soc. London, Ser. A*, 1981, **377,** 39.
128. Bassett, D. C. and Hodge, A. M., *Proc. R. Soc. London, Ser. A*, 1981, **377,** 61.
129. Mansfield, M. L., In preparation.
130. The number of *active* heterogeneities ν_0 at a crystallization temperature T_x is generally a strong function of the temperature T_1 above T_m to which the specimen is heated prior to cooling to T_x, the higher T_1 values leading to the lower ν_0 (see, e.g. ref. 48). Turnbull[131] treated the stability of crystals that persist above T_m in pores (or cracks) in heterogeneities which then act as seeds on cooling to T_x; crystals in large pores melt out just above T_m, but in small pores or cracks they can persist far above T_m. Given a distribution of pore or crack sizes, one has the explanation of the variation of ν_0 with T_1. Both stable and metastable crystal forms can be maintained well above T_m, with the result that the form that appears subsequently at T_x can depend on previous T, P history of specimens or surfaces in measuring apparatus. Inoculation of pores or cracks with the hexagonal PE phase above the triple point could lead thereafter to growth of this phase at T_x somewhat below the triple point.
131. Turnbull, D., *J. Chem. Phys.*, 1950, **18,** 198.
132. Perkins, T. T., Quake, S. R., Smith, D. E. and Chu, S., *Science*, 1994, **264,** 822.
133. Schonfeld, A., Wilke, W., Hohne, G. and Hosemann, R., *Kolloid. Z. Z. Polym.*, 1972, **250,** 102.
134. Vogel, W., Haase, J. and Hosemann, R., *Z. Naturforsch.* 1974, **29a,** 1152.
135. Baltá Calleja, F. J., Martinez Salazar, J., Čačković, H. and Loboda-Čačković, J., *J. Mater. Sci.*, 1981, **16,** 739.
136. The authors are indebted to Prof. F. J. Baltá Calleja, Institute

of Structure of Materials, CSIC, Madrid, for most helpful information concerning D_{110} values and discussions pertaining thereto.

137. The authors thank Prof. H. D. Keith, University of Connecticut, for a most helpful discussion concerning the nature of the growth front of a lamellar crystal generated at a screw dislocation in a previously-formed crystal.
138. Huang, J., Prasad, A. and Marand, H., *Polymer*, 1994, **35,** 1896.
139. Marand, H., *Macromolecules*, 1989, **22,** 3980.
140. Davis, G. T., Weeks, J. J., Martin, G. M. and Eby, R. K., *J. Appl. Phys.*, 1974, **45,** 4175.
141. Schmieg, C., Grossmann, H. P. and Hägele, P. C., *Polymer*, 1990, **31,** 631.
142. Bassett, D. C., Frank, F. C. and Keller, A., *Nature*, 1959, **184,** 810.
143. Bassett, D. C., Frank, F. C. and Keller, A., *Proc. Eur. Reg. Conf. on Electron Microscopy, Delft*, 1960, **I,** 244.
144. Harrison, I. R., *J. Polym. Sci., Polym. Phys. Ed.*, 1973, **11,** 991.
145. Organ, S. J. and Keller, A., *J. Mater. Sci.*, 1985, **20,** 1586.
146. Armitstead, K. and Goldbeck-Wood, G., *Adv. Polym. Sci.*, 1992, **100,** 219.
147. Dorset, D. L., *J. Macromol. Sci., Phys.*, 1986, **B25,** 1.
148. Fatou, J. G., Marco, C. and Mandelkern, L., *Polymer*, 1990, **31,** 1685.
149. Roitman, D. B., Marand, H., Miller, R. L. and Hoffman, J. D., *J. Phys. Chem.*, 1989, **93,** 6919.
150. Rodriguez-Arnold, J., Zhang, A., Cheng, S. Z. D., Lovinger, A. J., Hsieh, E. T., Chu, P., Johnson, T. W., Honnell, K. G., Geerts, R. G., Palackal, S. J., Hawley, G. R. and Welch, M. B., *Polymer*, 1994, **35,** 1884.
151. Clark, E. J. and Hoffman, J. D., *Macromolecules*, 1984, **17,** 878.
152. Mezghani, K., and Campbell, R. A. and Phillips, P. J., *Macromolecules*, 1994, **27,** 997.
153. Phillips, P. J. and Vatansever, N., *Macromolecules*, 1987, **20,** 2138.
154. Lazcano, S., Fatou, J. G., Marco, C. and Bello, A., *Polymer*, 1988, **29,** 2076.
155. Cheng, S. Z. D., Chen, J. and Janimak, J. J., *Polymer*, 1990, **31,** 1018.
156. At sufficiently high temperatures in regime I, it is possible that an onset of thermal 'roughening', i.e. thermal generation of steps with niches (or thermally-induced erasure or 'flickering' of stopping defects) might cause a reversion to regime II behaviour at all higher T_x. Such a reversion does not occur in PE but does so in *cis*-1,4-polyisoprene and PEO. In some polymers, these effects could prevent the appearance of regime I.
157. Lovinger, A. J., Davis, D. D. and Padden, F. J. Jr., *Polymer*, 1985, **26,** 1595.
158. Point, J. J. and Janimak, J. J., *J. Cryst. Growth*, 1993, **131,** 501.
159. Keith, H. D. and Loomis, T. C., *J. Polym. Sci., Polym. Phys. Ed.*, 1984, **22,** 295.
160. Keith, H. D., Personal communication.
161. Observable isothermal thickening occurs after an incubation time (induction period) t_{inc} of $\sim$1 min at $T_x = 126°C$, $\Delta T = 18.2°$, and on the order of 30 min at $T_x = 129°C$, $\Delta T = 15.2°$. (Personal communication, Dr P. J. Barham, Bristol.) Thereafter l_{obs} increases above its initial value according to a $K \log t$ law. Any very early thickening that occurred in times less than a few seconds would be subsumed in C_2. For the experiments cited in the text, it is evident that the initial lamellar thickness is separable from the effects of subsequent thickening.
162. Lieser, G. and Fischer, E. W., Personal communication reported in ref. 3.
163. Korenaga, T., Hamada, F. and Nakajima, A., *Polymer J.*, 1972, **3,** 21.
164. Fischer, E. W. and Lorenz, R., *Kolloid Z. Z. Polym.*, 1963, **189,** 97.
165. Martin, G. M. and Passaglia, E., *J. Res. Natl. Bur. Stand., Sect. A*, 1966, **70,** 221.
166. Hoffman, J. D., Lauritzen, J. I. Jr., Passaglia, E., Ross, G. S., Frolen, L. J. and Weeks, J. J., *Kolloid Z. Z. Polym.*, 1969, **231,** 564.
167. Ungar, G. and Keller, A., *Polymer*, 1986, **27,** 1835.
168. Phillips, P. J. and Lambert, W. S., *Macromolecules*, 1990, **23,** 2075.
169. Bank, M. I. and Krimm, S., *J. Appl. Phys.*, 1969, **40,** 4248.
170. de Gennes, P.-G., *Macromolecules*, 1984, **17,** 703.
171. Lacher, R. C., Bryant, J. L. and Howard, L. N., *J. Chem. Phys.*, 1986, **85,** 6147.
172. DiMarzio, E. A., *J. Chem. Phys.*, 1967, **47,** 3451.
173. Keith, H. D., Padden, F. J. Jr. and Vadimsky, R. G., *J. Appl. Phys.*, 1971, **42,** 4585.
174. Zachariades, A. E. and Logan, J. A., *J. Polym. Sci., Polym. Phys. Ed.*, 1983, **21,** 821.
175. Clark, E. J. and Hoffman, J. D., Unpublished observations.
176. Hoffman, J. D. and Miller, R. L., in *Advancing Materials Research*, ed. P. A. Psaras and H. D. Langford. National Academy Press, Washington, D.C., 1987, p. 245.
177. Phuong-Nguyen, H. and Delmas, G., *Macromolecules*, 1992, **25,** 408.
178. Rastogi, S. and Odell, J. A., *Polym. Commun.*, 1993, **34,** 1523.
179. Hoffman, J. D., in *Proceedings of the International Polymer Symposium Celebrating Professor Tohru Kawai's 70th Birthday*, ed. A. Shoji and N. Okui. Tokyo, 1994 (publ. 1995), p. 33.
180. Ungar, G., Stejny, J., Keller, A., Bidd, I. and Whiting, M. C., *Science*, 1985, **229,** 386.
181. Guttman, C. M., *Faraday Discuss. Chem. Soc.*, 1979, **68,** 457.
182. Lauritzen, J. I. and DiMarzio, E. A., *J. Res. Natl. Bur. Stand.*, 1978, **83,** 381.
183. Guttman, C. M., DiMarzio, E. A. and Hoffman, J. D., *J. Res. Natl. Bur. Stand.*, 1980, **85,** 273.
184. Broadhurst, M. G., *J. Res. Natl. Bur. Stand., Sect. A*, 1966, **70,** 481.
185. Stack, G. M., Mandelkern, L., Kröhnke, C. and Wegner, G., *Macromolecules*, 1989, **22,** 4351.
186. From a purely statistical mechanical point of view, unpairing (delocalization) of chain ends should increase T_{m_2} as noted by Stack *et al.*[185] and calculated by Broadhurst[184] (see his *Figure 4*). But unpairing is accompanied by other events which can have the opposite effect. If chain ends in an extended-chain lamellar crystal are unpaired by chain translation, there will be a (partially collapsed) row vacancy at the one end and a cilium at the other for each displaced chain. When such structures occur to a considerable extent for kinetic reasons during real-time crystallization, the heat of fusion will be somewhat deficient, and a perceptible '$\sigma_{cil}^{\perp}$' developed that will tend to lower the melting point below its equilibrium value. At low T_x near the extended-chain ($f = 0$) and once-folded ($f = 1$) transition, the effect of some 'buried' folds in the otherwise extended-chain crystal should be considered as a possible additional contributing cause for a lowered heat of fusion and the presence of premelting.
187. Holland, V. F. and Lindenmeyer, P. H., *Science*, 1965, **147,** 1296.
188. Holland, V. F. and Lindenmeyer, P. H., *J. Appl. Phys.*, 1965, **36,** 3049.
189. Holland, V. F., Lindenmeyer, P. H., Trivedi, R. and Amelinckx, S., *Phys. Stat. Sol.*, 1965, **10,** 543.
190. Schelten, J., Ballard, D. G. H., Wignall, G. D., Longman, G. and Schmatz, W., *Polymer*, 1976, **17,** 751.
191. Stamm, M., Fischer, E. W., Dettenmaier, M. and Convert, P., *Faraday Discuss. Chem. Soc.*, 1979, **68,** 263.
192. Bai, S. J., Thesis, Univ. of Michigan, 1979.
193. Summerfield, G. C., King, J. C. and Ullman, R., *J. Appl. Cryst.*, 1978, **11,** 534.
194. Sadler, D. M. and Keller, A., *Macromolecules*, 1977, **10,** 1128.
195. Sadler, D. M., *Faraday Discuss. Chem. Soc.*, 1979, **68,** 419, 429, 435.
196. Yoon, D. Y. and Flory, P. J., *Polymer*, 1977, **18,** 509.
197. Yoon, D. Y. and Flory, P. J., *Faraday Discuss. Chem. Soc.*, 1979, **68,** 288.
198. Yoon, D. Y. and Flory, P. J., *Polym. Bull. (Berlin)*, 1981, **4,** 693.
199. Guttman, C. M., Hoffman, J. D. and DiMarzio, E. A., *Faraday Discuss. Chem. Soc.*, 1979, **68,** 297.
200. Guttman, C. M., *Faraday Discuss. Chem. Soc.*, 1979, **68,** 433.
201. Mansfield, M. L., *Macromolecules*, 1986, **19,** 851.
202. Guenet, J. M., Picot, C. and Benoit, H., *Faraday Discuss. Chem. Soc.*, 1979, **68,** 251.
203. Backman, D. K. and Devries, K. L., *J. Polymer Sci., Part A-1*, 1969, **7,** 2125.
204. Jing, X. and Krimm, S., *J. Polym. Sci., Polym. Lett. Ed.*, 1983, **21,** 123.
205. Poly(tetramethyl *p*-phenylene disiloxanylene) [poly(TMPS)] has a K_g structure[206] that appears to us as typical of 'mixed' II and III-A from $\sim$10K to $\sim$30K and full III-A at

$M \sim 300$K to 1400K. The K_g in III-A is ~1.4–1.5 times higher than that in 'mixed' II and III-A from 10–30K, in parallel with PE in range D–D′ and E–E′ (cf. *Figure 7a*). This regime assignment is consistent with the fact that G at constant T_x shows but little variation with changing MW from ~40K and upward[207]. Recent experiments by Prof. H. Marand, Virginia Polytechnic Institute and State University, show that *it*-PS spherulites exhibit a virtually constant growth rate at constant T_x from $M = 214$K to 1540K. This holds for a set of isothermal T_x values and suggests that *it*-PS crystallizes in regime III-A in much of this molecular weight range[34]. The authors thank Prof. Marand for imparting this information to them.

206. Magill, J. H. and Li, H.-M., *Polymer*, 1978, **19,** 416.
207. Magill, J. H., *J. Polym. Sci., Part A-2*, 1967, **5,** 89.
208. Medellín-Rodríguez, F. J., Phillips, P. J. and Lin, J. S., *Macromolecules*, 1995, **28,** 7744.